Shear Behavior of Macro-Synthetic Fiber-Reinforced Concrete Panels

John Paul B. Gaston

A thesis
Submitted in partial fulfilment of the
Requirements of

Master of Science in Civil Engineering

University of Washington
2023

Committee:
Travis Thonstad
Paolo M. Calvi
Marc O. Eberhard

Program Authorized to Offer Degree:
Civil and Environmental Engineering

University of Washington

Abstract

Shear Behavior of Macro-Synthetic Fiber-Reinforced Concrete Panels

John Paul B. Gaston

Co-Chairs of the Supervisory Committee:

Travis Thonstad

Civil and Environmental Engineering

Paolo M. Calvi

Civil and Environmental Engineering

Macro-synthetic (polypropylene or polyolefin) fibers are often added to concrete mixtures as secondary reinforcement, designed to control shrinkage and temperature cracks. The contribution of these fibers to the strength of structural elements and the interactions and synergies between distributed fiber and deformed bar reinforcement are not well understood.

This research investigated the behavior of macro-synthetic fiber-reinforced concrete panels subjected to in-plane shear stresses. Twelve panel specimens were tested using the Panel Element Tester located in the Structure Engineering Testing Laboratory at the University of Washington. The panel specimens varied in their transverse reinforcement ratio (ranging from 0% to 1.1%) and fiber content (ranging from 0% to 0.5%). Additionally, companion specimens were cast and tested alongside each panel to determine material properties, including compressive strength, modulus of elasticity, and flexural toughness and strength.

The results of the tests showed that macro-synthetic fibers, at the dosage rates used, were effective at reducing both the average and maximum crack widths observed throughout testing. Generally, the addition of fibers led to finer, more distributed cracking in the panel specimens and no significant change to the panels' shear strengths. Comparisons to existing empirical shear equations from the literature showed overestimations of shear strength in panels containing no transverse reinforcement and tended toward more accurate estimates as the reinforcement ratio increased. In the larger project, the experimental data that was collected will be used to develop rational design guidelines for the shear strength of members that contain both macro-synthetic fibers and transverse deformed bar reinforcement.

Acknowledgements

There are countless people who deserve much more than words of thanks. Firstly, I would like to thank Professor Travis Thonstad and Professor Paolo Calvi for their constant support and guidance. This project provided many challenges and without their advice and encouragement, it would have been an insurmountable task. I would also like to thank Professor Marc Eberhard for his willing and enthusiastic service on my committee.

This project would not be possible without financial and material support. I would like to acknowledge both the ACI Foundation and the Accelerated Bridge Construction – University Transportation Center (ABC-UTC) at Florida International University for providing project funding. Lafarge, GCP Applied Technologies, and CalPortland were essential with providing the necessary aggregate, cement, fibers, and admixtures.

I would still be down in the Structures Lab without the help from all these individuals. Thanks to the lab manager, Vince Chaijaroen for ensuring that all the equipment was working properly and was being used safely. I appreciate all the effort of my first assistant, Clayton Black, for showing me the ropes on the construction process and how to use different pieces of equipment. Thanks to my three other assistants, Daniela Cao, Alexander Maldonado, and Kevin Truong, for learning quickly and helping with enthusiasm. I would also like to thank those who helped though not assigned to my project but helped anyways including Ed Kelly, Kira Twitchell, Grace Zhang, Benedikt Fadel, Francisco Felix, and Ryan Bader.

Finally, I would like to thank those who are closest to me. To all my friends, roommates, and family, you all have given me immense amounts of encouragement. You supported me through any means possible for which I am grateful.

Thank you all!

Table of Contents

List of Figures

List of Tables

Notation List

$A_{cyl} = area\ of\ advance\ (3.19\ in^2)\ or\ retract\ (6.49\ in^2)\ actuator$

$A_f = cross\ sectional\ area\ of\ test\ region$

$A_g = cross - sectional\ area$

$A_v = Area\ of\ Shear\ Reinforcing\ Steel$

$C_{Rd,c} = calibration\ factor\ for\ the\ design\ shear\ capacity$

$D_f = fiber\ diameter$

$E_s = Modulus\ of\ elasticity\ of\ reinforcing\ steel$

$F = fiber\ factor$

$F_{act} = force\ from\ actuator$

$L_f = fiber\ length$

$L_{hl} = Length\ of\ horizontal\ line$

$N_u = design\ axial\ force$

$V = shear\ force$

$V_{cd} = design\ value\ of\ concrete\ contribution\ to\ shear\ capacity$

$V_{fd} = design\ value\ of\ fiber\ contribution\ to\ shear\ capacity$

$V_f = volume\ fraction\ of\ steel\ fibers$

$a/d = shear\ span - depth\ ratio$

$b_w = web\ width$

$d = effective\ depth$

$d_f = bond\ factor$

$e = arch\ action\ factor$

$f_{ci} = Stress\ in\ concrete\ in\ direction\ "i"$

$f_{ck} = characteristic\ concrete\ cylinder\ compressive\ strength$

$f_{ctk} = characterisic\ tensile\ strength\ of\ concrete$

$f_{cuf} = cube\ strength\ of\ fiber\ concrete, MPa$

$f_{Ftuk} = characteristic\ value\ of\ post\ cracking\ strength\ for\ the\ ultimate\ crack\ opening$

$f_i = Stress\ on\ panel\ in\ direction\ "i"$

$f_{RK,4}$
$= characteristic\ residual\ flexural\ strength\ for\ the\ ultimate\ limit\ state\ at\ a\ CMOD\ of\ 3.5mm$

$f_{si} =\ Stress\ in\ the\ reinforcing\ steel\ in\ the\ "i"\ direction$

$f_{spfc} = computed\ value\ of\ split - cylinder\ strength\ of\ fiber\ concrete$

$f_{sy} = Yield\ Strength\ of\ Reinforcing\ Steel$

$f'c = concrete\ cylinder\ compressive\ strength$

$f'_t = split - cylinder\ tensile\ strength\ of\ concrete$

$k_f = factor\ that\ considers\ the\ contribution\ of\ the\ flanges\ in\ T - sections$

$n_c = Number\ of\ cracks\ crossing\ horizontal\ line$

$p_{act} = pressure\ of\ either\ advance\ or\ retract\ line$

$s = Crack\ spacing$

$w_{csl} = Average\ crack\ width\ of\ a\ single\ line\ crossing\ the\ horizontal\ line$

$\gamma = shear\ strain$

$\gamma_c = concrete\ material\ factor$

$\Delta L = change\ in\ length$

$\Delta L_x = change\ in\ x - direction\ length$

$\varepsilon = strain$

$\lambda = factor\ for\ standard\ or\ lightweight\ concrete$

$\rho = flexural\ reinforcement\ ratio$

$\rho_{si} = Reinforcement\ Ratio\ (\%)\ in\ direction\ "i"$

$\sigma_{cu} = Flexural\ Strength\ of\ Fiber\ Concrete$

$\tau = bond\ strength\ between\ fibers\ and\ matrix$

$\tau_f = design\ value\ of\ bond\ strength\ between\ fibers\ and\ matrix$

$\upsilon = shear\ stress$

$v_b = shear\ strength\ attributed\ to\ fibers$

$v_u = average\ shear\ stress\ at\ shear\ failure$

Chapter 1: Introduction

1.1 Introduction

Macro-synthetic fibers are often added to concrete mixtures as secondary reinforcement, designed to control shrinkage, temperature cracks, and improve the durability of structural elements. The addition of fibers to concrete improves the tensile behavior of the material, which leads to more durable concrete elements with increased ductility and better crack control. In addition to these desirable effects, the tensile strength of the fibers also contributes to the strength of the member, however this benefit is not included in current design codes [e.g., ACI 318-19, (2019)]. The lack of provisions regarding the use of macro-synthetic fibers as supplemental reinforcement is of detriment to the construction industry because the use of fibers would result in a reduction of bar reinforcement and congestion, lighter members, smaller crack sizes, better distribution of localized stresses, and increased confinement and performance of member ends.

Prior tests of fiber-reinforced concrete elements have generally focused on steel fiber-reinforced concrete (SFRC) beams without stirrups. A much smaller number of researchers have investigated the use of deformed bar reinforcement and fibers together to resist shear, and lesser still have investigated the shear strength of macro-synthetic fiber-reinforced concrete with or without transverse reinforcement. This thesis describes the results from experimental tests investigating the shear strength of panel elements containing both conventional transverse deformed bar and macro-synthetic fiber reinforcement. To the knowledge of the author, this was the first test series to investigate the behavior of panel elements with both types of reinforcement (deformed bars and macro-synthetic fibers). The panel tests, where specimens were subjected to pure in-plane shear stresses, were used to isolate the shear strength contributions of the fibers. This is in contrast to previous studies where specimens (beams) were subjected to a combination of shear and flexural stresses. The test series aimed to quantify any positive interactions, or synergies, that arise when using both deformed bar and macro-synthetic fiber reinforcements to resist shear forces.

1.2 Research Objective

The objective of this research was to experimentally measure the shear behavior of reinforced concrete panel elements containing both macro-synthetic fibers and transverse deformed bar reinforcement. This was done through the use of the Panel Element Tester at the Large-Scale Structure Engineering Testing Laboratory at the University of Washington. Quantifying the potential interaction between deformed bar and macro-synthetic fiber reinforcement was a critical component of the testing program, so the test matrix included panels with different levels of both types of reinforcement.

1.3 Thesis Organization

The organization of the thesis is as follows:

- **Chapter 2: Literature Review** explores the background information on both the PFRC material and methods of testing in shear. There is also a focus on related shear equations for steel fiber reinforced elements which will be used in Chapter 5.
- **Chapter 3: Experimental Test Program** discusses the specimen construction and test procedure, including the concrete mixture design, mixing and casting procedure, reinforcement layouts, material testing, instrumentation, tests setup, and loading procedure.
- **Chapter 4: Experimental Results** describes the data processing and test results for a typical panel specimen with summary tables, plots, and photos.
- **Chapter 5: Analysis and Comparison of Results** presents key measurements from the experimental test series, analyzes the results to identify trends, and compares the measured values to empirical equations used to predict the shear strength of fiber reinforced structural elements.
- **Chapter 6: Summary. Conclusions, and Future Work** summarizes the completed work, develops conclusions based on the experimental results, and proposes several areas for future work in this area.

Chapter 2: Literature Review

2.1 Introduction

The potential utilization of fibers in structural applications has garnered the sustained interest of researchers and engineers for over 50 years. Experiments have studied the influence of concrete strength, fiber type, fiber percentage by volume, fiber aspect ratio, and longitudinal reinforcement ratio on the strength and deformability of fiber reinforced concrete (FRC) beams [e.g., Shah et al., (1971)], and a significant amount of research since the early research in the 1960's has focused on steel fiber-reinforced concrete (SFRC) beams without stirrups and with fiber volumes in the range of 2%-4%, as shown by the grey bars in Fig. 2-1 with data from Lantsoght, (2019). This body of experimental evidence formed the basis for the code change in ACI 318-08 (2008) exempting SFRC beams from the minimum shear reinforcement requirements. In order to qualify for the exemption, SFRC beams must contain at least 100 lbs/yd^3 of steel fibers (0.75% by volume) and the fiber-reinforced concrete mixture must meet specific tensile strength properties measured indirectly through bending tests conducted according to ASTM C1609 (2019). This code change was supported by the analysis of a database of 147 SFRC beam specimens tested without stirrups by Parra-Montesinos and Gustavo (2006). In this analysis, beams with at least 0.75% steel fibers by volume had shear strengths exceeding $3.5\sqrt{f'_c}$.

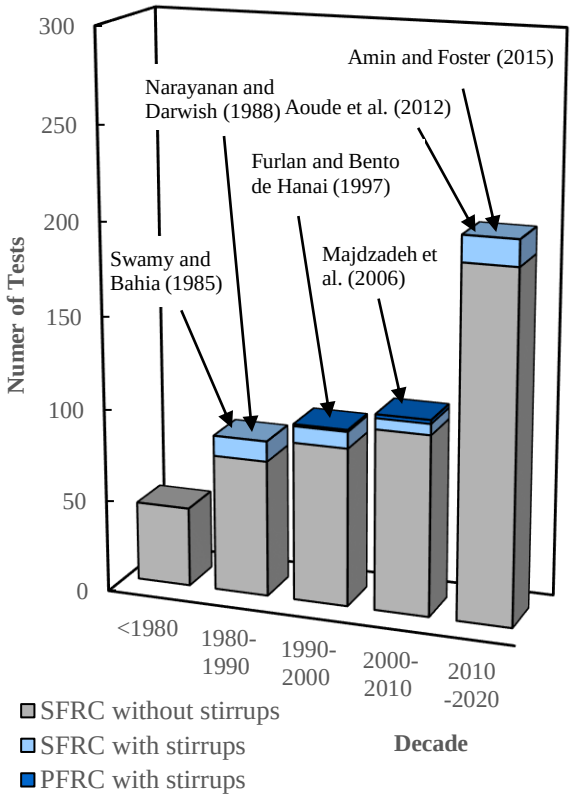

Figure 2-1: Tests of FRC Beams, Data Partially from Lantsoght (2019)

In current practice, fiber addition rates are often less than 0.75% and deformed bars are designed to carry all the necessary shear forces. In comparison with SFRC beams without stirrups, little research has been done to examine the behavior of fiber-reinforced concrete elements that also contain conventional shear reinforcement (shown by the blue bars in Figure 2-1). The limited

evidence available [e.g., Narayanan et al., (1987)] demonstrates that the addition of fibers to beams with conventional shear reinforcement improves the shear strength of the beams and can shift failure from brittle to ductile modes [e.g., Li et al., (1992)]. While this limited test data suggests potential benefits of using fibers as supplemental reinforcement, potentially leading to improved designs including relief of reinforcement congestion in critical regions, the interactions and synergies between distributed fiber reinforcement and conventional deformed bars in resisting shear is not well understood.

The purpose of this chapter is to summarize key background information and past research in the field of macro-synthetic fiber-reinforced concrete. The chapter contains five sections, summarizing:

- the different types of macro-synthetic fibers that are commercially available and their mechanical properties,
- the mechanical properties of macro-synthetic fiber-reinforced concrete elements,
- the performance of macro-synthetic fiber-reinforced concrete beams with and without stirrups,
- the behavior of steel and macro-synthetic fiber-reinforced concrete shear panels, and
- existing empirical and code equations for estimating the shear strength contribution of (steel) fiber-reinforced concrete.

The objective of this chapter is to identify the critical knowledge gaps that are addressed in this project, illustrating the contribution of this work in the context of advancing the understanding of macro-synthetic fiber-reinforced concrete.

2.2 Mechanical Properties of Macro-Synthetic Fibers

Table 2-1 lists the mechanical properties of several types of polymer fibers that are currently in production, showing the substantial variability that exists. For example, carbon or Kevlar fibers have a much higher modulus of elasticity (up to 480,000 MPa) in comparison with polypropylene or polyethylene (less than 5,000 MPa).

Table 2-1: Mechanical Properties of Typical Synthetic Fibers (Daniel, 1991; Bentur, 2007)

Fiber Type	Diameter (mm)	Tensile Strength (MPa)	Elastic Modulus (MPa)	Ultimate Elongation (%)
Acrylic	0.020-0.350	200-1,000	14,000-19,000	10-50
Carbon	0.008-0.019	500-4,000	30,000-480,000	0.5-2.4
Kevlar	0.010-0.012	2,300-3,500	63,000-120,000	2-4.5
Nylon	0.023-0.400	750-1,000	4,100-5,200	16-20
Polyester	0.010-0.200	230-1,200	10,000-18,000	10-50
Polyethylene	0.025-1.000	80-600	5,000	3-100
Polyolefin	0.150-0.640	275	2,700	15
Polypropylene				
-Monofilament	0.100-0.200	450-500	3,500-5,000	15-25
-Fibrillated	0.300-1.000	550-760	3,500-9,000	8
PVA	0.014-0.650	800-1,500	29,000-36,000	5.7

Note: Comparable values for typical steel fibers are diameter 0.100 mm-1.000 mm, tensile strengths 500 MPa-2,600 MPa, modulus 210 GPa, and elongation 0.5%-3.5%.

The most used polymer for macro-synthetic fibers is polypropylene, and many advancements have been made to modify the fiber properties through changes in the material itself or implementing more optimal shapes (Bentur, 2007). Like steel, polypropylene can be cold rolled which provides the benefits of increased modulus of elasticity and tensile strength (Gregor-Svetec and Sluga, 2005) at the expense of ductility (Chatterjee and Deopura, 2006), though reductions in ductility are not a major concern since polypropylene fibers tend to pull-out prior to fracturing in tension. This is consistent with other fiber types, which tend to have relatively low bond strength that limits any benefits gained from increasing the moduli or strengths of the fibers (since their ability to transmit stress across cracks is controlled by bond) (Bentur, 2007). To improve the fiber bond characteristics, the geometry, surface texture, or ends of the fiber can be modified (Wang et al., 1987). Some examples of this include end-hooked, fibrillated, and twisted fibers though many other shapes and finishes exist. Polypropylene fibers are also susceptible to fire or sun damage, although they are protected by the surrounding concrete, and are hydrophobic, which can cause reduced cement paste coverage, low bond capacity, and poor fiber dispersion (Bentur, 2007).

Manufacturers are keenly aware of these issues and have developed many improvements to their proprietary fiber technologies, however comprehensive test data is not widely available in the literature (Richardson and Landless, 2009).

2.3 Mechanical Properties of Macro-Synthetic Fiber-Reinforced Concrete

In general, adding fibers to concrete mixtures tends to increase ductility and toughness, while reducing crack propagation (Shah and Rangan, 1971) and reduces the normal brittle post cracking response of plain concrete. These benefits appear to increase proportionally to the fiber volume content (Bentur, 2007), though adding more fibers can affect the workability of the concrete, leading to possible issues with fiber distribution or concrete consolidation. Additionally, there seems to be a "fiber saturation point" for steel fibers (at about one percent volume ratio), where adding more fibers provides only marginal benefits (Susetyo, 2009, Mirasayah and Banthia, 2002).

In direct tension, the addition of macro-synthetic fibers does not significantly affect the cracking strength (Bentur, 2007). However, post cracking, the macro-synthetic fiber-reinforced concrete exhibits ductile behavior (Carnovale, 2013). It has also been reported that a dosage of 0.33-0.5% volume of fibers increases splitting tensile strength by 10 to 15% (Hasan et al., 2011). The compressive strength does not seem to be influenced by fiber addition (Bentur, 2007), while peak strain and ductility show increases proportionally to the addition of macro-synthetic fibres (Hasan et al., 2011).

The flexural behavior of beams, rupture strength, flexural toughness, and residual strength, are improved through the addition of macro-synthetic fibers. For slender beams, an approximately 20% flexural strength increase was observed for a fiber volume of 0.75 (Altoubat et al., 2009). The flexural toughness and residual strength increases can be seen below in Figure 2-2 from Majdzadeh et al. (2006) with the latter improving by approximately 70% with only slight increases seen beyond addition of more than 0.5% fiber volume.

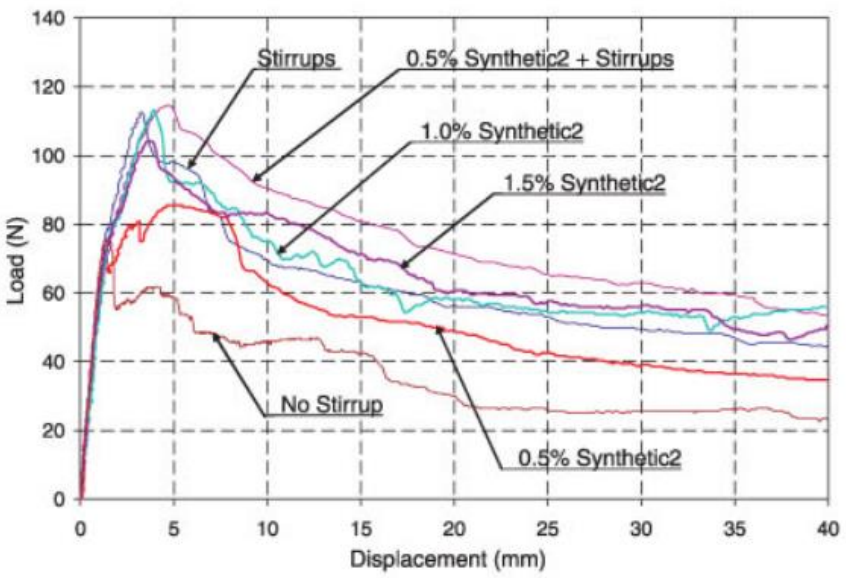

Figure 2-2: Flexural Response of Fiber Beams (Majdzadeh et al., 2006)

2.4 Performance of Macro-Synthetic Fiber-Reinforced Concrete Beams

Table 2-2 summarizes experimental tests investigating macro-synthetic fiber-reinforced concrete beams, both with and without transverse deformed bar reinforcement. The conclusions from each study are summarized in the column on the right side.

Table 2-2: Structural Testing of Synthetic Fiber Concrete Beams with and without Conventional Deformed Bar Reinforcement

Author	Test	Specimen	Fiber Length (mm)	Fiber Aspect Ratio	Fiber Modulus (GPa)	Fiber Geometry	Fiber volume	Conventional reinforcement	Key conclusions
Li et al. 1992	Flexure /Shear	Beams	12.7	334	100	Straight	V_f = 1.0%	ρ_ℓ = 1.1% / 2.2% ρ_v = 0%	Strength increased between 100-200% when a 1% volume fraction of fibers was used. Possible to obtain ductile flexural failures for variety of reinforcement and span-to-depth ratios.
Li et al. 1994	Shear	Ohno shear beams	12.7	334	100	Straight	V_f = 2.0%	ρ_ℓ = 0% / 0.75% ρ_v = 0% / 0.75%	Fiber reinforced beam exhibited higher shear strength than plain concrete specimen and lower strength than reinforced one Fibers did not improve first cracking load. Fiber reinforced specimen had improved ultimate strain over beam with conventional concrete and welded wire fabric reinforcement.
Furlan and Bento de Hanai 1997	Flexure /Shear	Beams	42	840		Multi-filament	V_f = 0% / 0.50%	ρ_ℓ = 1.58% ρ_v = 0.18%	Addition of fibers increased stiffness, improved ductility, increased the shear strength, and led to the formation of multiple cracks at failure in the beams Addition of fibers modified the failure mode of the beams from shear to flexure in the presence of stirrups.
Majdzadeh et al. 2006	Flexure /Shear	Beams	50 54	85 360	9.5 3.5	Straight Self-fibrillating	V_f = 0% / 0.5% / 1.0% / 1.5%	ρ_ℓ = 2.62% ρ_v = 0% / 0.14%	Fiber reinforcement enhanced the capacity of the beams. No benefits were noted when the volume fraction was increased beyond 1%. Beams with both stirrups and fibers had higher strengths than beams containing only stirrups, and the increase was larger than expected given the resistance of the

Author	Test	Specimen	Fiber Length (mm)	Fiber Aspect Ratio	Fiber Modulus (GPa)	Fiber Geometry	Fiber volume	Conventional reinforcement	Key conclusions
									beams tested with only fibers or stirrups alone.
Altoubat et al. 2009	Flexure /Shear	Beams	40	90	9.5	Straight	V_f = 0% / 0.5% / 0.75% / 1.0%	ρ_ℓ = 2.15% / 3.18% ρ_v = 0%	Addition of fibers increased first diagonal cracking strength and ultimate strength roughly of 20-30% Beam response with fibers was more ductile than control RC beams Fibers changed the cracking pattern and mode of failure of the beams. The fiber-reinforced beams exhibited multiple diagonal cracks before failure occurred. Fibers did not change the load at which the diagonal cracks initiated but did slow down propagation and widening
Alhassan et al. 2017	Flexure /Shear	Beams	40	90	9.5	Straight	V_f = 0% / 0.33% / 0.55% / 0.77%	ρ_ℓ = 1.26% / 1.81% / 2.46% / 3.22% ρ_v = 3.33%	Slight increase in strength: roughly 20% increase in strength for a fiber volume fraction of 0.77% Initial, service, and post-cracking stiffness increased with fiber volume fraction

There is limited evidence on the benefits of macro-synthetic fibers with respect to shear strength. In most cases, it has been observed that the fibers contribute to increase the ductility and crack response of the beam specimens, somewhat proportionally to the employed fiber volume. The ultimate strength and failure response have also been observed to improve, shifting the failure mode from a brittle shear failure to a more ductile flexural one. Key results from several references from Table 2-2 are described in greater detail below.

Li (1992)

The goal of this study was to determine the effects of fibers on the shear strength of longitudinally reinforced beams. Two beam sizes were used with the larger section having a height of 228 millimeters and a width of 127 millimeters while the smaller section had a height of 127 millimeters and a width of 63.5 millimeters. The span to depth ratio varied between 1 and 4.25. The authors tested a total of 312 beams in three-point displacement-controlled flexure with 252 being cast from mortar mixes and the last 60 being concrete. Two separate, mortar mixes were used with slightly different water to cement ratios. Fibers of varied surface types and shapes were used with the majority being steel but also some were synthetic such as aramid, acrylic, and polyethylene. Each beam was cast with only one type of fiber.

The addition of fibers provided benefits to both strength and type of failure. When one percent volume fraction of fibers was added, the shear strength saw increases of 100-200%. The fibers also seemed to improve the first cracking shear stress and ultimate shear strength of beams more quickly as reinforcement was added compared to plain concrete. The presumed mechanism is that the fibers reduce the crack propagation along the reinforcing steel which increases the capacity to resist tensile forces across the diagonal cracks. Finally, beams with a span to depth ratio of 3.0 that were reinforced with 1% 50mm steel fibers experienced flexural failures. This showed that ductile flexural failures can be achieved for beams with span to depth ratios that would normally cause shear failures.

Majdzadeh (2006):

This study looked at the effects of both fiber addition and transverse reinforcement on the shear strength of concrete elements. Two different setups were used, including a four-point bending test and a direct shear test (seen below in Figures 2-3 and 2-4). Three different types, hooked steel fibers, a self-fibrillating synthetic fibers, and straight synthetic fibers, were added at 0.5%, 1.0%,

and 1.5% to both types of specimens. Plain concrete specimens were also cast to create a baseline for comparison. The beam specimens had a height and width of 150 millimeters with a clear span of 800 millimeters. Some beams were reinforced with stirrups which were spaced apart further than allowable minimums to study the fiber contribution. The specimens tested for direct shear had dimension in accordance with JSCE-SF3 which has a width and height of 30 centimeters and a length of 60 centimeters. The direct shear specimens were tested in accordance with Japan Society of Civil Engineers procedure JSCE-SF6 with modification including securing the ends from rotation and adding notches in the specimen's ends to ensure the failure plane.

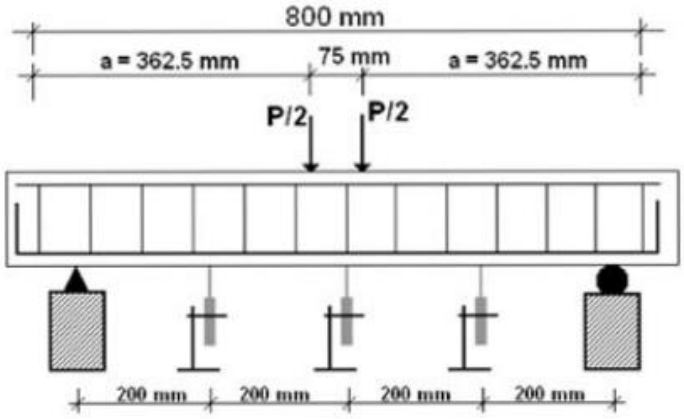

Figure 2-3: Four-Point Beam Bending Test Setup (Majdzadeh et al., 2006)

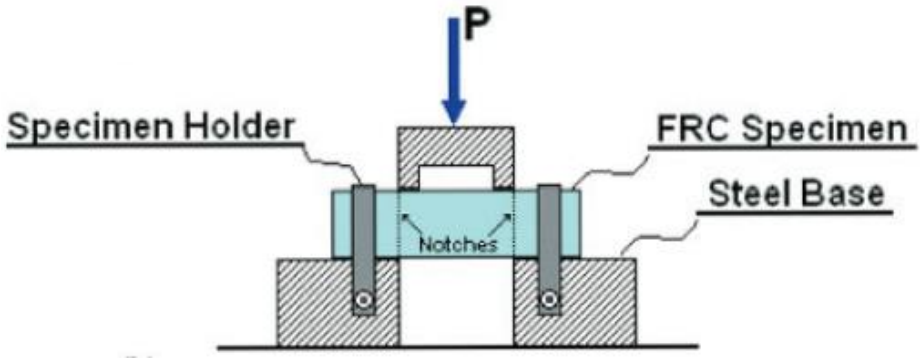

Figure 2-4: Direct Shear Test Setup (Majdzadeh et al., 2006)

Several key conclusions were drawn from the results: (i) the addition of fibers increases the capacity of the beams, while providing residual strength after failure; (ii) fiber volumes over one percent do not improve the behavior and, in some cases, can negatively affect workability which can cause quality issues; and (iii) beams with both fibers and stirrups saw some extra strength (referred to as "synergy strength") when compared to their reinforced concrete companions. The additional strength was attributed to the reduction in crack propagation provided by the fibers, which contributes to maintaining the strength of the confined concrete.

Altoubat (2009):

This experimental program consisted of twenty-seven large-scale concrete beams which were tested under monotonic three-point displacement-controlled flexure. Two specimen sizes were used with the larger set having a height of 460 millimeters and a width of 280 millimeters while the smaller beams had a height of 390 millimeters and a width of 230 millimeters. The parameters which were varied included span to depth ratio, amount of flexural reinforcement, and volume percent of fibers. Companion cylinders were cast and tested to determine the material compressive strength and smaller beams were used to obtain the flexural toughness. The span to depth ratio was also selected to represent both slender and short beams. Fiber volumes varied from zero percent to one percent in quarter percent increments.

The addition of fibers increased both the ultimate strength by about 20-30% and the ductility when compared to the control plain reinforced concrete specimens. Crack patterns and modes of failure were also affected, with the fiber-reinforced beams exhibiting multiple diagonal cracks before failure. Additionally, while the initial cracking load remained similar, crack propagation and widening were also reduced in the presence of fibers. The results from these tests were also analyzed against previous fiber beam shear strength equations from Yazdanbakhsh (2015). It was found that fib-MC (2010), Swamy et al. (1985), Mansur et al. (1986), and RILEM (2003) and Ashour et al. (1992) were the best at accurately predicting the specimens' strength.

2.5 Fiber-Reinforced Concrete Panel Tests

Tests of panel elements (shown in Figure 2-5), rectangular reinforced concrete elements representing portions of reinforced concrete beams or walls subjected to in-plane shear and axial

stresses, allow for the precise control of the shear and axial stress acting on the structural element. This experimental method allows for the direct determination of the shear behavior of reinforced concrete elements, in contrast to beam tests where the underlying shear behavior must be separated from the total response, which includes stresses due to flexure and any accidental torsion caused by the test setup.

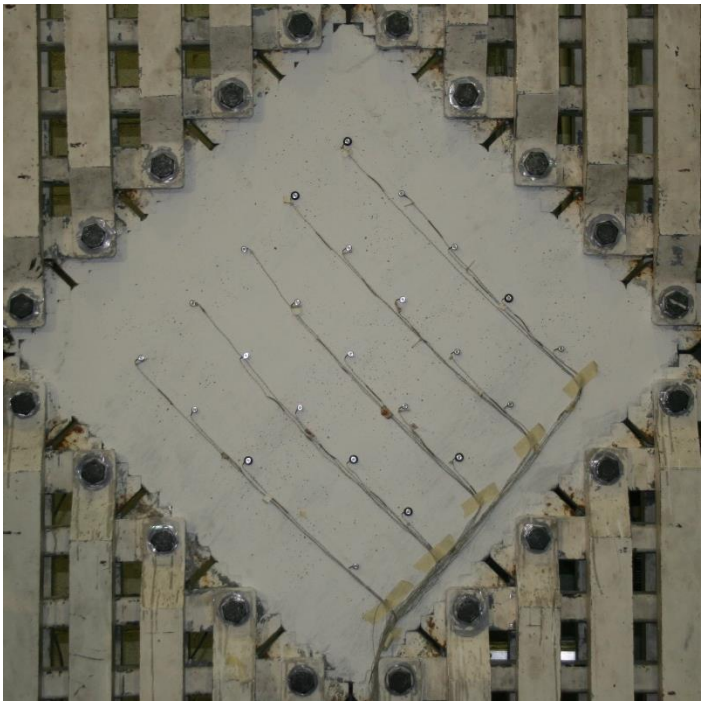

Figure 2-5: Panel Element in Tester

While the current study is the first to test macro-synthetic fiber-reinforced concrete panels with transverse deformed bar reinforcement under shear loads, there have been several studies that investigated the shear response of steel and macro-synthetic fiber-reinforced panel elements without transverse reinforcement and steel fiber-reinforced concrete panel elements with transverse reinforcement. These studies are summarized in the following paragraphs.

Carnovale (2013):

Carnovale tested five panels (890 x 890 x 70 mm) at the panel element tester facility at the University of Toronto with varied amounts of steel or macro-synthetic fibers at constant reinforcement percentages under in-plane shear loads. The fiber volumes chosen after trial batches

were plain, one percent, and two percent with each fiber type present at each level. The authors reported that, due to the high number of fibers, it was difficult to achieve uniform fiber distribution over the cross section during casting. All the panel tests were subject to reversed cyclic loading. Cylinders, direct tension specimens, and beams were cast and tested to determine the material properties of each batch.

This project showed that adding steel fibers to the concrete matrix leads to improvements with respect to cracking response, residual strength, and ductility of the panel elements (seen below in Figure 2-6). Further, the degradation under cyclic loading is not substantial. These benefits come at the cost of concrete workability, especially at higher fiber levels. Also, the study demonstrated that steel fibers increase concrete strength more considerably than macro-synthetic fibers. Finally, due to their geometry and surface, macro-synthetic fibers tend to fail due to bond issues. This is concerning, particularly with respect to attempting to utilize fibers in place of the minimum transverse steel currently recommended.

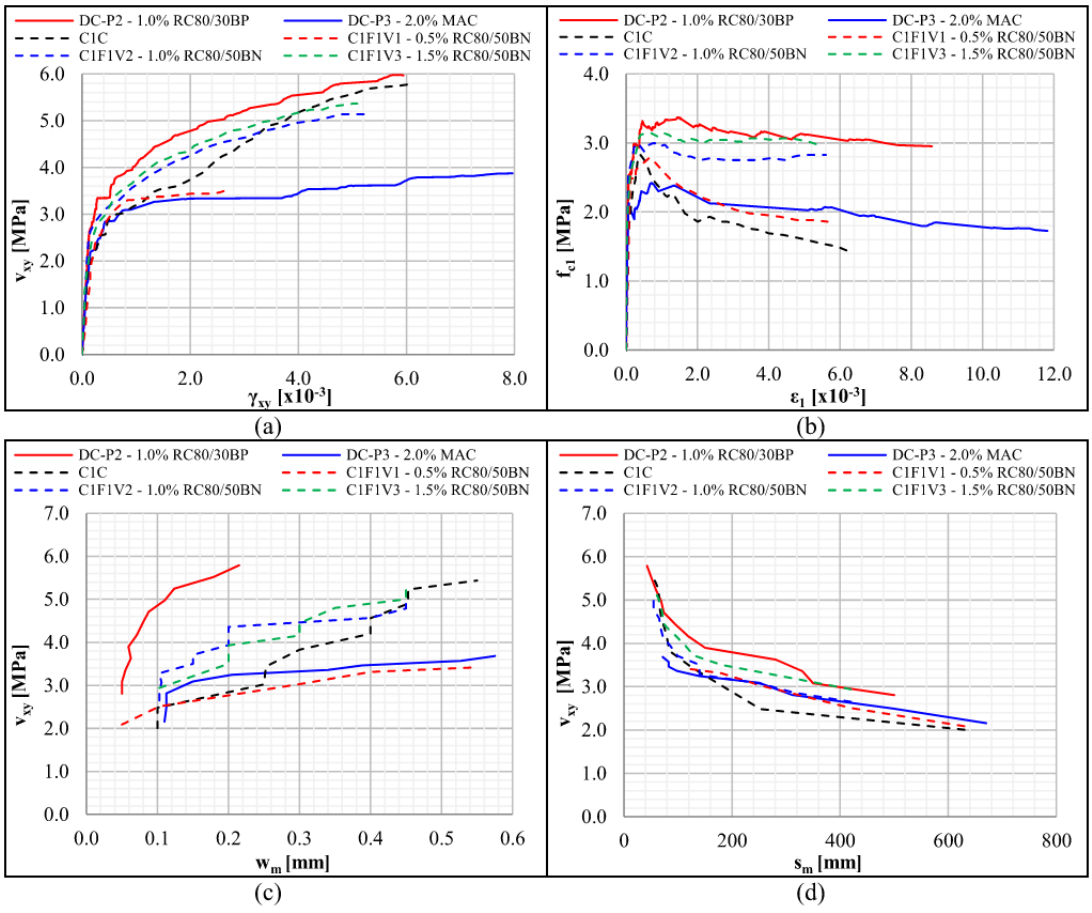

Figure 2-6: Influence of Fibre Type on Panel Test Response (Carnovale, 2013)

Chasioti (2017):

The focus of this investigation was the response of hybrid fiber reinforced concrete on shear dominated stress states. Fourteen panel elements (890 x 890 x 70 mm) were tested at the panel element tester facility at the University of Toronto. Many variables were considered within the test matrix of this experimental program, including types of fibers used, load state, and type of loading. Though the goal was to study hybrid mixtures some baseline mixes were cast with either micro or macro fibers exclusively. Further, both steel and synthetic fibers were considered. Most of the panels were tested in pure shear, with only a set of two specimens subjected to simultaneous biaxial tension and shear. The loading protocol was either monotonic or reversed cyclic. Some panels were purposefully pre-damaged as another possible variable. Alongside the panel elements, material specimens were tested including cubes, cylinders, dog bones, and prisms.

The results of the material testing showed that with the addition of hybrid fibers, ultimate strength and ductility increase in both compression and tension. Regarding the shear panels, the same strength benefits were also observed. Further, serviceability improvements were also quantified regarding limiting drift, improving damage control, lowering crack widths, and crack spacing. These material property increases were seen when compared to both plain concrete samples and those that contain only one type of fiber.

2.6 Fiber Concrete Shear Empirical Equations

The existing literature on fiber-reinforced concrete includes numerous proposed equations for the shear strength of fiber-reinforced concrete (compiled into a database by Lantoght, 2019). The remainder of this section will present several of these empirical and code equations, which were developed using databases of SFRC beams without stirrups and therefore may be unsuitable for elements that contain stirrups and macro-synthetic fibers, even after accounting for the differences between the fiber types. These equations will be assessed in Chapter 5 using the experimental results from this project.

Swamy (1985)

Swamy tested nine T-beams and two rectangular beams under four-point bending. Three variables were considered in the T-beams, namely the amount of longitudinal steel, web steel, and fiber volume. All other parameters were kept constant. Another T-beam was cast with fibers only in the stem and rectangular beams were also fabricated and tested for comparison purposes. The rectangular beams had the same web width, overall depth, and effective depth as the T-beams. Least squares regression was used to relate the ultimate shear strength of the beam with the flexural strength of the same beam as shown in Equation 2.1.

$$v_u = 0.517 + 0.283\sigma_{cu} \quad \text{(MPa)} \tag{2.1}$$

where v_u is the average shear stress at shear failure and σ_{cu} is the flexural strength of fiber-reinforced concrete.

Sharma (1986)

Sharma tested both plain concrete and fiber-reinforced concrete beams under combined bending and shear loading. The beams were reinforced with both longitudinal and transverse steel. The shear strength measured in the tests was related to the transverse reinforcement and fiber volume. Equation 2.2 shows the empirical equation developed to predict the shear strength of the tests. This equation has the benefit of simplicity but incorporates the influence of fiber volume and geometry of the fibers indirectly through the split cylinder strength, and neglects contributions from the flexural reinforcement. The influence of the shear span-depth ratio is also conservatively underestimated.

$$v_u = \left[k f'_t \left(\frac{d}{a}\right)^2\right] b_w d \quad \text{(MPa)} \tag{2.2}$$

where k = 2/3 is a shape fitting parameter; a/d is the shear span-to-depth ratio; f'_t is the split-cylinder tensile strength of the concrete, which can be approximated as 0.79 $\sqrt{f'c}$ if not known; $f'c$ is the specified 28-day compressive strength of the concrete; b_w is the width of the web of the beam; and d is the effective depth of the beam section.

Narayanan and Darwish (1987)

This research followed the work done by Sharma (1986). 50 beams containing fibers were tested in shear. A fiber factor, F, was introduced into the equation to account for the fiber volume, geometry, and bond due to anchorage. The proposed expression is given below in Equation 2.3.

$$v_u = [e\left[0.24f_{spfc} + 80\rho\frac{d}{a}\right] + v_b]b_w d \quad \text{(MPa)} \tag{2.3}$$

$$f_{spfc} = \frac{f_{cuf}}{20-\sqrt{F}} + 0.7 + \sqrt{F} \tag{2.4}$$

$$F = (\frac{L_f}{D_f})V_f d_f \tag{2.5}$$

where f_{spfc} is the computed value of the split-cylinder strength of fiber concrete; ρ is the flexural reinforcement ratio; F is the fiber factor; e is the arching factor, which is taken as $2.8\frac{d}{a}$ if $\frac{a}{d} \leq 2.8$ and 1.0 if $\frac{a}{d} > 2.8$; f_{cuf} is the cube strength of fiber concrete in MPa; L_f is the fiber length; D_f is the fiber diameter; V_f is the volume fraction of steel fibers; d_f is the bond factor, which is taken as 0.5 for rounded, 0.75 for crimped, and 1.00 for indented; v_b is the shear strength attributed to fibers, which is taken as $0.41\tau F$ for this model; and τ is the bond strength between fibers and matrix, which is taken as $4.15\ MPa$ for this model.

Ashour, Hasanain, and Wafa (1992)

This experimental program focused on testing steel fiber reinforced beams without any transverse reinforcement. Two different equations were proposed by the authors. One was based on Zsutty's equation with extra factors added to the base equations to account for the influence of adding fibers.

For $\frac{a}{d} \geq 2.5$

$$v_u = \ [\left(2.11\sqrt[3]{f'c} + 7F\right)\left(\rho\frac{d}{a}\right)^{0.333}]b_w d \qquad \text{(MPa)} \tag{2.6a}$$

For $\frac{a}{d} \leq 2.5$

$$[v_u = \ [Eq\ 2.6a]\frac{2.5}{\frac{a}{d}} + v_b(2.5 - \frac{a}{d})]b_w d \qquad \text{(MPa)} \tag{2.6b}$$

The other was a modified version of the shear equation present in ACI 318-19. Though according to Yazdanbakhsh et al. (2015), this version is not as accurate.

$$v_u = \left[\left(0.7\sqrt[2]{f'c} + 7F\right)\frac{d}{a} + 17.2\rho\frac{d}{a}\right]b_w d \quad \text{(MPa)} \tag{2.7}$$

Kwak, Eberhard, Kim, and Kim (2002)

This investigation reviewed 139 steel fiber reinforced concrete with longitudinal steel but without transverse bars. All the beams were tested in flexure. The equation proposed in this paper was built on Zsutty's equation with additional parameters to account for the fiber influence on both tensile strength on arching action and directly on shear resistance.

$$v_u = [Aef_{spfc}^{exp1}(\rho\frac{d}{a})^{exp2} + Bv_b]b_w d \quad \text{(MPa)} \tag{2.8}$$

where $A = 3.7$ is a shape fitting parameter; e is the arching factor, taken as 1.0 if $\frac{a}{d} > \frac{a}{d_{transition}}$ or $\left(\frac{\frac{a}{d_{transition}}}{\frac{a}{d}}\right)$ if $\frac{a}{d} < \frac{a}{d_{transition}}$; $exp1 = 2/3$ is a shape fitting parameter; $exp2 = 1/3$ is a shape fitting parameter; and $B = 0.8$ is a shape fitting parameter.

Code Equations

Several different code references also provide strength predictions for the shear strength of concrete.

American Concrete Institute (ACI-318):

ACI does not have a specific equation for the shear strength of fiber-reinforced concrete. Therefore, the shear strength equation from Table 22.5.5.1, given by Equation 2.9, would be used, regardless of the fiber volume fraction used.

$$v_u = [2\lambda\sqrt{f'_c} + \frac{N_u}{6A_g}]b_w d \tag{2.9}$$

where λ is a factor for standard or lightweight concrete; N_u is the design axial force; and A_g is the cross-sectional area.

fib. (Model Code 2010: Final Draft):

The fib. model equation for the shear strength of fiber-reinforced concrete is listed below. Note most of this project's samples are underneath the C50 grade.

$$v_u = \frac{C_{Rd,c}}{\gamma_c} k(100\rho\left(1 + 7.5\frac{f_{Ftuk}}{f_{ctk}}\right)f_{ck})^{1/3} b_w d \tag{2.10}$$

$$f_{ctk} = \begin{cases} 0.3(f_{ck})^{2/3} \; for \; concrete \; grades \; \leq C50 \\ 2.12\ln\left(1 + 0.1(f_{ck} + 8MPa)\right) for \; concrete \; grades \; > C50 \end{cases} \tag{2.11}$$

where $C_{Rd,c}$ is the calibration factor for the design shear capacity; γ_c is the concrete material factor; f_{Ftuk} is the characteristic value of post cracking strength for the ultimate crack opening; f_{ctk} is the characteristic tensile strength of concrete; and f_{ck} is the characteristic concrete cylinder compressive strength.

RILEM (Design Method for Steel Fiber Reinforced Concrete):

The RILEM code has an equation that takes into account the contributions from concrete and fibers separately. The equations and subsequent equation necessary to calculate the shear strength predictions are listed below.

$$v_u = V_{cd} + V_{fd} \tag{2.12}$$

$$V_{cd} = 0.12k(100\rho f_{ck})^{1/3} \; b_w d \tag{2.13}$$

$$V_{fd} = 0.7k_f k\tau_{fd} b_w d \tag{2.14}$$

$$k_f = 1 + n(\frac{h_f}{b_w})(\frac{h_f}{d}) \leq 1.5 \tag{2.15}$$

$$n = \frac{b_f - b_w}{h_f} \leq 3 \; and \leq \frac{3b_w}{h_f} \tag{2.16}$$

$$\tau_{fd} = 0.12 f_{RK,4} \tag{2.17}$$

where V_{cd} is the design value of the concrete contribution to shear capacity; V_{fd} is the design value of the fiber contribution to shear capacity; k_f is the factor that considers the contribution of the flanges in T-sections; τ_{fd} is the design value of bond strength between fibers and matrix; and $f_{RK,4}$ is the characteristic residual flexural strength for the ultimate limit state at a CMOD of 3.5mm.

Chapter 3: Experimental Test Program

The objective of the testing program was to quantify the benefits of the combined use of deformed bar reinforcement and macro-synthetic fibers to resist shear forces. To this end, an experimental test matrix was selected with variations in both the transverse steel reinforcement and the amount of added synthetic fibers, allowing for the isolation of the contributions from each type of reinforcement, similar to the study by Majdzadeh et al. (2006).

Table 3-1. Panel Test Matrix

Panel	Specimen Name	V_f (%)	ρ_v (%)
P1	PFRC-000-000	0	0
P2	PFRC-000-029	0	0.29
P3	PFRC-000-058	0	0.58
P4	PFRC-000-114	0	1.14
P5	PFRC-026-000	0.26	0
P6	PFRC-026-029	0.26	0.29
P7	PFRC-026-058	0.26	0.58
P8	PFRC-026-114	0.26	1.14
P9	PFRC-052-000	0.52	0
P10	PFRC-052-029	0.52	0.29
P11	PFRC-052-058	0.52	0.58
P12	PFRC-052-114	0.52	1.14

Table 3-1 summarizes the testing program, showing the values used for each of the experimental variables, i.e., the transverse reinforcement ratio and fiber volume fraction, along with the naming convention for each panel. The naming convention consists of three parts, from left to right, polymer fiber reinforced concrete (PFRC), the fiber volume fraction (×100), and the transverse reinforcement ratio (×100). The fiber volume fraction (fiber volume/ total volume) values were chosen based on recommendations from the manufacturer with 0.26% representing the typical amount used on construction sites (4 lb/yd^3) and 0.52% being the maximum suggested (8 lb/yd^3). The transverse reinforcement ratio (the y-direction based on the coordinate system assigned to each panel) increase from a baseline of 0.0% to 1.14% which is the maximum allowable by the casting setup. The reinforcement ratio in the longitudinal direction, ρ_x, was held at a constant 2.28% to ensure a shear failure in the panels.

In addition to the panel specimens, companion cylinders and beams were also cast at the same time as each of the panels in order to measure the concrete material properties, including compressive strength, the modulus of elasticity, and flexural strength and toughness properties for each batch of concrete used.

3.1 Concrete Mixture Design

Table 3-2 shows the mixture design for the panel specimen test series. Three different admixtures, WRDA64, ADVA 195, and V-MAR, were used in the concrete mix at dosages of 21.3 fl. oz / yd^3, 18.3 fl. oz / yd^3, 15.1 fl. oz / yd^3, respectively.

Table 3-2. Concrete Mixture Design for Panel Specimens

	Absorp (%)	Specific Gravity	**M1:** 0% Fiber*	**M2:** 0.25 % Fibers*	**M3:** 0.52% Fibers*
			Mass [Volume] (lb [ft^3])		
Cement		3.15	534 [2.72]	534 [2.72]	534 [2.72]
Fine Aggregate	2.10	2.65	1447 [8.75]	1413 [8.55]	1380 [8.34]
Coarse Aggregate	1.12	2.68	1815 [10.85]	1838 [11.06]	1860 [11.12]
Water			267 [4.28]	267 [4.28]	267 [4.28]
Air (1.5%)			0 [0.41]	0 [0.41]	0 [0.41]
Fibers		0.92	0	4 [0.07]	8 [0.13]
Total			4062 [27.00]	4059 [27.00]	4056 [27.00]

Each of the mixture proportions in Table 3-2 were based off an existing mixture design provided by a ready-mix supplier using local aggregates. This was done intentionally, to enable the results of the test to be scalable for larger subassembly test specimens in future test programs. The exact batch size and admixture addition volumes were refined to apply for the specific equipment and materials available at the University of Washington (UW) Civil Engineering Materials Laboratory. Because the initial mixture design produced concrete strengths that were higher than desired for the panel testing program (10,000 psi versus the target strength of 6,000 psi), the water-to-cement ratio was increased to 0.5. Each panel was constructed using aggregate and cement from the same supplier. The constitutive materials were stored in bulk bags in the laboratory until use.

3.2 Reinforcement Layout

Figure 3-1 shows the four reinforcement layouts used in the test series. For all configurations, the longitudinal reinforcement ratio was held constant at 2.28%. This reinforcement ratio was

selected to force failure in the transverse direction and was based on previous experience with similarly reinforced specimens tested with the panel tester [e.g., Zhang et al., 2020].

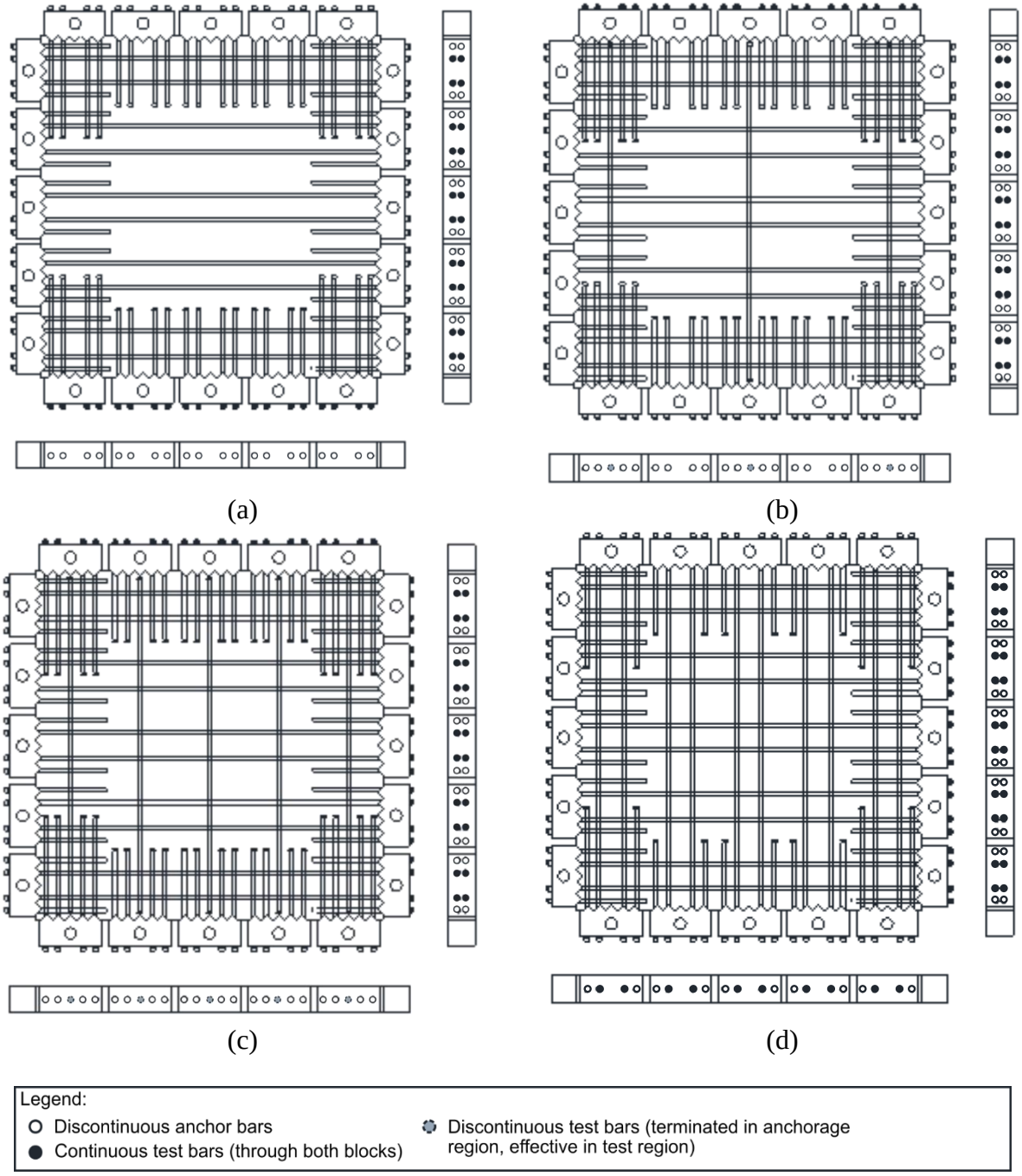

Figure 3-1: Panel Rebar Layouts

In the transverse direction, the spacing of the continuous reinforcement varied between panels, ordered from (a) to (d) from the least amount of transverse reinforcement (0%) to the greatest (1.14%). The discontinuous boundary zone reinforcement around the edge of the panels, which is required to grip the panel with the Panel Element Tester and force failure into the central test region, was also the identical between the specimens.

3.3 Panel Element Construction

The construction sequence for the panels included several steps, which are summarized here and described in more detail the subsequent paragraphs.

- The casting table was prepared and the anchor blocks, which were used to connect the panel specimens to the Panel Element Tester were installed (see Figure 3-2).
- Threaded rebar was slid through the anchor blocks, tied together, and fastened to the anchor blocks (see Figure 3-3).
- Concrete was mixed and placed into the steel panel element form around the reinforcement, consolidated primarily through external vibration of the casting table.
- The specimens were finished and wet cured for a minimum of 7 days before being stored in the lab for testing (see Figure 3-4).

Figure 3-2 shows the casting table before and after the blocks were attached. The shear keys and casting table were designed to ensure proper dimensions for conformity with the tester. Each of the blocks were bolted to the casting table with each numbered key going in the same position around the table each time. The threaded reinforcement was then installed based on the specified layout in the testing matrix.

Figure 3-2: Casting Table with and without Shear Keys

Figure 3-3 shows a representative panel specimen ready for casting. The discontinuous reinforcement in the transverse direction was headed using a standard 3/8-inch UNC hex nut to ensure proper anchorage which was found to be an issue in previous projects. On the end of the bars protruding through the steel anchor blocks, the bars were attached the blocks using an assembly which consists of one washer, one 3/8-inch UNC hex nut, and one 3/8-inch UNC jam nut. Once all of the reinforcement was placed, tie wire was used to connect the bars to prevent movement during casting.

Prior to placing the concrete, the gaps between the anchor blocks and around the reinforcement were filled with plasticine clay and the bottoms of the form were oiled. The plasticine clay was used to prevent concrete from leaking into and around the anchor blocks, which would hinder block removal and use on future casts. The oil on the top surface of the casting table eased panel removal. Special attention was made to avoid getting oil on the reinforcement as that would bond with the concrete.

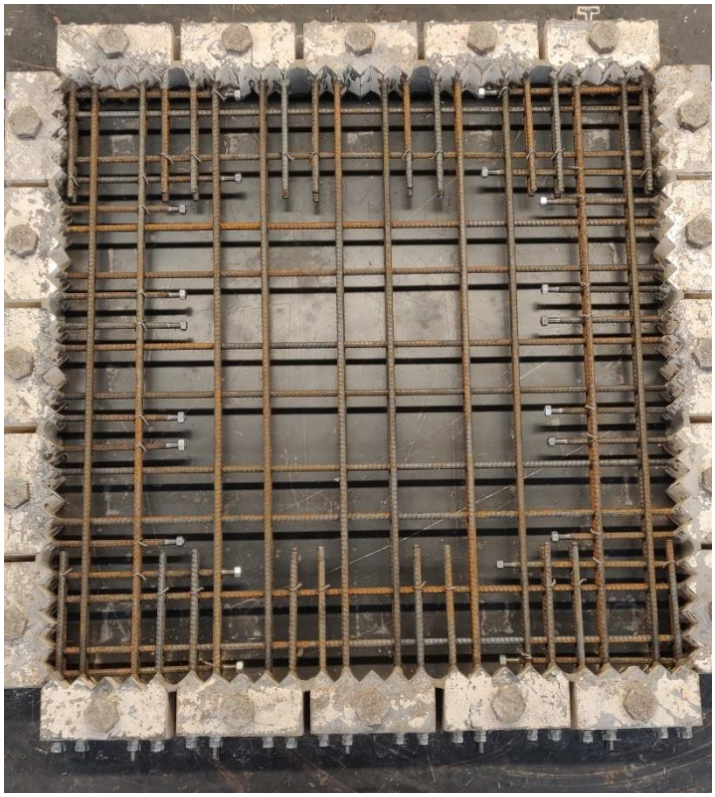

Figure 3-3: Panel Form Ready for Cast

Figure 3-4 shows a panel element specimen curing in the laboratory. The moisture contents of the coarse and fine aggregates were found in accordance with ASTM C566 the day before casting. Moisture corrections were then applied to the mixture design in Table 3-2 and the mixture constituents (water, cement, fine aggregate, and coarse aggregate) were weighed out in and stored in sealed 5-gal buckets until casting. The concrete was mixed in accordance with ASTM C172 with fibers being added at the end of the mixing procedure. The panel form and companion specimens were then filled and externally vibrated in two lifts. The first lift filled the panel to roughly the level of the first layer of reinforcement, and the second lift filled the remainder of the panel. This procedure attempted to minimize the number of fibers that draped over the reinforcement during concrete placement. After being finished, the specimens were covered with wet burlap and plastic and left to cure.

Figure 3-4: Panel Specimen Curing

After 7-day wet cure, the panels were removed from the casting table and stored, adjacent to the demolded companion specimens, at ambient conditions in the laboratory. After at least 28 days after casting, the panels were lifted into the Panel Element Tester and instrumented.

3.4 Project Schedule

Table 3-3 lists the panel specimens cast and test dates, in order of testing, as well as the time between the two dates. The test series took one year to complete, and the amount of time between casting and testing the panels varied between panels due to several factors. The second test was delayed due to a mechanical issue with the load maintainer; the third panel to be tested

was broken in the tester during installation; and after casting the sixth panel, consolidation issues were observed, and additional test mixes and placements were performed before additional panels were cast.

Table 3-3: Panel Series Cast and Test Days

Panel Specimen	Cast Date	Test Date	Days @ testing
PFRC-000-000	1/13/2022	3/8/2022	54
PFRC-000-058	3/11/2022	7/7/2022	118
PFRC-052-000	4/27/2022	N/A*	N/A*
PFRC-052-058	5/27/2022	8/5/2022	70
PFRC-026-000	6/27/2022	11/8/2022	134
PFRC-026-058	7/11/2022	9/15/2022	66
PFRC-052-000 (recast)	7/29/2022	8/26/2022	28
PFRC-000-029	8/25/2022	12/16/2022	113
PFRC-052-029	12/15/2022	2/8/2023	55
PFRC-026-029	1/11/2023	2/14/2023	34
PFRC-000-114	1/19/2023	2/22/2023	34
PFRC-052-114	1/26/2023	3/1/2023	34
PFRC-026-114	2/2/2023	3/8/2023	34

*PFRC-052-000 was damaged during installation and was recast

3.5 Material Properties

Table 3-4 summarizes the measured test day material properties of companion specimens that were cast at the same time as the panels. Concrete compressive strength was determined according to ASTM C39 (Figure 3-5a), elastic modulus was determined according to ASTM C469 (Figure 3-5b), and flexural strength and toughness values were determined according to ASTM C1609 (Figure 3-5c). For non-fiber-reinforced specimens the modulus of rupture was determined according to ASTM C78.

Table 3-4: Companion Specimen Properties on Test Day

Panel Specimen	Compressive Strength (psi)	Modulus of Elasticity (ksi)	Flexural Strength (psi)
PFRC-000-000	6454	4661	749
PFRC-000-029	5467	4083	846
PFRC-000-058	4520	4339	441
PFRC-000-114	6127	4682	767
PFRC-026-000	4735	3776	860
PFRC-026-029	5427	4402	635
PFRC-026-058	4767	3918	700
PFRC-026-114	6334	4604	560
PFRC-052-000	4066	7587	535
PFRC-052-029	6533	4309	630
PFRC-052-058	5149	4746	635
PFRC-052-114	5236	4140	500

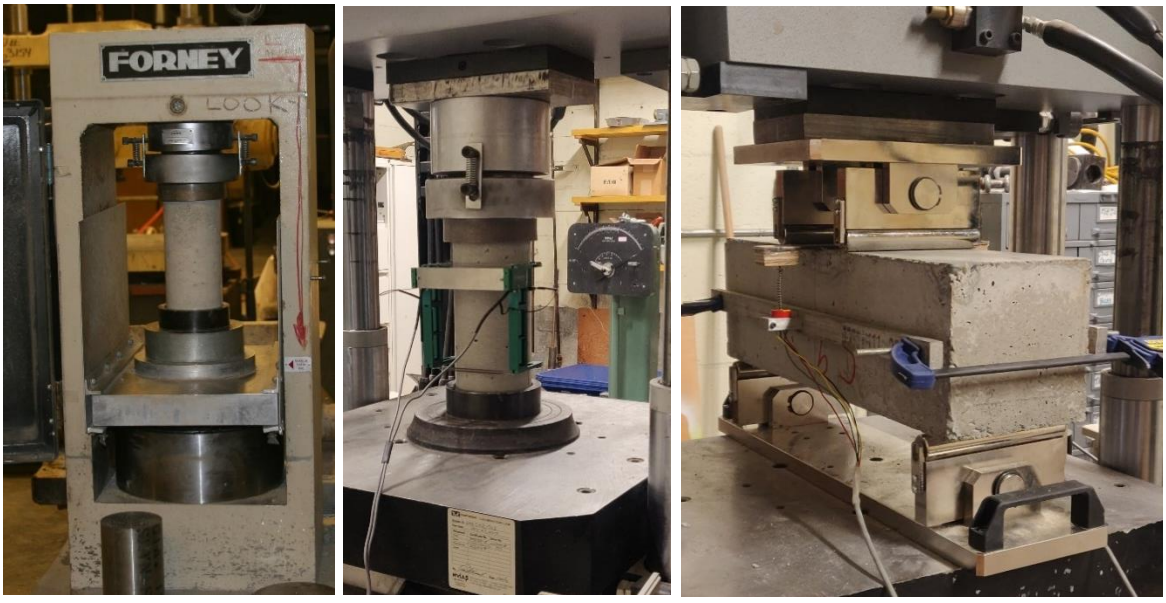

Figure 3-5: Material Testing (a) Compressive Strength (b) Compressive Modulus (c) Flexural Strength and Toughness

Companion specimens were stripped from their molds at the same time the panels were removed from the casting table and were kept under the same ambient conditions until they were tested. A sensor temperature and humidity sensor monitored laboratory conditions while the panels and

companion specimen cured following removal from the casting table. The average temperature of the lab during testing was 26.2 °C and tended to fluctuate approximately 5 °C between the summer and winter. The maximum temperature recorded during the test series was 32.4 °C and the low was 7.14 °C. The relative humidity varied similarly with an average of 36.2 %, a high of 73.4%, and a low of 14.9%.

3.3.1 Concrete Compressive Strength

Table 3-5 summarizes the cylinder compressive strengths at three ages: at panel removal, 28 days, and test day. It was measured when the panel was removed from the casting table, which varied between 3 and 19 days after casting; at 28-days; and on test day, which varied between 28 and 134 days. The target 28-day compressive strength for all the mixture designs was 6000 psi, and the average measured 28-day value was 5400 psi with a COV of 14.4%.

Table 3-5: Development of Cylinder Compressive Strengths

Panel Specimen	Removal (psi)	28 Day (psi)	Test Day (psi)
PFRC-000-000	4297	5769	6454
PFRC-000-029	4409	5841	5467
PFRC-000-058	3064	4520	4520
PFRC-000-114	3804	6016	6127
PFRC-026-000	3366	4568	4735
PFRC-026-029	3708	5284	5427
PFRC-026-058	2785	4799	4767
PFRC-026-114	3947	6390	6334
PFRC-052-000	4472	4337	4066
PFRC-052-029	5364	6207	6533
PFRC-052-058	3295	4942	5149
PFRC-052-114	3478	5475	5236

3.3.2 Reinforcement Properties

Figure 3-6 shows the axial stress versus strain graph for five A706 No. 3 deformed bar reinforcement samples. Strains were measured using an extensometer with a 2-inch gauge length. The average yield stress for the samples was 512 MPa with a standard deviation of 12 MPa, and the average ultimate stress for the samples was 698 MPa with a standard deviation of 3 MPa. The extensometer measuring strains was removed just prior to bar fracture, therefore the fracture

strain was not directly measured. However, the smallest last reliable strain reading prior to fracture was 0.18.

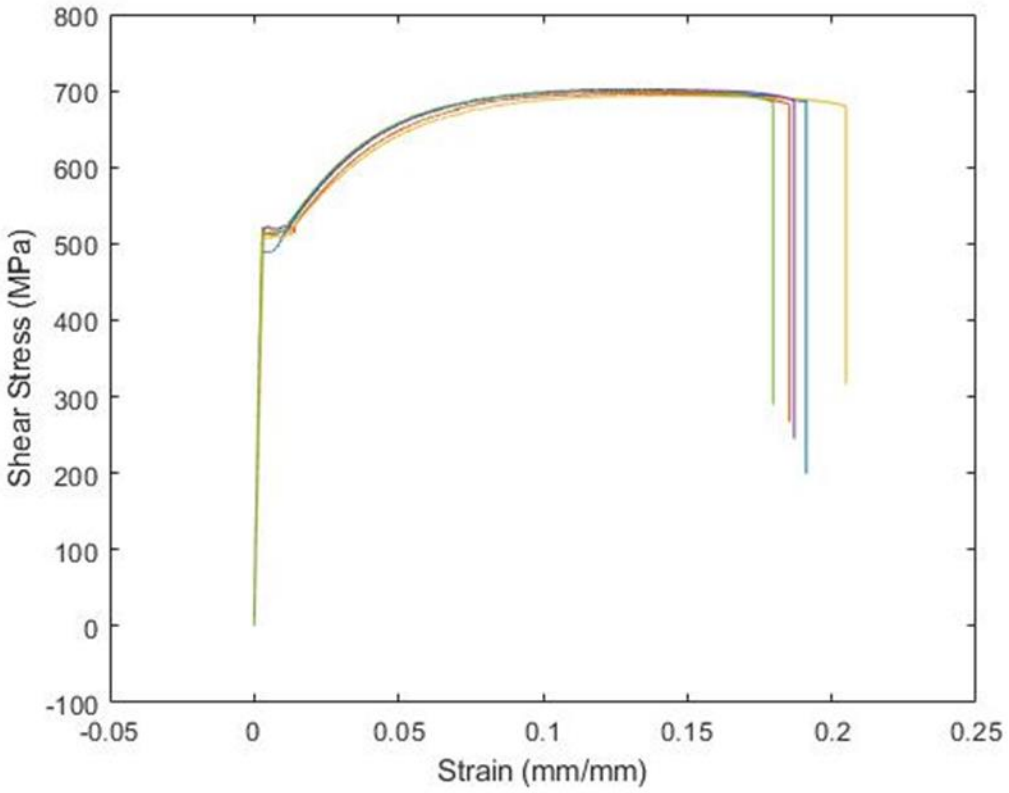

Figure 3-6: Steel Rebar Stress Versus Strain

3.3.3 Concrete Flexural Properties

Figure 3-7 shows typical flexural (tensile) stress versus midspan deflection behaviors for 6 in×6 in×21 in macro-synthetic fiber-reinforced concrete companion beam specimens. At first cracking (peak strength), the load capacity of the beams dropped rapidly, and the test machine struggled to control the descending branch of the response. The number of fibers bridging the initial crack determined the residual strength, as shown in the graph with the concrete containing a higher percent volume (0.52%) of fibers holds approximately twice the load as the lower fiber percent volume (0.26%).

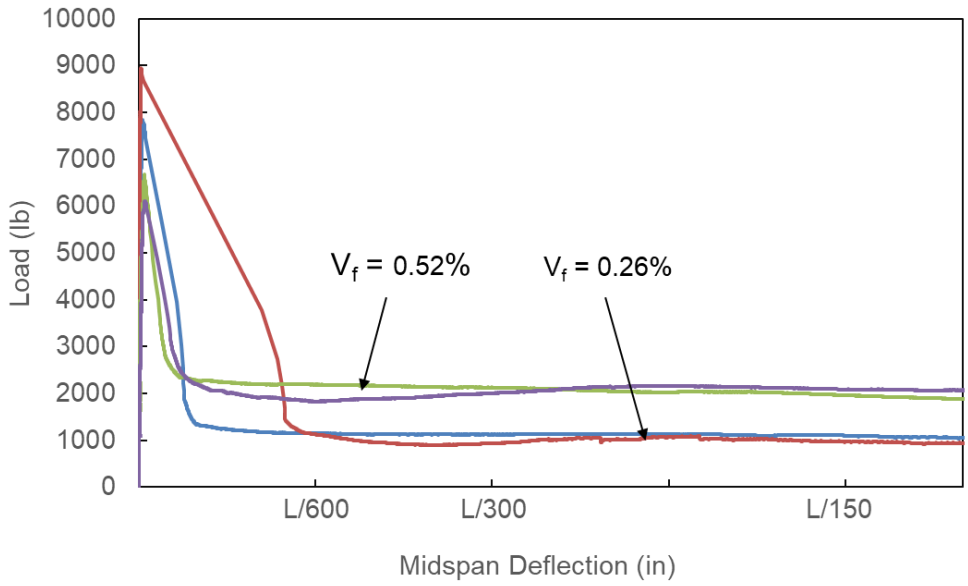

Figure 3-7: Fiber Beam Test Results

Table 3-6 summarizes the relevant values from ASTM C1609 (or from ASTM C78 for beams that did not contain fibers). Note that the toughness values are not reported due to the precision of the test setup, which did not capture enough of the response immediately after first cracking.

Table 3-6: Concrete Flexural Properties

Panel Specimen	4 in×4 in Beams			6 in×6 in Beams		
Panel Series	f1 (psi)	f150 (psi)	f600 (psi)	f1 (psi)	f150 (psi)	f600 (psi)
PFRC-000-000	750					
PFRC-000-029	846			789		
PFRC-000-058	441					
PFRC-000-114	767			650		
PFRC-026-000	715	70	75	860	105	110
PFRC-026-029	735	155	135	635	145	160
PFRC-026-058	780	65	100	700	95	95
PFRC-026-114	710	60	75	560	105	110
PFRC-052-000	590	145	150	535	175	170
PFRC-052-029	795	180	190	630	205	195
PFRC-052-058	565	125	160	635	115	145
PFRC-052-114	665	185	170	500	190	195

3.4 Panel Element Tests

Figure 3-8 and Figure 3-9 show the UW Panel Element Tester that was used to test the panel specimens. The frame connects to the panel element through 20 vertical and 20 horizontal links. Of these 40 links, 37 are connected to 60-kip hydraulic actuators (blue and green arrows in Figure 3-8) and 3 are fixed (yellow rectangles in Figure 3-8) that act as supports. At each vertical and horizontal link intersection the links are pin connected to the steel anchor blocks that are in turn attached to the reinforced bars embedded in each panel. The actuators are connected into control groups of five which allow for easier application of types of in-plane stresses. In these tests, groups 1 and 2 (shown in green arrows) are set to advance while groups 3 and 4 (shown in blue arrows) are set to retract. This applied pure shear loading (shown in red arrows) to the panel element. To avoid out-of-plane movement, restraints are added on the backside of the panel from the shear key to the rigid frame (see Figure 3-9).

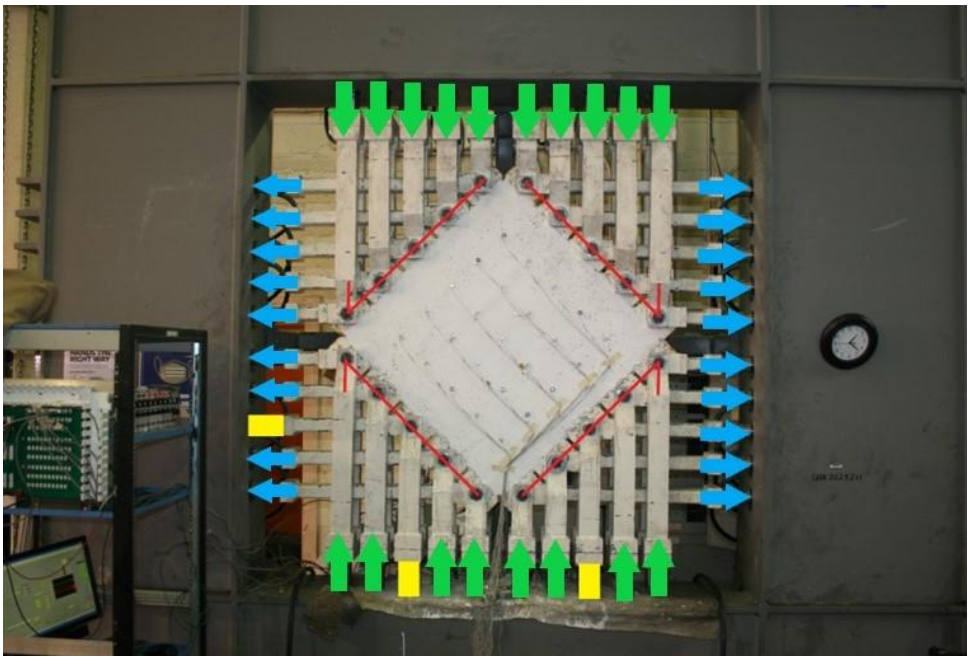

Figure 3-8: Front of Panel Element Tester

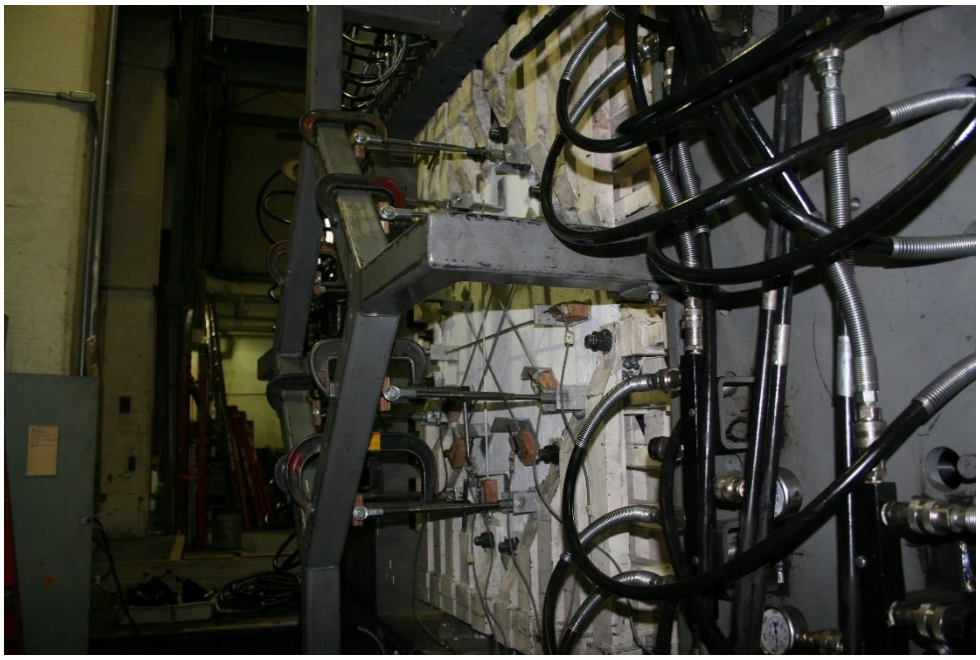

Figure 3-9: Back of Panel Element Tester

Figure 3-10 shows a test in progress. The panel tester is controlled through pressure supplied by a hydraulic system comprising a hydraulic power unit (red unit in Fig 3-10) and a hydraulic load maintainer (bottom right corner of Fig 3-10). Together, the hydraulic system is capable of providing up to 6 proportional channels of hydraulic pressure, up to 10,000 psi. For direct shear, the ratio between advancing and retracting actuators was 0.4915 to account for the different areas of the piston in the two directions. If a different ratio is used, then the panel would be subjected to tension or compression in addition to the desired shear loads.

Figure 3-10: Panel Element Test

3.5 Instrumentation

Each panel specimen was instrumented with a number of sensors to monitor stresses and deformations during loading. Stresses were determined by converting pressures in the actuators to stresses in the panels. Two pressure transducers were attached to each of the outputs of the load maintainer. These sensors were also used to verify that the proper pressure ratio was maintained between advancing and retracting cylinders. Additional pressure gauges were also connected to each control group to check that the pressures were similar between the groups.

The deformations of the panels specimens were determined using two different instrument systems, connected to independent data acquisition systems (DAQ). This provided redundancy and assisted in syncing the data from the two systems.

Figure 3-11 shows the conventional instrumentation system applied to the back (finished surface) of the panel specimen. The first system utilized conventional contact measurements, which consists of linear potentiometers. Each potentiometer was mounted on brackets connected to

aluminum rods which spanned the test region length. A total of six were used with two for each of the principal directions and one on each of the diagonals.

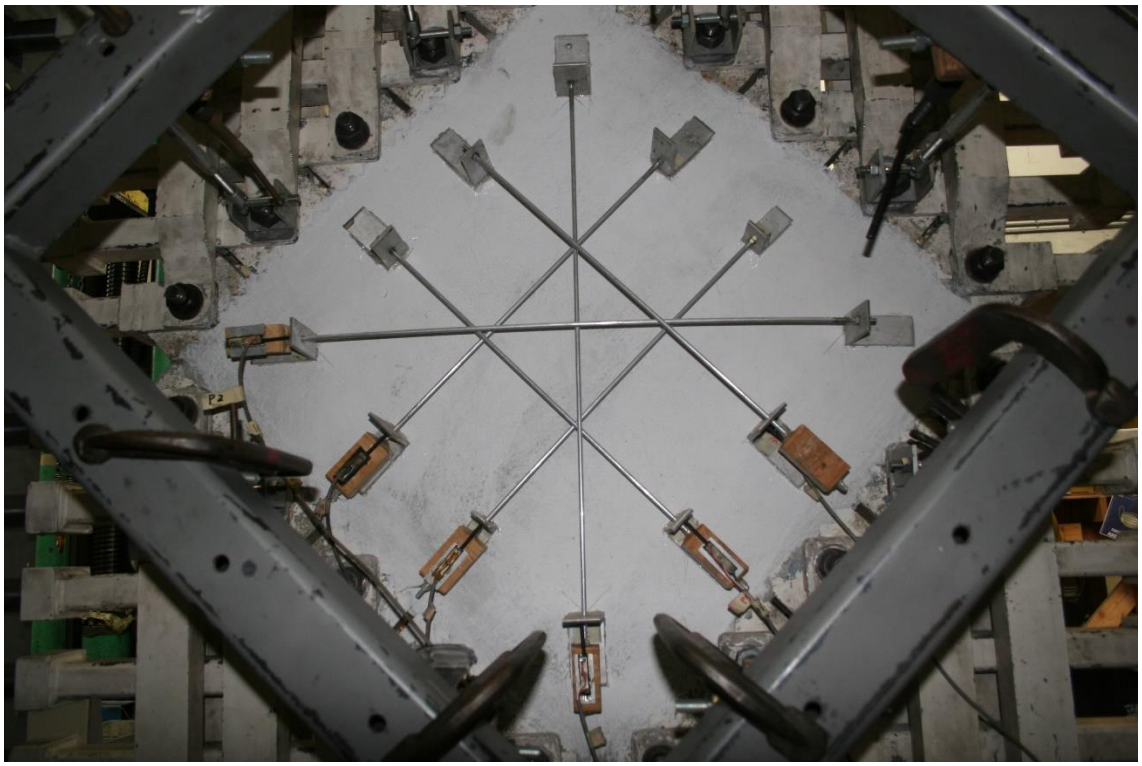

Figure 3-11: Contact Displacement Instrumentation

Figure 3-12 and Figure 3-13 show the non-contact instrumentation that was used on the front (bottom casting surface) of the panel specimens. The location of infrared LED targets adhered to the surface of the panel were resolved in three-dimensional space using an OptoTrak camera and corresponding software. The LED targets were placed in a 5x5 grid spaced evenly across the 540mm x 540mm test region. The OptoTrak camera was set up directly in front of the panel with good line of sight on all the targets. The output from the system was the x, y, and z coordinates of the targets in the camera's coordinate system, which was collected at 10 Hz to match the contact readings.

Figure 3-12: OptoTrak Camera Setup

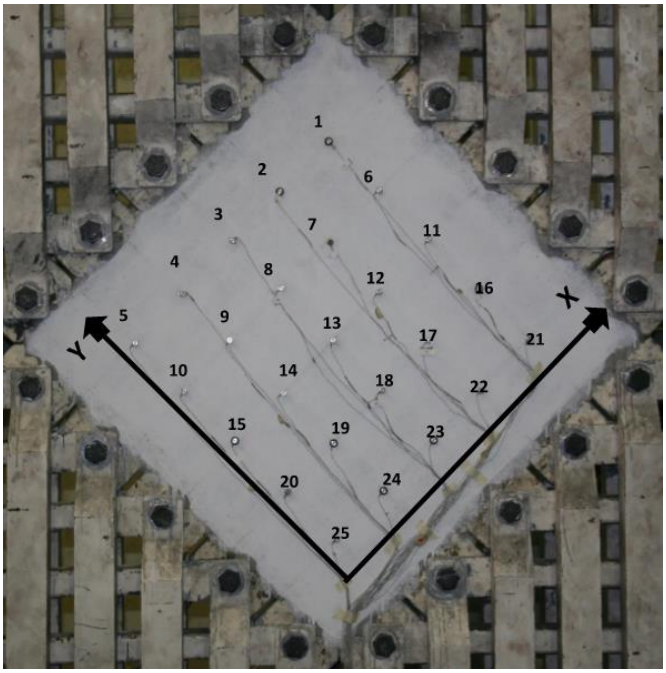

Figure 3-13: LED Target Layout

3.6 Test Procedure

Figure 3-14 below shows the pressure versus time for panel specimen PFRC-026-029. Pressures were applied to the panel slowly, increasing load on the panel until first cracking was achieved. At this point the load was then reduced by roughly ten percent of the cracking load to limit additional deformation while visible cracks were marked, measured, and photographed. Photos of both the front and back of the panel were also taken. After first cracking, loads were slowly increased in stages until failure with the second pause for crack mapping occurring at 1500 psi output pressure (at a shear stress of 313 psi) and all subsequent occurring at 500 psi intervals (corresponding to a shear stress increment of 104 psi). Each stage followed the same process of marking, measuring, and photographing. This procedure was repeated for each panel.

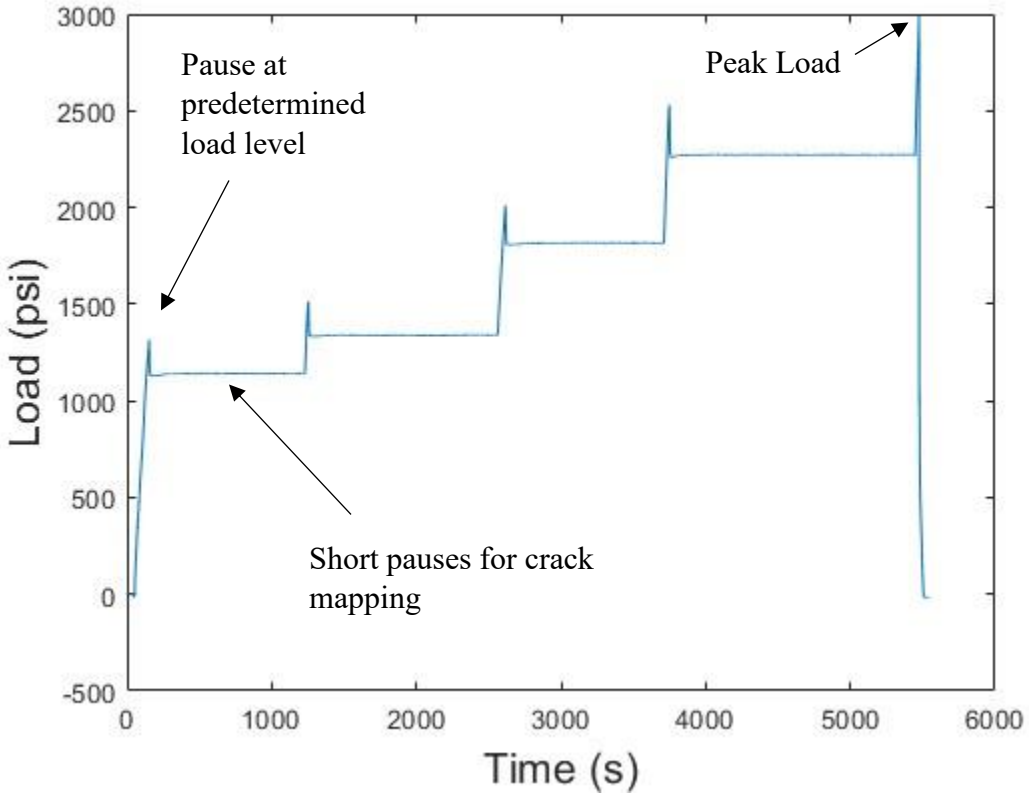

Figure 3-14: Test Procedure

Chapter 4: Experimental Results

4.1 Introduction

This chapter presents the measurements taken during the panel tests and the physical quantities (i.e. shear stress and strain) that were derived from the measurements. This includes shear stress-strain behavior, principal stress and strain in concrete and crack widths. Each section will describe the equations and steps used in the calculations. Results from PFRC-026-029 are presented be at the end of each section to show the behavior seen in a typical panel test. Note that the results from all the panels can be found in Appendix A.

4.2 Shear Stress-Strain Behavior

The shear stress, v, was computed directly from the recorded output pressures from the load maintainer using Equation 4.1. The pressure in either the advancing or retracting actuators, p_{act}, is multiplied by the cross-sectional area of the hydraulic cylinders, A_{cyl}, which is different for the two directions in the dual acting cylinders. The total shear force acting on the panel is then found by the vector sum of the actuator forces on one edge of the panel, $\sqrt{2}N_{\text{blocks}}$, where N_{blocks} = 5 for the UW Panel Element Tester. The shear force is then divided by the cross-sectional area of the panel, A_{f} = 62,300 mm^2 (890mm × 70 mm) to obtain shear stress.

$$v = \frac{\sqrt{2}N_{\text{blocks}}p_{\text{act}}A_{\text{cyl}}}{A_{\text{f}}} \tag{4.1}$$

Average shear strains in the test region were computed using two separate sets of instruments: from the displacements recorded by the crisscrossing linear potentiometers affixed to the back of the panel (see Figure 3-11) and through the relative motion of the non-contact instrumentation targets affixed to the front of the panel (see Figure 3-13).

The linear, engineering strains of the panel in the test region (ε_x , ε_y, and ε_{45}) were computed by dividing the potentiometer readings by the dimensions of the test region (540 mm for the x- and y-directions and 764 mm for the diagonal measurements). Six measurements were taken in all, 2 in each direction, so some redundancy existed between the measurements. The average of the two measurements in the x- and y-directions were used along with one of the diagonal measurements (the average was not used here, since the measurements differ in sign). The linear

strains (ε_x , ε_y, and ε_{45}) were converted to shear strain, γ, using the strain transformation equation shown in Equation 4.2.

$$\gamma = 2\varepsilon_{45} - \varepsilon_x - \varepsilon_y \tag{4.2}$$

The OptoTrak non-contact instrumentation system outputs the target locations in a 3D space. The coordinate system is local to the camera by default. Figure 4-1 shows the location of the targets in the camera coordinate system for a typical panel specimen.

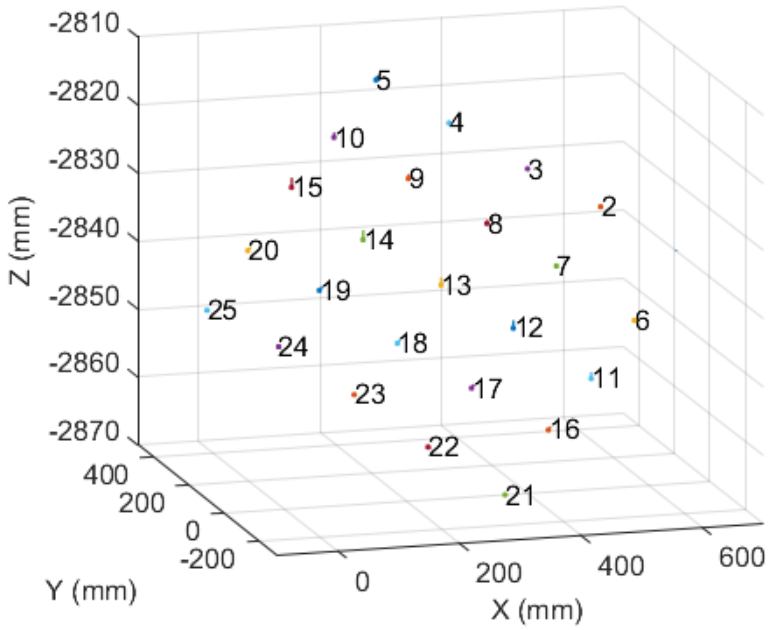

Figure 4-1: LED Targets in 3D Space

To compute in-plane deformations and strains, the target locations were first converted into a 2D panel coordinate system. Point 25 was chosen as the origin (see Figure 3-13 for the location of the targets). The x-axis was defined from the origin to point 21. A cross product was then used to find the y-axis, which was nearly identical to the direction from the origin to point 5. Another cross product was used to find the z-direction, which was then perpendicular to the panel's surface. With the panel coordinate system defined, the locations of the targets in the camera coordinate system were transformed and the z-coordinates were discarded, since motion in the z-direction (out-of-plane) was small.

The average strains in the test region were calculated using the four corner points (25, 21, 5, and 1) by tracking the distance between the four points throughout testing. With the initial distance between points and change in this distance known, the x- and y-direction strains and the strains at 45 ° and 135 ° were calculated. The average shear strain in the test region was then computed using Equation 4.2.

Figure 4-2 compares the computed shear strain values for the two instrumentation systems during a typical panel test. In general, the two sets of instruments measure similar values, although the conventional instrumentation tended to give lower readings at lower shear strains (i.e., less than 5×10^{-3}) and higher readings at higher strains (i.e., greater than 10×10^{-3}). Given the anticipated uncertainty of the conventional instruments at these low shear strains, the non-contact instrumentation values were used for the remainder of the data analysis.

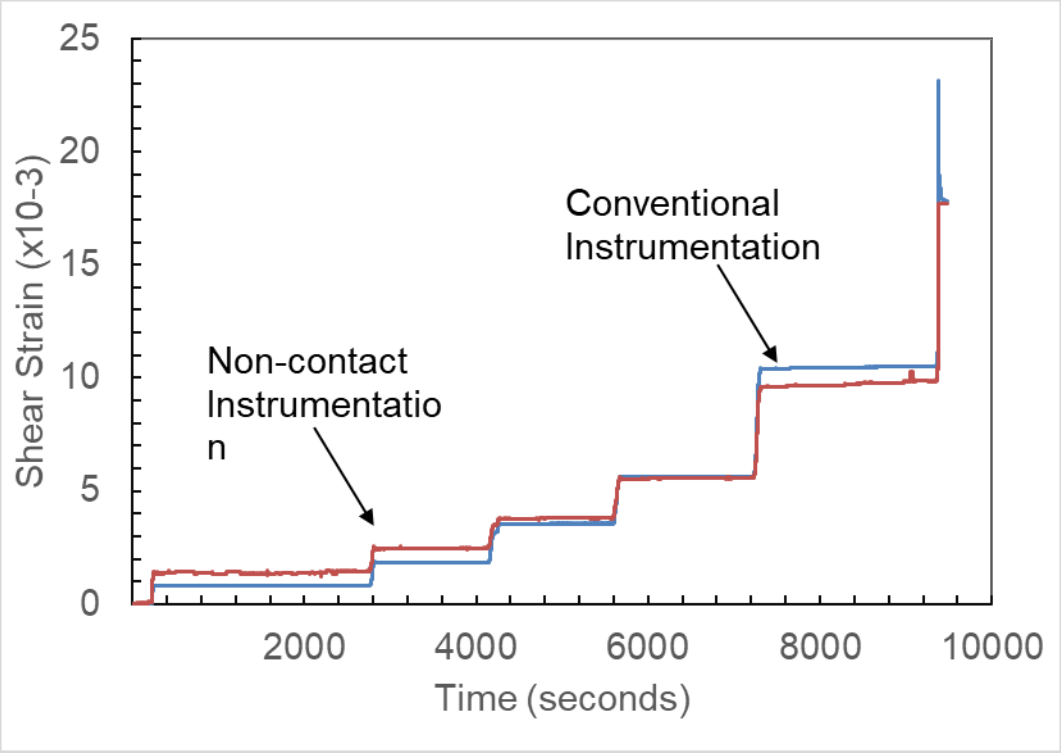

Figure 4-2: Comparison of Computed Shear Strain Values from Contact and Non-Contact Instrumentation Systems

Figure 4-3 shows the shear stress-shear strain backbone behavior for of a typical panel specimen with transverse deformed bar reinforcement (PFRC-26-029). Note that the diamonds indicate points at first cracking, each load stage, and failure. Backbone curves were developed for each panel from the computed shear stress and shear strain data by extracting the point at first cracking, the maximum stress reached in each load increment, and the failure point. Additional points were selected at the midpoint of each load increment if significant curvature was observed between beginning and end points.

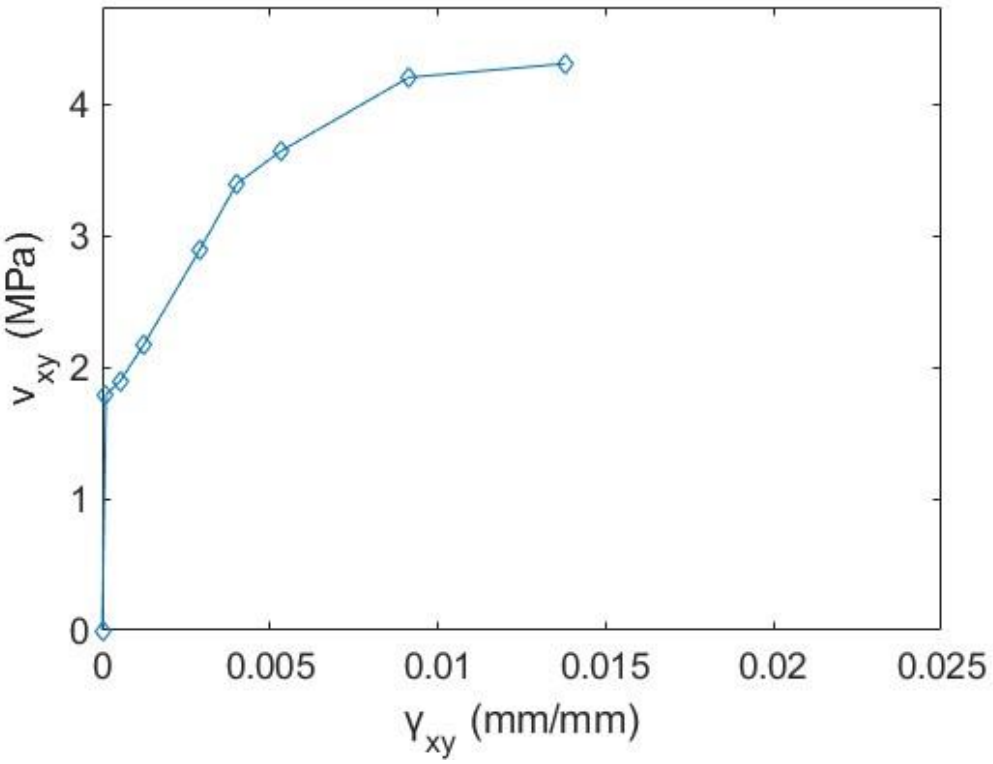

Figure 4-3: Shear Stress-Strain Behavior of PFRC-026-029

Initially, the panel was uncracked, and the shear stress-shear strain behavior was linear (with a modulus of roughly 15.7 GPa). After first cracking occurred, at a shear stress of 1.80 MPa for this panel, the response progressively softened until the panel failed in shear, at a shear stress of 4.31 MPa and a shear strain of 0.0138.

4.3 Principal Stresses and Strains in the Concrete

From equilibrium in an arbitrary i-direction, the relationship between the normal stress in the steel, f_{si}, the normal stress in the concrete, f_{ci}, and the normal applied stress, f_i, is given by Equation 4.3:

$$f_i = f_{ci} + \rho_{si} f_{si} \tag{4.3}$$

where ρ_{si} is the reinforcement ratio in the i-direction. Since the tested panels were subjected to pure shear, the applied normal stress in the x- and y-directions were zero, and the stress in the concrete and steel can be related using Equation 4.4,

$$f_{ci} = -\rho_{si} f_{si} \tag{4.4}$$

To compute the stress in the concrete, the stress in the reinforcement was determined using the elastic modulus of the steel, E_s, and the measured strain in the i -direction, ϵ_i, using equation 4.5, which was limited to the yield stress of the steel, f_{sy}.

$$f_{si} = \epsilon_i E_s \leq f_{sy} \tag{4.5}$$

The shear stress in the concrete was assumed to be equal to the applied shear stress, v_{xy}. From these relationships, the principal stresses in the concrete, $f_{c1,2}$, can be computed using the stress transformation equation given by Equation 4.6.

$$f_{c1,2} = \frac{f_{cx}+f_{cy}}{2} \pm \sqrt{\left(\frac{f_{cx}-f_{cy}}{2}\right)^2 + (v_{xy})^2} \tag{4.6}$$

where the calculated concrete stresses in the x- and y-directions are given by f_{cx} and f_{cy}, respectively, and the applied shear stress is given by v_{xy}. The principal strain orientation, θ_ε, and magnitude, $\varepsilon_{1,2}$, can also be calculated for the panel, in a similar fashion, using Equations 4.7 and 4.8

$$\varepsilon_{1,2} = \frac{\varepsilon_x+\varepsilon_y}{2} \pm \sqrt{\left(\frac{\varepsilon_x-\varepsilon_y}{2}\right)^2 + (\frac{\gamma_{xy}}{2})^2} \tag{4.7}$$

$$\theta_\varepsilon = \frac{1}{2}\tan^{-1}(\frac{\gamma_{xy}}{\varepsilon_x-\varepsilon_y}) \tag{4.8}$$

Where ε_x and ε_y are the average strains in the test region in the x- and y-directions, and γ_{xy} is the computed average shear strain in the test region.

Figure 4-4 shows the calculated principal tension stress (f_{c1}) for a typical panel specimen (PFRC-026-029) versus the principal tension strain (ε_1). Th concrete tensile behavior used in the Modified Compression Field Theory (Vecchio, 1986) is also shown for reference.

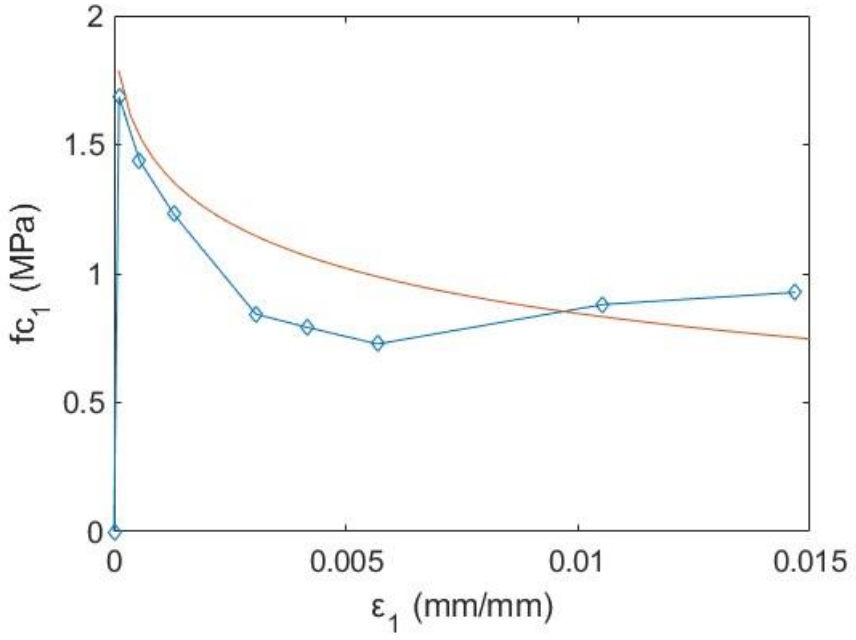

Figure 4-4: Principal Tensile Response of PFRC-026-029

The principal tension response was initially linear, reached a peak value corresponding to first cracking, and then gradually softened to a value roughly half that of the peak. The panels containing macro-synthetic fibers had higher residual tension strengths when compared to the panels that did not contain fibers.

Figure 4-5 shows the principal compression stress (f_{c2}) for a typical panel specimen (PFRC-026-029) versus the principal compression strain (ε_2). The concrete compression behavior used in the Modified Compression Field Theory (Vecchio and Collins, 1986) is also shown for reference.

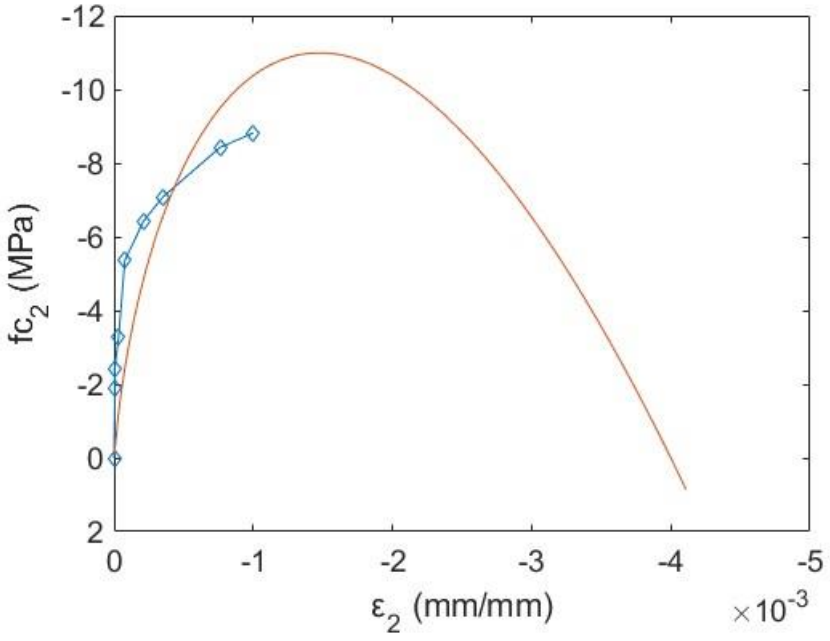

Figure 4-5: Principal Compressive Response of PFRC-026-029

The principal compressive stress-strain response followed a roughly parabolic curve, and the panels failed in shear prior to the principal compressive stress reaching the peak value predicted by the MCFT equations (Vecchio and Collins, 1986). This supports the assertion that the panels did not fail by concrete crushing along the compression diagonal but rather through shear and yielding of the reinforcement.

4.4 Crack Spacing and Width

Figure 4-6 shows a photo of specimen PFRC-026-029 at a shear stress level of $4.24\sqrt{f'_c}$ (visible cracks were identified with black marker during testing) and the corresponding digital crack map developed from visual crack comparator measurements. The box on the digital crack map specifies the test region. Loading was paused at regular intervals during testing, at first cracking and then at specified load levels, to document crack propagation, spacing, and crack widths.

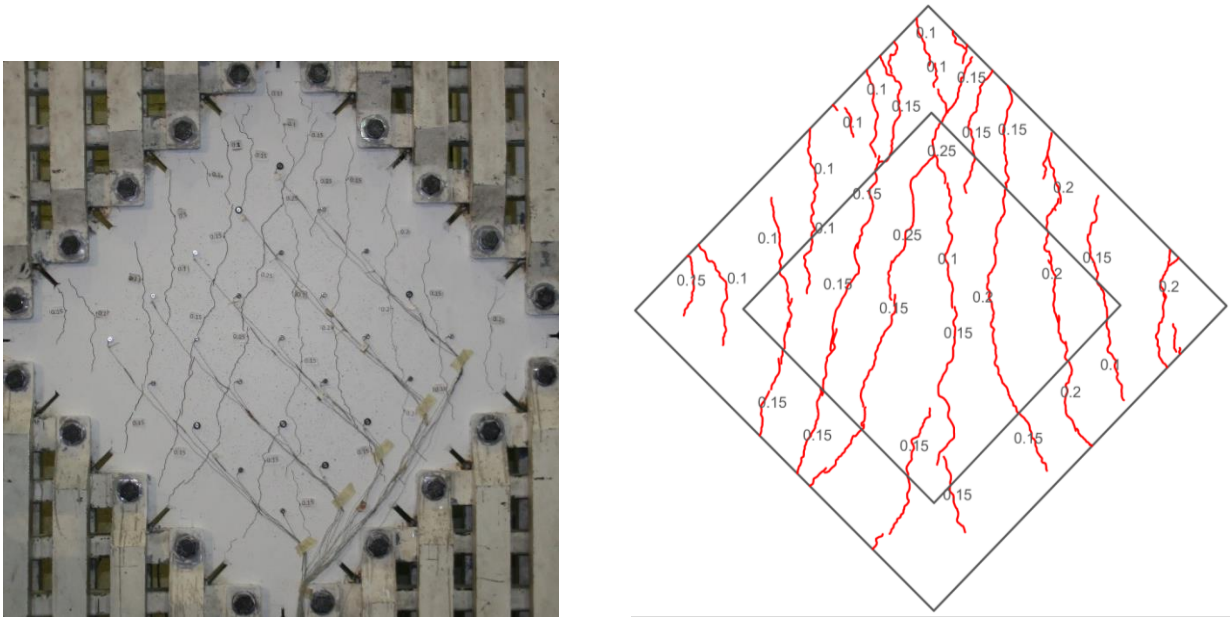

Figure 4-6: PFRC-026-114 Crack Map at Second Marking Level

Figure 4-7 shows the visually identified cracks in the test region of PFRC-026-029 at a shear stress level of $4.24\sqrt{f'_c}$. To determine average crack width and crack spacing, the cracks that crossed a horizontal line through the diagonals were counted (so for this case it would be seven cracks as noted in the figure).

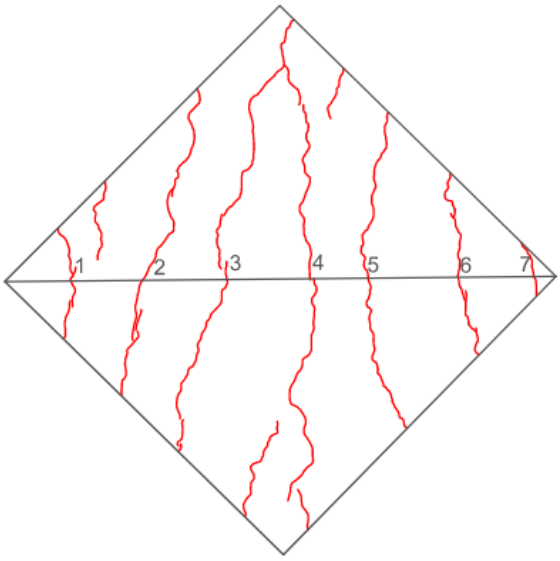

Figure 4-7: Number of Cracks Across Horizontal Line in Test Region

Figure 4-8 shows crack spacing in the test region versus average shear stress for the PFRC-026-029 specimen. Crack spacing, s_m, was determined by dividing the diagonal length of the test region, 764 mm, by the number of cracks crossing the horizontal diagonal line in Figure 4-9. As stress increased, crack spacing decreased, indicating the formation of more cracks across the test region. Crack spacing continued to decrease, reaching a value of 69 mm at failure. Panels with higher transverse reinforcement ratios (greater than 0.58 %) behaved similarly, except they exhibited a plateau where crack spacing stabilized (see Appendix A).

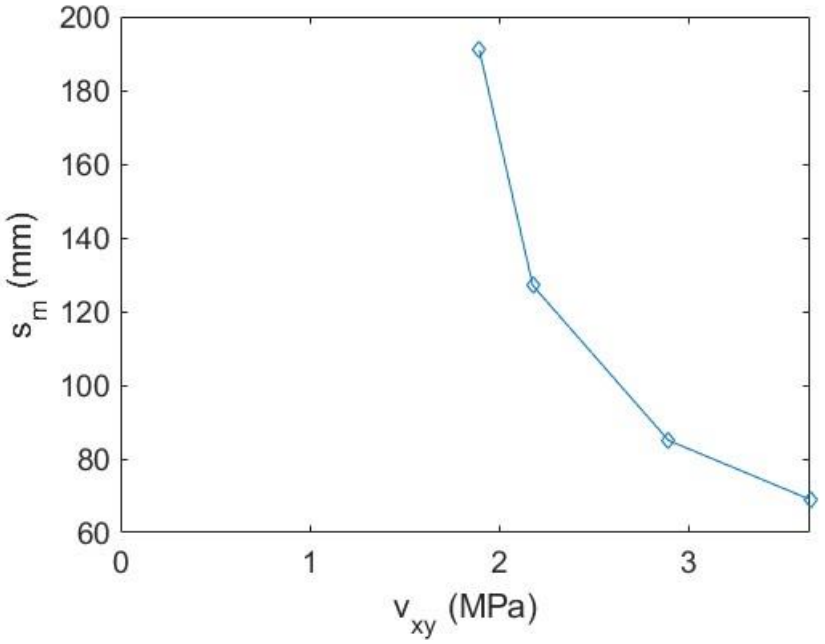

Figure 4-8: Crack Spacing Versus Shear Stress for PFRC-026-029

Figure 4-9 shows the measured widths of the cracks in the test region of PFRC-026-029 at a shear stress of $4.24\sqrt{f'_c}$. Average crack widths in the panel, w_c, were computed by averaging the widths of the cracks crossing the horizontal diagonal line.

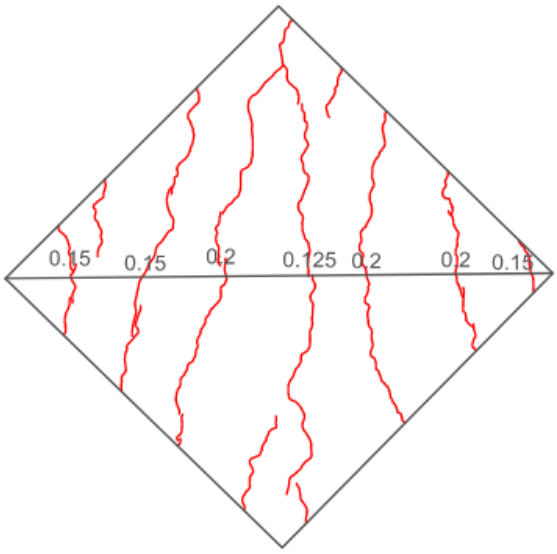

Figure 4-9: Average Crack Width of Each Single Crack

Figure 4-10 shows the average crack width of PFRC-026-029 versus shear stress. The average crack width and shear stress increased roughly proportionally to one another. The increase in average crack width is mostly driven by widening of existing cracks, rather than the formation of additional cracks.

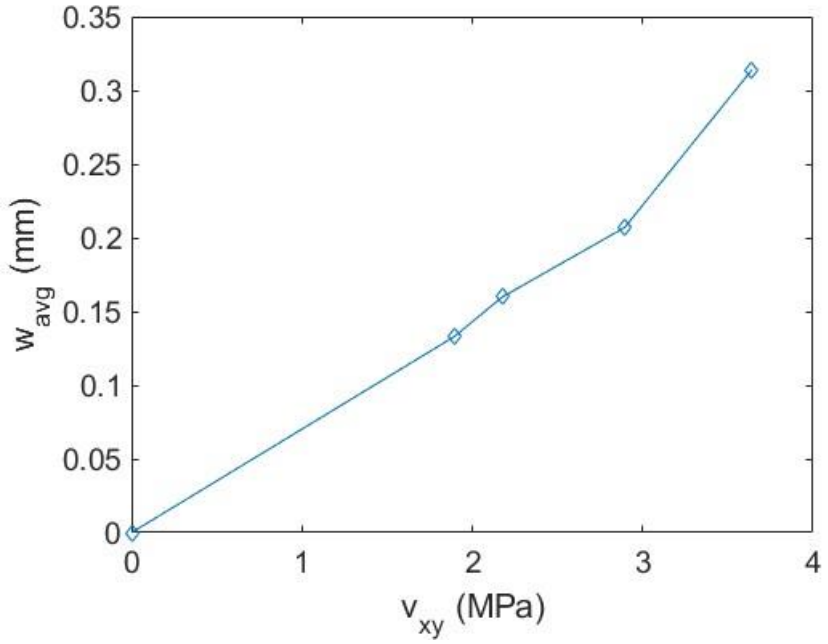

Figure 4-10: Average Crack Width Versus Shear Stress for PFRC-026-029

Chapter 5: Analysis and Comparison of Results

This chapter is organized into two separate sections. The first section (Section 5.1) outlines the key data derived from the panel tests. The panels are compared to each other, and trends are identified with respect to the main test parameters of interest, such as peak shear strength, shear strain at failure, and crack widths. These results are normalized with respect to the square root of the compressive strength found from the companion cylinder tests. The second section (Section 5.2) provides comparisons between the experimental shear strengths measured in this experimental program and the strength predictions obtained from a set of empirical equations and design codes, which are referenced in Chapter 2.

Table 5-1 summarizes key results from the test series including the cracking stress and strain and values of the shear stress, shear strain, concrete principal stresses, concrete principal strains, crack width, and crack spacing at the final load stage before failure for all twelve panels, determined following the process described in Chapter 4.

The average concrete compressive strength on test day was 37.5 MPa which was decently below the goal value of 41.4 MPa. Further, the standard deviation and coefficient of variation of this value was very high with values of 5.96 MPa and 14.4% respectively. It is also important to note that the ultimate shear strength is highly dependent on the compressive strength so normalization would be needed for proper comparisons. The final thing to note is that none of the panels failed in crushing along the principal compression direction (see fc2). This table corroborates the graph seen in Section 4.3 but for every panel series.

Table 5-1: Panel Element Test Properties

Specimen ID	f'_c (MPa)	ν_{cr} (MPa)	γ_{cr} (10^{-3})	ν_u (MPa)	γ_{xy} (10^{-3})	ε_x (10^{-3})	ε_y (10^{-3})	f_{c1} (MPa)	f_{c2} (MPa)	ε_1 (10^{-3})	ε_2 (10^{-3})	f_{sx} (MPa)	f_{sy} (MPa)	w_m (mm)	s_m (mm)
PFRC-000-000	44.5	1.98	0.10	2.12	0.71	0.11	0.42	1.884	-2.388	0.65	-0.13	22.13	87.79	-	-
PFRC-000-029	37.7	1.38	0.11	4.27	13.31	2.04	13.74	1.810	-10.076	16.75	-0.97	428.67	512.43	0.522	109
PFRC-000-058	31.2	1.52	0.10	5.41	12.21	2.76	9.72	2.565	-11.405	13.27	-0.79	512.43	512.43	0.500	69
PFRC-000-114	42.2	1.87	0.16	7.82	13.73	4.21	8.35	5.399	-11.327	13.45	-0.89	512.43	512.43	0.326	64
PFRC-026-000	32.6	1.16	0.15	1.39	1.69	0.81	0.33	0.446	-4.345	1.30	-0.16	171.00	68.63	-	-
PFRC-026-029	38.3	1.80	0.11	4.31	13.80	1.60	11.05	2.215	-8.383	14.68	-2.03	336.66	512.43	0.314	69
PFRC-026-058	34.4	1.54	0.44	4.24	5.49	1.44	4.45	2.720	-6.622	6.08	-0.18	303.43	512.43	0.250	69
PFRC-026-114	43.7	1.25	0.19	7.43	11.95	2.26	7.92	5.382	-10.269	11.71	-1.52	474.32	512.43	0.410	69
PFRC-052-000	29.4	1.41	0.28	1.50	3.59	0.07	0.18	1.340	-1.684	0.31	-0.06	15.08	37.11	-	-
PFRC-052-029	45.0	1.02	0.06	5.00	20.75	2.38	19.75	2.084	-11.988	24.60	-2.46	500.50	512.43	0.470	64
PFRC-052-058	35.5	1.26	0.08	4.94	8.09	2.02	7.04	2.636	-9.275	9.29	-0.23	423.50	512.43	0.297	69
PFRC-052-114	36.1	1.47	0.11	7.47	13.03	2.54	8.52	5.071	-10.999	12.70	-1.63	512.43	512.43	0.426	64

5.1 Shear Stress-Strain Behavior

Figure 5-1 shows the normalized shear stress versus shear strain graph for all the panels. To make an equivalent comparison, the applied shear stress for each panel was normalized by the square root of the average compressive strength of the concrete cylinders tested on the same day as the panel. In general, the panels all had cracking stresses around $2.91\sqrt{f'_c}$ (standard deviation of $0.52\sqrt{f'_c}$ with a COV of 18%) and panels with higher transverse reinforcement ratios exhibited greater shear strengths, as anticipated.

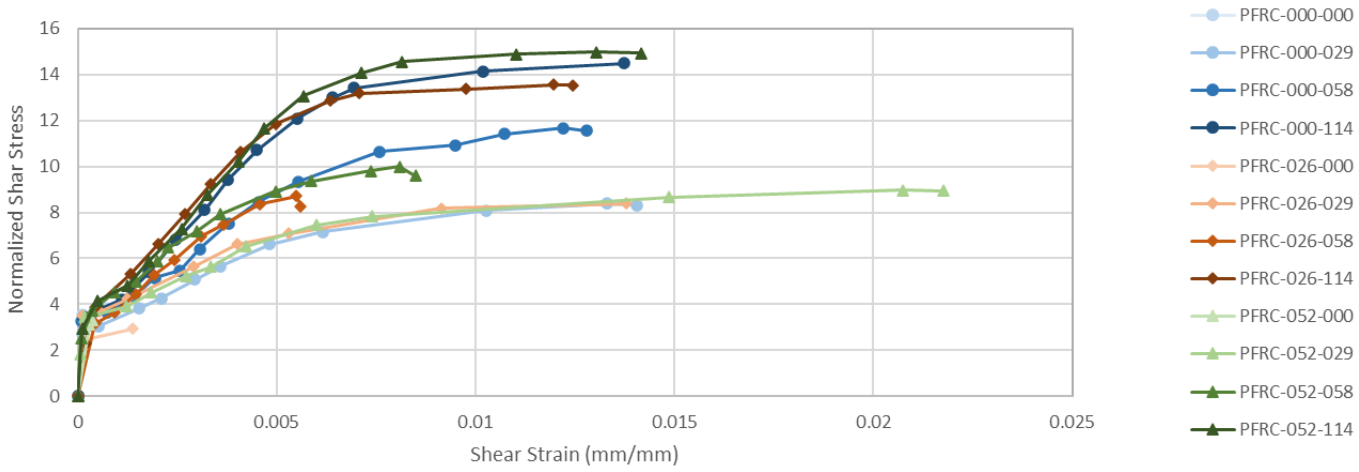

Figure 5-1: Normalized Shear Stress versus Shear Strain for All Panel Tests

In subsequent sections, key points on these graphs (e.g., peak shear stress) will be compared between the twelve panels to elucidate the influence of transverse reinforcement ratio or the fiber volume on the responses.

5.2 Shear Strength

Figure 5-2 shows that the shear strength of all twelve panels plotted against the transverse reinforcement ratio. Fiber volume is indicated in the figures by marker color and type. Also shown in the plot is the shear strength of the panels estimated using the ACI 318-19 one-way shear strength equations in Section 22.5 (ACI 2019), assuming a transverse yield stress of 74.3 ksi and a nominal 28-day concrete compressive strength of 5443 psi.

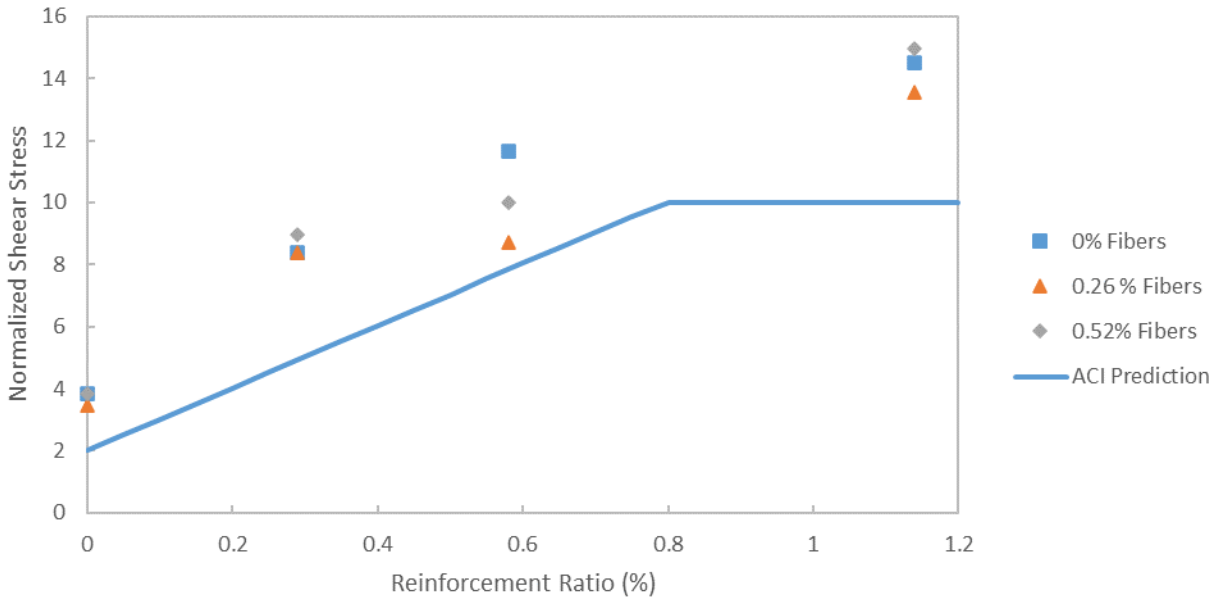

Figure 5-2: Reinforcement Ratio's Effect on Panel Shear Strength

The shear strength of the panels was positively correlated to the transverse reinforcement ratio, as expected. The increase in strength was consistent with ACI estimates for reinforced concrete elements with transverse reinforcement ratios in the range considered in this study, although the actual strength values were quite conservative, by a factor of roughly 2. The normalized shear strength at each reinforcement level shows small variation. The main exception to this was the panels at 0.58% transverse reinforcement which experienced consolidation issues which led to lower strengths.

Figure 5-3 shows the normalized shear strength of all twelve panels plotted against fiber volume fraction. Unlike transverse reinforcement ratio, there is no clear relationship that can be identified between fiber volume and shear strength. In fact, the shear strength appears to remain roughly constant for all fiber volumes, for given transverse reinforcement ratios. The one exception is the 0.58% reinforcement ratio panels containing fibers which experienced consolidations issues, thus exhibiting lower strength than their reference companion.

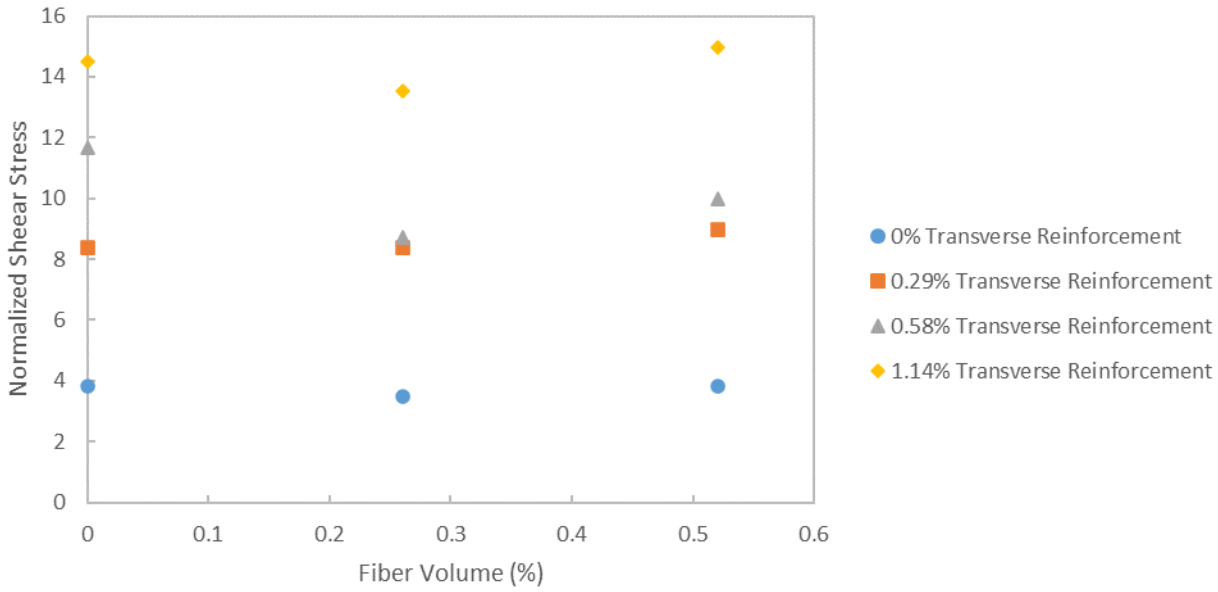

Figure 5-3: Fiber Volume's Effect on Panel Shear Strength

5.2 Shear Strain at Failure

Figure 5-4 shows the shear strain at failure for all twelve panels plotted against transverse reinforcement ratio. Fiber volume is indicated in the figures by marker color and type. The shear strain at failure increased transitioning from specimens with no shear reinforcement to specimens containing at least the minimum transverse reinforcement required by the ACI 318 code (i.e., comparing strain values at 0 and 0.29 transverse reinforcement ratios). However, as the reinforcement ratio was further increased, the shear strain at failure remained almost constant or decreased slightly for the transverse reinforcement ratios considered in this experimental program.

It should be noted that for the two fiber-reinforced specimens with 0.58% transverse reinforcement, namely PFRC-026-058 and PFRC-052-058, the relatively lower maximum shear strain values were attributed to the consolidation issues which occurred in the heavily reinforced edges of those panels.

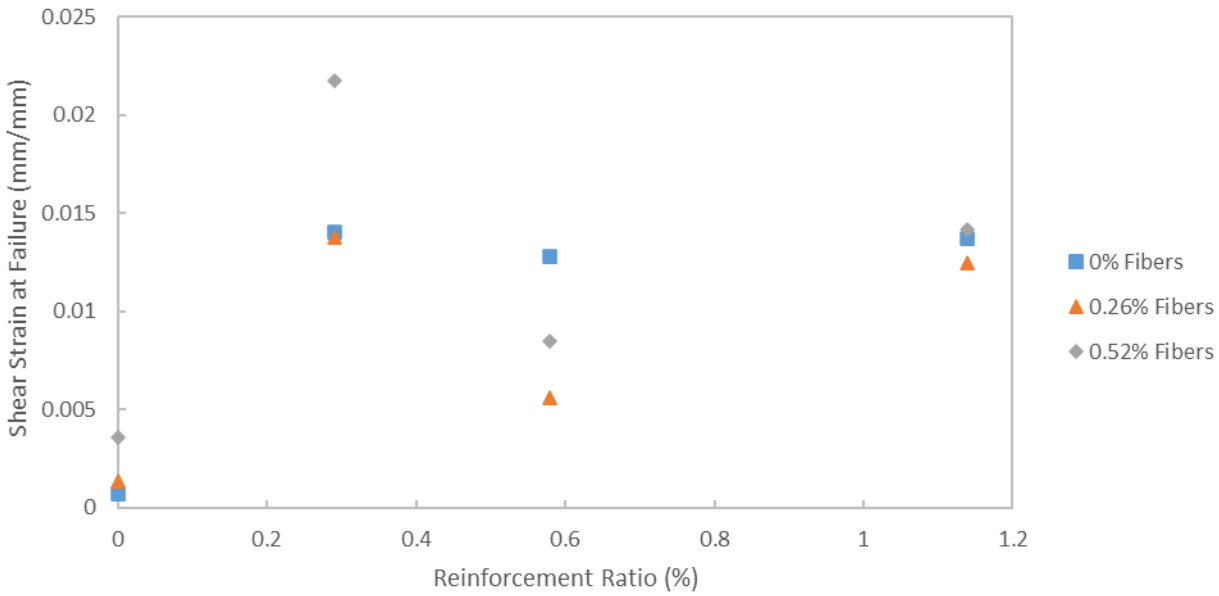

Figure 5-4: Reinforcement Ratio's Effect on Shear Strain at Failure

Figure 5-5 shows the shear strain at failure plotted against fiber volume fraction for the panels that contained transverse deformed bar reinforcement. In the plot, transverse reinforcement ratio is indicated by marker type and color. As before, two of the points in the 0.58% reinforcement series, PFRC-026-058 and PFRC-052-058, had significant consolidation issues during construction and were found to have lower-than-expected shear strengths and strains at failure.

The influence of fiber volume fraction on the shear strain at failure was found to depend on reinforcement ratio. Panels with 1.14% transverse reinforcement had consistent shear strains at failure despite the addition of fibers. However, at a transverse reinforcement ratio 0.29%, an increase in shear strain at failure was observed with the addition of macro-synthetic fibers, especially for the panel with 0.58% fibers.

Figure 5-6 shows the shear strain at failure plotted against fiber volume fraction for the panels that did not contain transverse deformed bar reinforcement (0% reinforcement series). Similar to the panels with 0.29% transverse reinforcement, the shear strain at failure increased with fiber volume ratio, roughly proportionally in this instance.

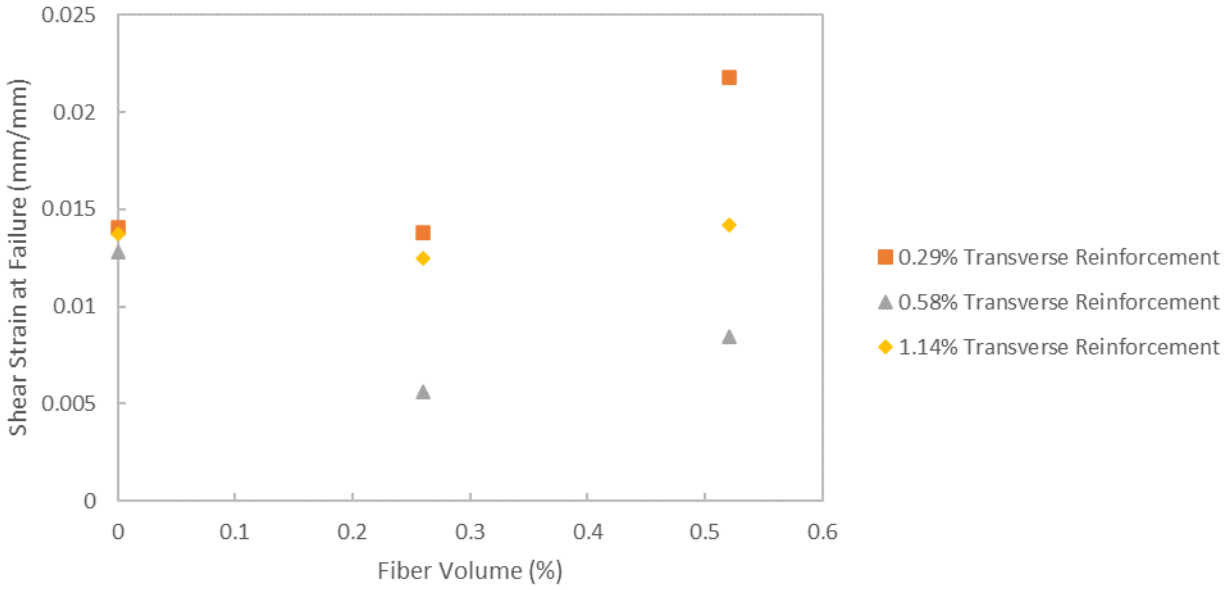

Figure 5-5: Fiber Volume Effect on Shear Strain at Failure for Panels Containing Transverse Reinforcement

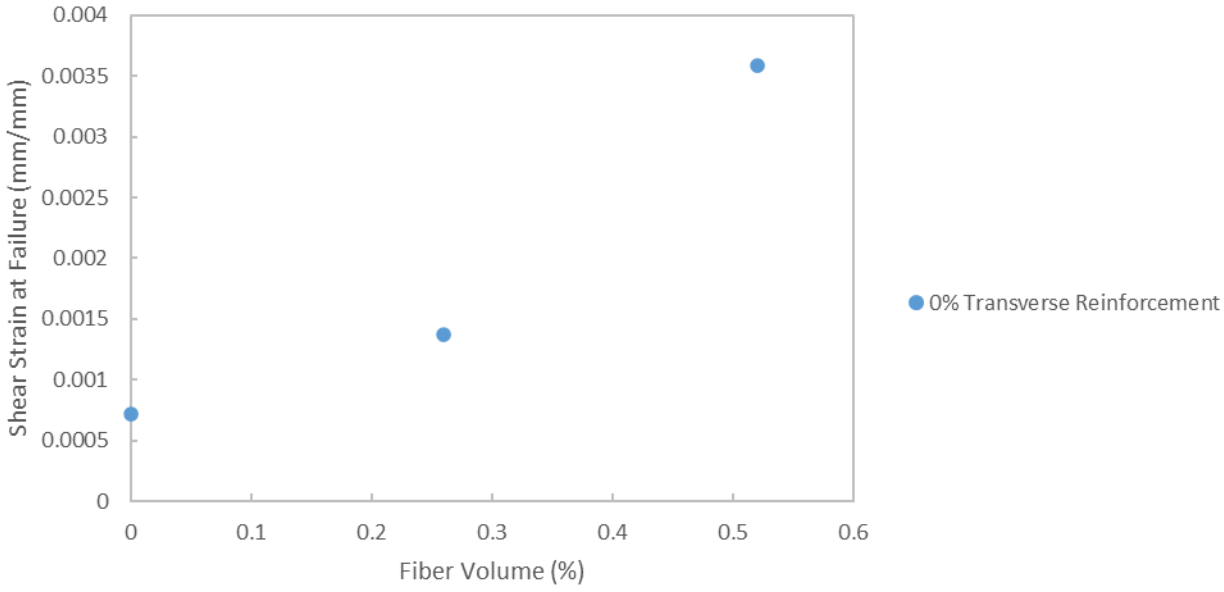

Figure 5-6: Fiber Volume Effect on Shear Strain at Failure for 0% Transverse Reinforcement

5.1.1 Average Crack Width

Figure 5-7 shows the average crack width in each panel at a normalized shear stress of $4\sqrt{f'c}$ versus the reinforcement ratio. The panels without transverse reinforcement did not reach this shear stress level and are, therefore, not shown in the plot. In general, the average crack width at a normalized shear stress of $4\sqrt{f'c}$ tended to decrease as the transverse reinforcement ratio increased, with a slope of roughly -0.03 mm/%.

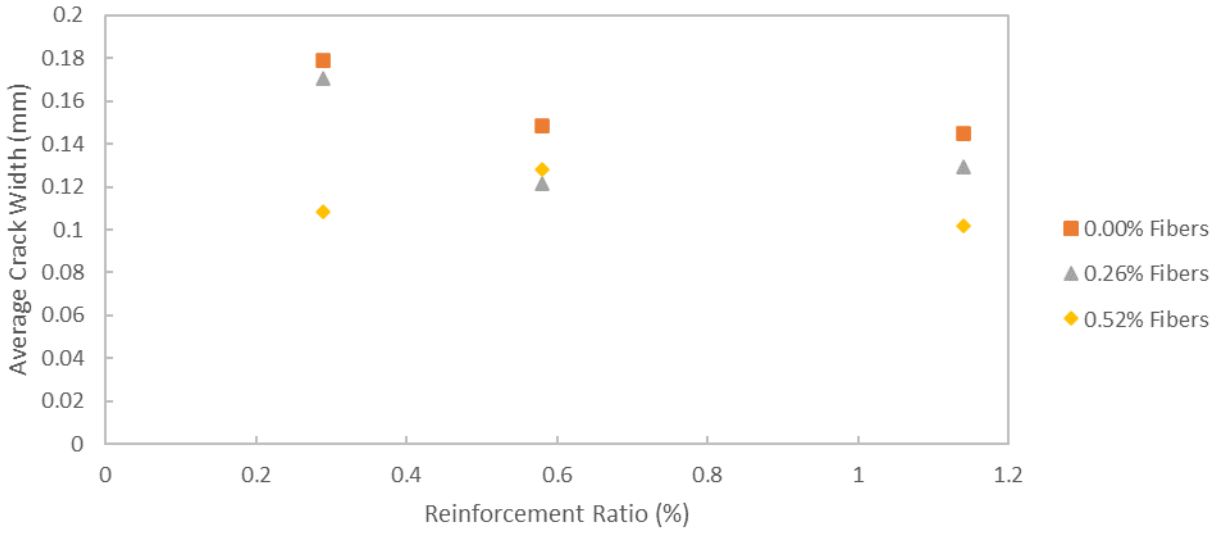

Figure 5-7: Reinforcement Ratio's Effect on Average Crack Width at $4\sqrt{f'c}$ Shear Stress

Figure 5-8 shows the average crack width versus fiber volume at a normalized shear stress of $4\sqrt{f'c}$. The panels without transverse reinforcement did not reach this shear stress level and are, therefore, not shown in the plot. In general, the average crack width at a normalized shear stress of $4\sqrt{f'c}$ tended to decrease as the fiber volume fraction increased, with a slope of roughly -0.05 mm/%.

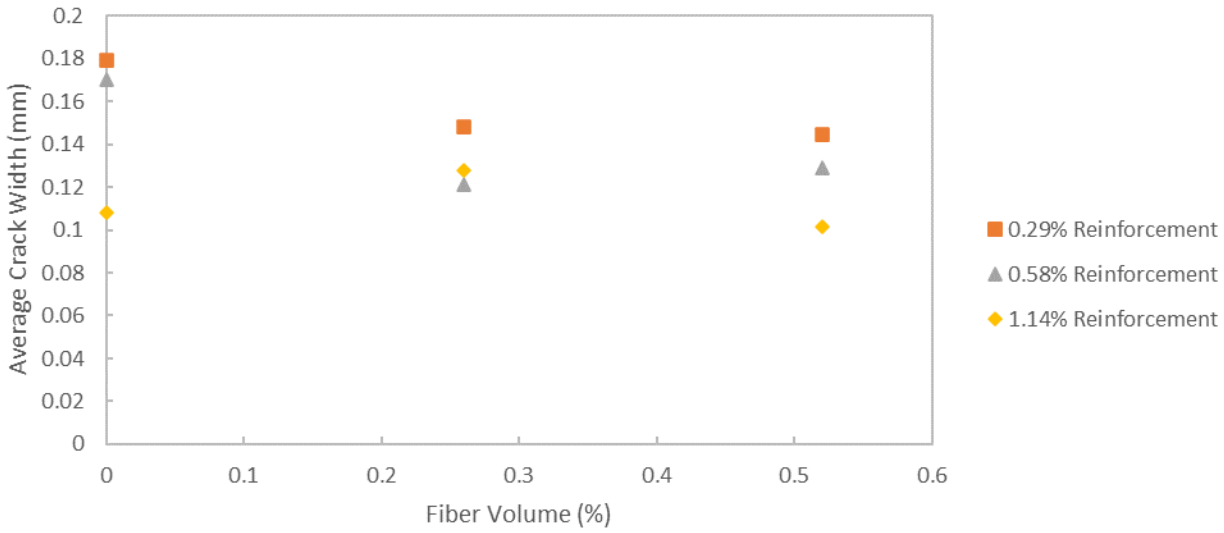

Figure 5-8: Fiber Volume Effect on Average Crack Width at $4\sqrt{f'c}$ Shear Stress

5.1.1 Maximum Crack Width

Figure 5-9 shows the maximum crack width plotted against transverse reinforcement ratio at a normalized shear stress of $4\sqrt{f'c}$. The panels without transverse reinforcement did not reach this shear stress level and are, therefore, not shown in the plot. In general, the maximum crack width at a normalized shear stress of $4\sqrt{f'c}$ tended to decrease as the transverse reinforcement ratio increased, with a slope of roughly -0.2 mm/%.

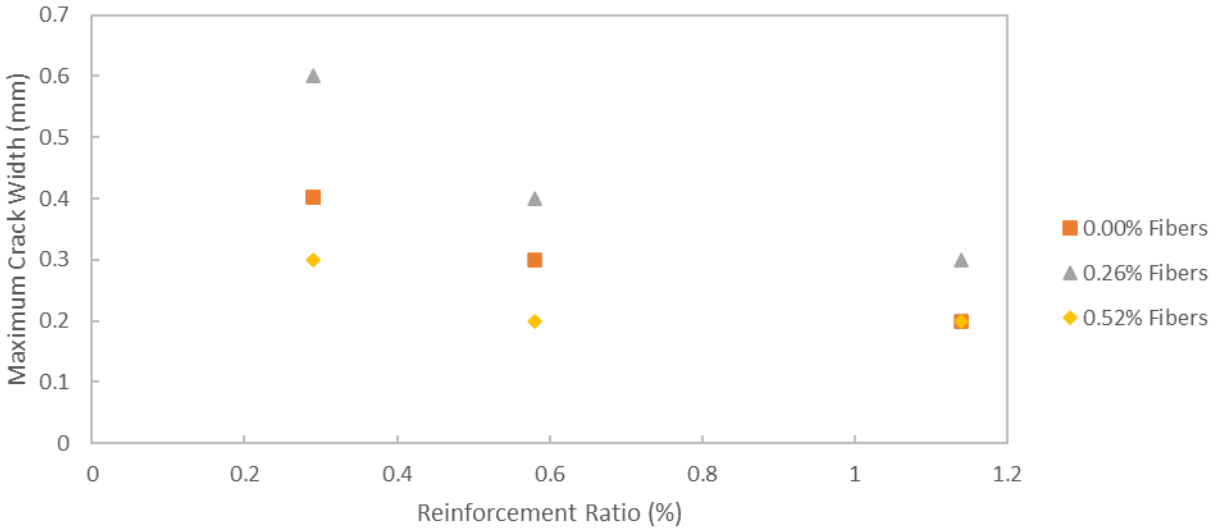

Figure 5-9: Reinforcement Ratio's Effect on Maximum Crack Width at $4\sqrt{f'c}$ Shear Stress

Figure 5-10 shows the maximum crack width plotted against fiber volume fraction at a normalized shear stress of $4\sqrt{f'c}$. Note that the point for PFRC-026-029 is covered since it is at the exact same point as PFRC-026-114. In general, the maximum crack width at a normalized shear stress of $4\sqrt{f'c}$ tended to decrease as the fiber volume fraction increased, with a slope of roughly -0.2 mm/%.

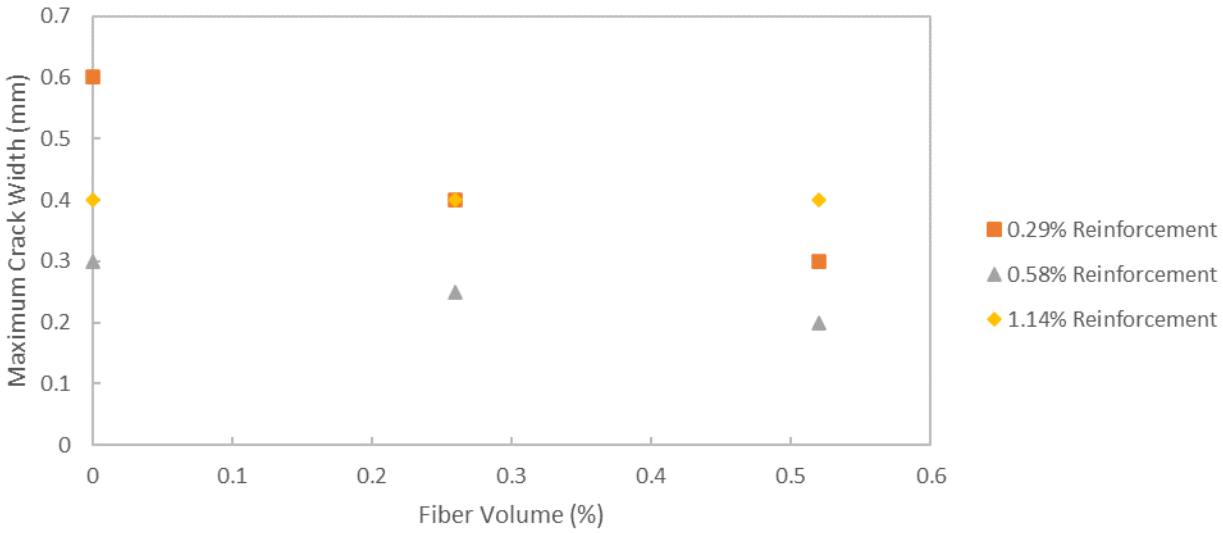

Figure 5-10: Fiber Volume Effect on Maximum Crack Width at $4\sqrt{f'c}$ Shear Stress

5.2 Comparison to Empirical Shear Strength Relationships

The measured shear strengths of the panel elements were compared to the estimated strengths determined using the shear strength equations highlighted at the end of Chapter 2. To enable comparison to the empirical formulas, which estimate the contribution of (steel) fiber-reinforced concrete to shear strength only, an estimate of the transverse reinforcement contribution was needed as well. For consistency, the shear strength contribution from the deformed bar reinforcement was estimated to be $v_s = \rho_v f_{yt}$ for all the empirical models, where ρ_v is the transverse reinforcement ratio and f_{yt} is the measured yield stress of the transverse deformed bar reinforcement.

An additional point to highlight with respect to the literature equations is the longitudinal reinforcement ratio selected for this project, which was constant between the panels at 2.28%. This is an important value to note since most of the empirical equations are dependent upon this value excluding the models proposed by Swamy et al. (1985) and Sharma (1986). The reason for selecting a longitudinal reinforcement ratio at least twice that of the maximum transverse reinforcement ratio was to ensure that the longitudinal steel would remain elastic and that shear failure would occur without the possibility of biaxial yielding of the reinforcement. The longitudinal reinforcement ratio was still below the maximum allowable 4.0% specified by ACI-318 (ACI 2019).

Table 5-2: Predicted/Observed Ratio for Literature Equations

Specimen ID	Swamy et al.	Sharma	Narayann et al.	Ashour	Kwak et al.	ACI	fib.	RILEM
pfrc-000-000	0.93	1.66	1.22	2.50	1.07	0.52	0.53	0.53
pfrc-000-029	0.80	1.05	0.88	1.47	0.80	0.53	0.54	0.54
pfrc-000-058	0.64	0.93	0.83	1.25	0.75	0.55	0.57	0.57
pfrc-000-114	0.79	0.97	0.86	1.20	0.82	0.67	0.67	0.67
pfrc-026-000	1.58	2.16	1.87	3.76	1.56	0.68	0.86	0.82
pfrc-026-029	0.70	1.04	0.91	1.56	0.84	0.53	0.59	0.58
pfrc-026-058	0.93	1.22	1.10	1.74	1.00	0.72	0.77	0.76
pfrc-026-114	0.78	1.03	0.93	1.33	0.89	0.71	0.73	0.72
pfrc-052-000	1.04	1.90	1.76	3.67	1.42	0.60	0.84	0.78
pfrc-052-029	0.60	0.96	0.84	1.49	0.80	0.47	0.53	0.52
pfrc-052-058	0.78	1.05	0.99	1.60	0.93	0.62	0.67	0.66
pfrc-052-114	0.76	0.98	0.93	1.34	0.89	0.69	0.73	0.72

Table 5-2 shows the ratio between the observed strength in the panel tests and the predicted strength from both the empirical and design code equations. Table 5-3 presents the average, standard deviation, coefficient of variation, minimum, and maximum values of the predicted strength ratios. The intent behind the development of each type of equation is evident with the empirical equations being much closer to 1.0 with a value of 1.05 while the code design equations are very conservatively underpredicting with an average of 0.65. The standard deviation and coefficient of variation of all the empirical equations were quite high with values of about 0.3 and 26% respectively. Though the empirical equations have most of the contribution with a standard deviation of 0.31 and coefficient of variation of 29% when compared to the small magnitude spread of the design code equation predictions which had a standard deviation of 0.10 and coefficient of variation of 15%.

Table 5-3: Predicted/Observed Ratio Statistics

Model	Avg	STD	COV	Min	Max
Swamy et al.	0.86	0.25	29%	0.60	1.58
Sharma	1.25	0.40	32%	0.93	2.16
Narayann et al.	1.10	0.34	31%	0.83	1.87
Kwak et al.	0.98	0.25	25%	0.75	1.56
ACI	0.61	0.08	13%	0.47	0.72
fib.	0.67	0.11	17%	0.53	0.86
RILEM	0.66	0.10	16%	0.52	0.82

Figure 5-11 shows the predicted panel strength from the empirical equations versus the observed strengths seen in this project. The solid line indicates a 1:1 relationship and the dashed lines indicate 20% bounds. Overall, the strengths were overpredicted at lower strength values and were underpredicted at higher strengths with some variation between the empirical equations. The equation developed by Swamy et al. (1985) consistently underestimated the strength by nearly 20% and the equation developed by Narayann et al. (1987) tended to give the closest estimates overall for the different strength levels, although they overestimated the strength of the panels without transverse reinforcement by more than 20% (the datapoints with observed strengths less than 2 MPa).

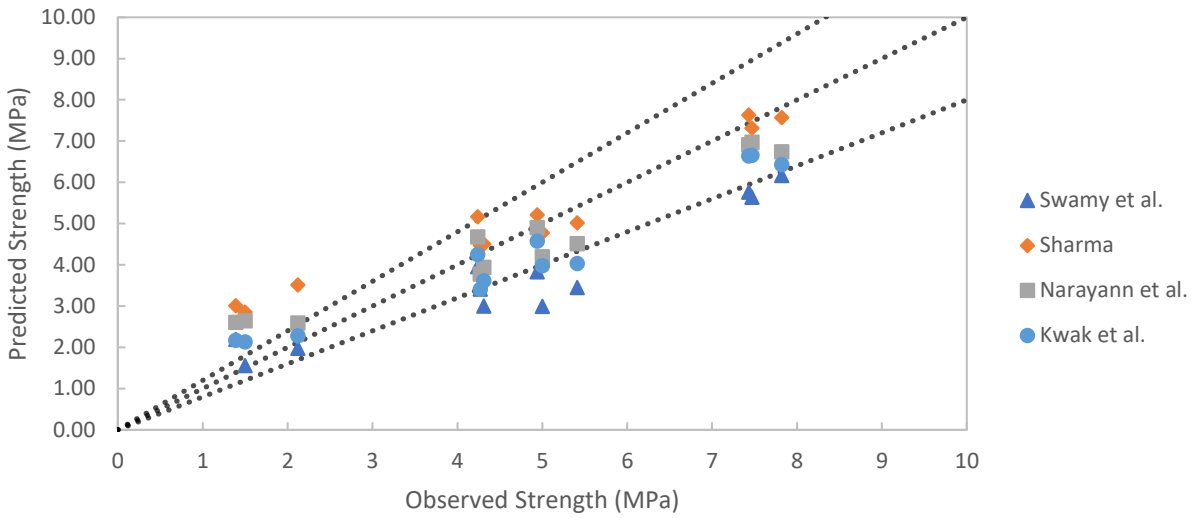

Figure 5-11: Observed versus Predicted Strength for Empirical Equations

Figure 5-12 shows the predicted/observed ratio for the concrete alone versus the transverse reinforcement ratio. Note that the vertical axis is logarithmic to show deviation from 1.0 consistently between values that are higher and lower than the reference line. Overall, the empirical equations overpredicted the strength of the panels without transverse deformed bar reinforcement, by roughly 40%. For panels with deformed bar transverse reinforcement, the empirical equations tended to underpredict the strength by roughly 20%, and the variation remains constant with higher reinforcement ratios as the steel response was normalized out.

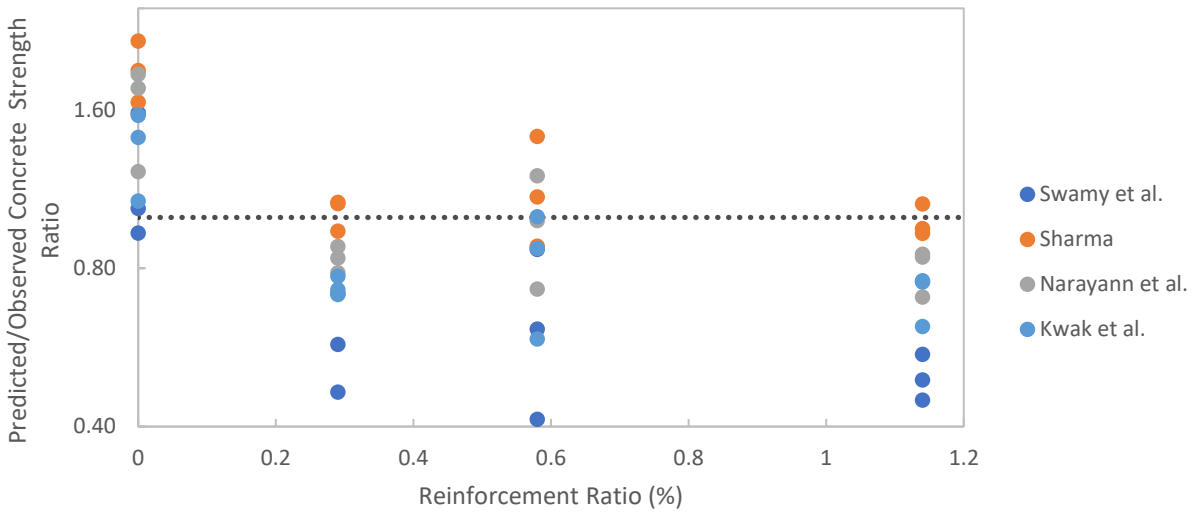

Figure 5-12: Predicted to Observed Concrete Strength Ratio versus Reinforcement Ratio for Empirical Equations

Figure 5-13 shows the fiber volume's effect on the predicted/observed concrete strength ratio with the steel response normalized out. Note that the vertical axis is logarithmic to show deviation from 1.0 consistently between values that are higher and lower than the reference line. The points show a large vertical spread that is flat between points calculated using the same empirical equation. From this, it seems that the fiber volume does not affect the accuracy of predicted strength for the empirical equations.

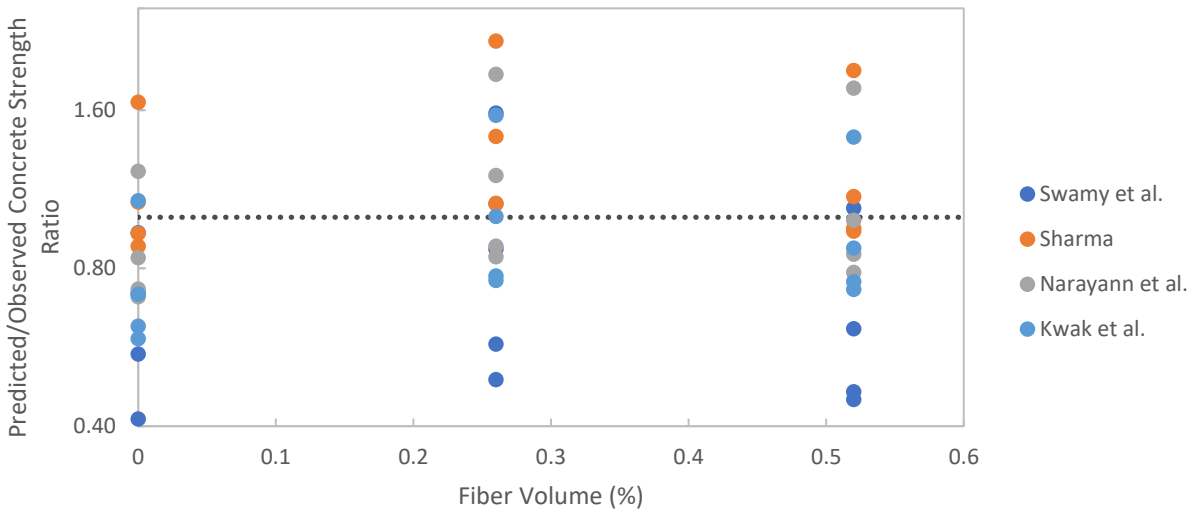

Figure 5-13: Predicted to Observed Concrete Strength Ratio versus Fiber Volume for Empirical Equations

Figure 5-14 below shows the predicted shear strength from the code equations (ACI 318, *fib*, and RILEM) versus the observed shear strength. These are discussed separately from the empirical equations here, since code provisions are intentionally conservative estimates. The solid line indicates a 1:1 relationship and the dashed lines indicate 20% bounds. In general, the code equations estimate similar strengths for the panels and underpredict the observed strength, as anticipated. For each panel, the equations developed by RILEM and *fib* estimate higher shear strengths than the ACI equation that does not account for the presence of fibers to an approximate 8% difference.

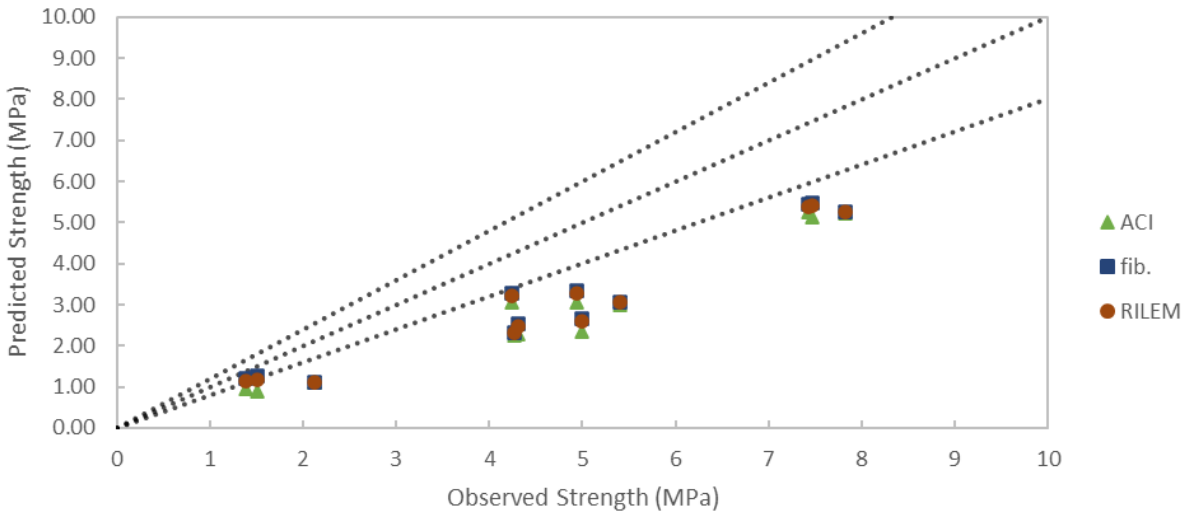

Figure 5-14: Observed versus Predicted Concrete Strength for Design Code Equations

Figure 5-15 shows the predicted concrete strength ratio from the design code equations versus the reinforcement ratio. Note that the vertical axis is logarithmic to show deviation from 1.0 consistently between values that are higher and lower than the reference line. The points show underpredictions over the whole response with the closest being when no transverse steel is present at roughly 25%. The underprediction at any of the steel levels used in this project seems to be almost constantly 75%.

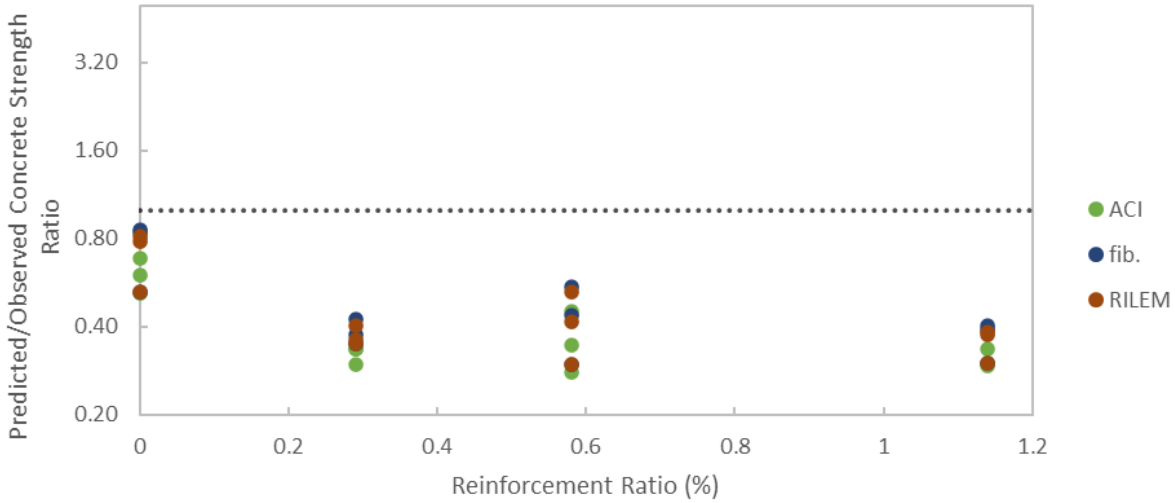

Figure 5-15: Predicted to Observed Concrete Strength Ratio versus Reinforcement Ratio for Design Code Equations

Figure 5-16 shows the predicted concrete strength ratio from the design code equations versus the fiber volume. Note that the vertical axis is logarithmic to show deviation from 1.0 consistently between values that are higher and lower than the reference line. The overall trend is flat between the points which show that the fiber volume does not significantly affect the strength predictions made by the design equations.

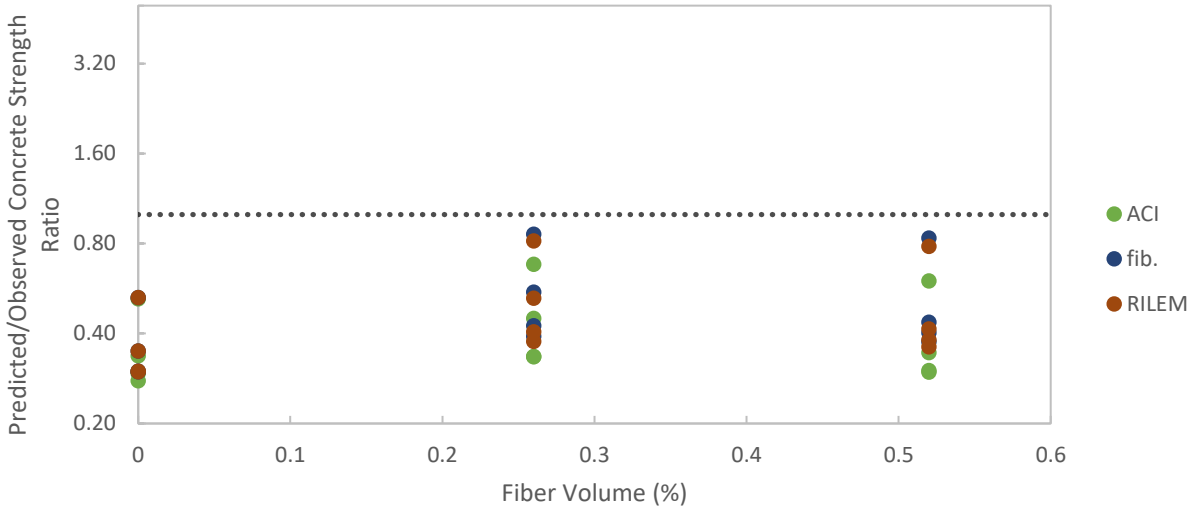

Figure 5-16: Predicted to Observed Strength Ratio versus Fiber Volume for Design Code Equations

Chapter 6: Summary, Conclusions, and Future Work

6.1 Summary

This research program investigated the use of both deformed bar reinforcement and distributed macro-synthetic fibers to resist shear forces. Twelve panel element specimens were tested under in-plane shear loading with transverse deformed bar reinforcement ratios, ranging from $\rho_t = 0\%$ to $\rho_t = 1.14\%$, and macro-synthetic fiber content, ranging from $V_f = 0\%$ to $V_f = 0.52\%$ fibers by volume. Companion specimens were cast alongside each panel to quantify the compressive strength, modulus of elasticity, and flexural toughness and strength of the concrete. The results were then compared to shear strength models provided by Swamy et al. (1985), Sharma (1986), Narayanan et al. (1987), and Kwak et al. (2002). Additionally, code equations from ACI 318-19 (2019), fib. Model Code 2010 (2013), and RILEM (2003) were also compared to the results.

6.2 Conclusions

In the range of the parameters investigated, the following conclusions were reached:

- Macro-synthetic fibers were effective in decreasing both the maximum and average crack widths during shear loading. For panels with a transverse reinforcement ratio of 0.29%, increasing the fiber volume from 0% to 0.52% reduced the maximum crack width at a shear stress of $6\sqrt{f'_c}$ from 0.6 mm to 0.3 mm (50% decrease), and reduced the corresponding average crack widths from 0.32 mm to 0.25 mm (22% decrease).
- No significant increases in shear strength were observed by adding macro-synthetic fibers at the addition rates used in this study. This is in contrast to previous test series (e.g., Li et al. 1992) where the addition of 1.0% fibers by volume led to an increase in beam strength of roughly 100% to 200% depending on fiber type. This discrepancy is at least partially attributed to the different testing methods, since the previously tested specimens were subjected to a combination of shear and flexure under displacement control.
- At transverse reinforcement ratios of 0% and 0.29%, the shear strain capacity at failure increased as fiber volume increased, however no improvements were observed at the transverse reinforcement ratio of 1.14%. This is consistent with the results of Carnovale (2013) who found that the addition of fibers to panels containing no transverse reinforcement improved the shear ductility of the panels when tested cyclically.

- The benefits of adding macro-synthetic fibers on the shear strength of structural members may depend on the transverse reinforcement ratio (i.e., there may be more benefit at lower reinforcement ratios). This is consistent with previous studies (e.g., Altoubat et al. 2009) that found a 20% to 28% increase in shear strength for macro-synthetic fiber-reinforced beams without transverse reinforcement.
- Current predictive equations, based on the results of beams containing steel fibers without transverse reinforcement, tend to overestimate fiber contributions by 37.4%. when applied to the panel elements reinforced with macro-synthetic fibers and no transverse steel. On average, the strength predictions with transverse steel were 9.5% lower than the measured values at a transverse reinforcement ratio of 0.29%, and 6.7% lower at a transverse reinforcement ratio of 1.14%.

6.3 Future Work

The following are suggestions for future work investigating the combined use of deformed bar transverse reinforcement and macro-synthetic fibers:

- The two panel specimen tests that suffered from consolidation issues should be repeated to strengthen the trends observed in the current study.
- Additional tests that use different macro-synthetic fibers should be performed. Only one type of macro-synthetic fiber was used in this work, however macro-synthetic fibers come in many different sizes, shapes, materials, and coatings which all could affect their benefit when used with transverse bars.
- Additional shear tests should be conducted with similar or larger macro-synthetic fiber volumes and lower reinforcing levels (i.e. less than 0.58%), since greater benefit from fibers were seen there.
- The panel testing could be repeated under displacement control to capture the post peak response of the panels, and any identify any benefits to the residual shear capacity of PFRC elements.
- To extend the results of the current experimental campaign, the shear response of the PFRC panels should be modeled in available software programs (e.g., VecTor2), using the experimental results for validation.

- Design equations for the shear strength of structural elements containing macro-synthetic fibers and transverse reinforcement should be developed.

References

318-19 building code requirements for structural concrete and commentary. (2019). https://doi.org/10.14359/51716937

ACI (2008) Building code requirements for structural concrete (ACI 318-08) and commentary, Committee 318, American Concrete Institute Farmington Hills, MI, USA.

ASTM Standard C1609/C1609M-12, 2019, "Standard Test Method for Flexural Performance of Fiber-Reinforced Concrete (Using Beam With Third-Point Loading)" ASTM International, West Conshohocken, PA, 2003, DOI: 10.1520/C1609_C1609M-12, www.astm.org

Alhassan, M., Al-Rousan, R., Ababneh, A. (2017) "Flexural behavior of lightweight concrete beams encompassing various dosages of macro synthetic fibers and steel ratios." *Case Studies in Constr Mat*, 7: 280-293.

Altoubat, S., Yazdanbakhsh, A., & Rieder, K.-A. (2009). Shear behavior of macro-synthetic fiber-reinforced concrete beams without stirrups. *ACI Materials Journal, 106*(4). https://doi.org/10.14359/56659

Ashour, A. S., Hasanain, G. S., & Wafa, F. F. (1992). Shear behavior of high-strength fiber reinforced concrete beams. *ACI Structural Journal, 89*(2). https://doi.org/10.14359/2946

Bentur, A., & Mindess, S. (2007). *Fibre reinforced cementitious composites*. Taylor & Francis.

Carnovale, D. J. (2013). *Behavior and analysis of steel and macro-synthetic fibre reinforced concrete subjected to reversed cyclic loading: A pilot investigation* (thesis). University of Toronto, Toronto.

Chasioti, S. (2017). *Hybrid steel fibre reinforced concrete in shear: From the material to the structural level* (thesis). University of Toronto, Toronto.

Chatterjee, A., and Deopura, B., (2006). High modulus and high strength PP nanocomposite filament. *Composites Part A: Applied Science and Manufacturing, 37*(5), May 2006

Daniel, J. I., (1991). *Fiber reinforced concrete.* Illinois, USA: Portland Cement Association, pp. 48

fib. (2013). *FIB Model Code for Concrete Structures 2010*. https://doi.org/10.1002/9783433604090

Final recommendation of Rilem TC 162-TDF: Test and design methods for steel fibre reinforced concretesigma-epsilon-design method. (2003). *Materials and Structures, 36*(262), 560–567. https://doi.org/10.1617/14007

Furlan, S. and Bento-de-Hanai, J.B. (1997). Shear behavior of fiber reinforced concrete beams. Cement and Concrete Composites, 19: 359–366.

Gregor-Svetec, D., and Sluga, F., (2005). High modulus polypropylene fibers. I. mechanical properties. *Journal of Applied Polymer Science, 98*(1), January 2005

Hasan, M. J., Afroz, M., and Mahmud, H. M. I., (2011) An experimental investigation on mechanical behavior of macro synthetic fiber reinforced concrete. *International Journal of Civil and Environmental Engineering, 11*(3), June 2011

Kwak, Y.-K., Kim, J., Kim, W.-suk, & Eberhard, M. (2002). Shear strength of steel fiber-reinforced concrete beams without stirrups. *ACI Structural Journal*, *99*(4). https://doi.org/10.14359/12122

Lantsoght, E. O. L. (2019). Database of shear experiments on steel fiber reinforced concrete beams without stirrups. https://doi.org/10.20944/preprints201902.0264.v1

Li, V.C., Ward, R., Hamza, A.M. (1992) "Steel and Synthetic Fibers as Shear Reinforcement." *ACI Mat J*, 89(5): 499-508.

Li, V.C., Mishra, D.K., Naaman, A.E., Wight, J.K., LaFave, J.M., Wu, H., and Inada, Y. (1994) "On the Shear Behavior of Engineered Cementitious Composites." *Advn Cem Bas Mat,* 1994(1): 142-149.

Majdzadeh, F., Soeimani, S. M., & Banthia, N. (2006). Shear strength of reinforced concrete beams with a fiber concrete matrix. https://doi.org/https//cjce.nrc.ca

Mirsayah, A. A., & Banthia, N. (2002). Shear strength of steel fiber-reinforced concrete. *ACI Materials Journal*, *99*(5). https://doi.org/10.14359/12326

Narayanan, R., & Darwish, I. Y. S. (1987). Use of steel fibers as shear reinforcement. *ACI Structural Journal*, *84*(3). https://doi.org/10.14359/2654

Parra-Montesinos, G. J., (2006). Shear strength of beams with deformed steel fibers. Concrete Intl, 28 (11): 57-66.

Richardson, A. E., and Landless, S., (2009). Synthetic fibres and steel fibres in concrete with regard to bond strength and toughness. *Northumbria Working Paper Series: Interdisciplinary Studies in the Built and Virtual Environment,* December 2009

Shah, S. P., & Rangan, B. V. (1971). Fiber reinforced concrete properties. *ACI Journal Proceedings*, *68*(2). https://doi.org/10.14359/11299

Sharma, A. K. (1986). Shear strength of steel fiber reinforced concrete beams. *ACI Journal Proceedings*, *83*(4). https://doi.org/10.14359/10559

Swamy, R. N., & Bahia, H. M. (1985). The effectiveness of steel fibers as shear reinforcement. *Concrete International*.

Susetyo, J. (2009). *Fibre reinforcement for shrinkage crack control in prestressed, precast segmental bridges* (thesis).

Vecchio, F. J., & Collins, M. P. (1986). The modified compression-field theory for reinforced concrete elements subjected to shear. *ACI Journal Proceedings*, *83*(2). https://doi.org/10.14359/10416

Wang, Y., Backer, S., and Li, V. C., (1987). An experimental study of synthetic fibre reinforced cementitious composites. *Journal of Materials Science, 22*(12), December 1987

Yazdanbakhsh, A., Altoubat, S., & Rieder, K.-A. (2015). Analytical study on shear strength of macro synthetic fiber reinforced concrete beams. *Engineering Structures, 100*, 622–632. https://doi.org/10.1016/j.engstruct.2015.06.034

Zhang, H., Calvi, P. M., Lehman, D., Kuder, K., & Roeder, C. (2020). Response of recycled coarse aggregate concrete subjected to pure shear. *Journal of Structural Engineering*, *146*(5). https://doi.org/10.1061/(asce)st.1943-541x.0002620

Appendix

A.1 Complete Panel Results

A.1.1 Shear Stress and Strain Behavior, Principal Tension and Compression, and Crack Width and Spacing

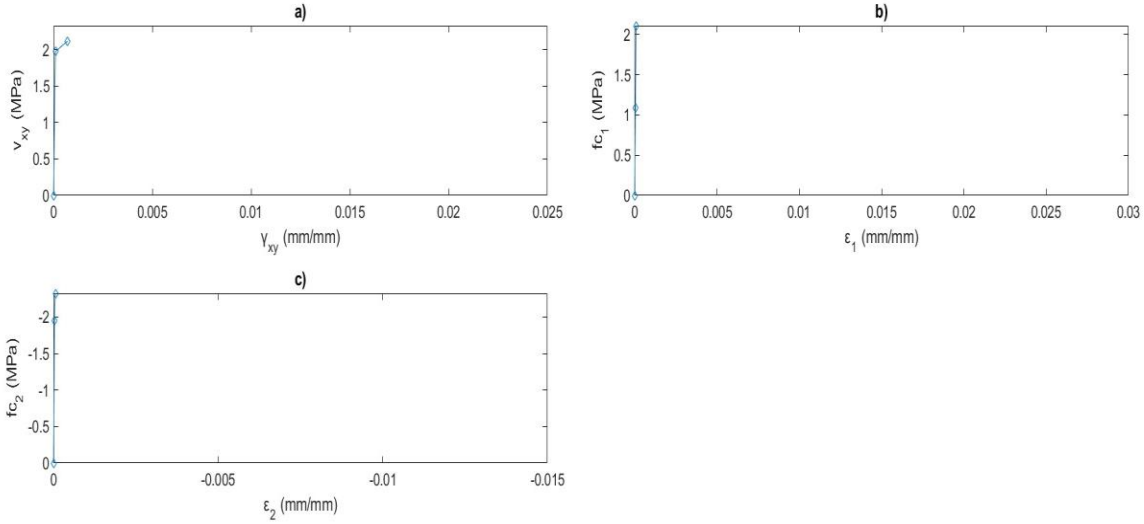

Figure A-1: PFRC-000-000 Results Graphs a) Shear Stress Versus Strain b) Principal Tension c) Principal Compression

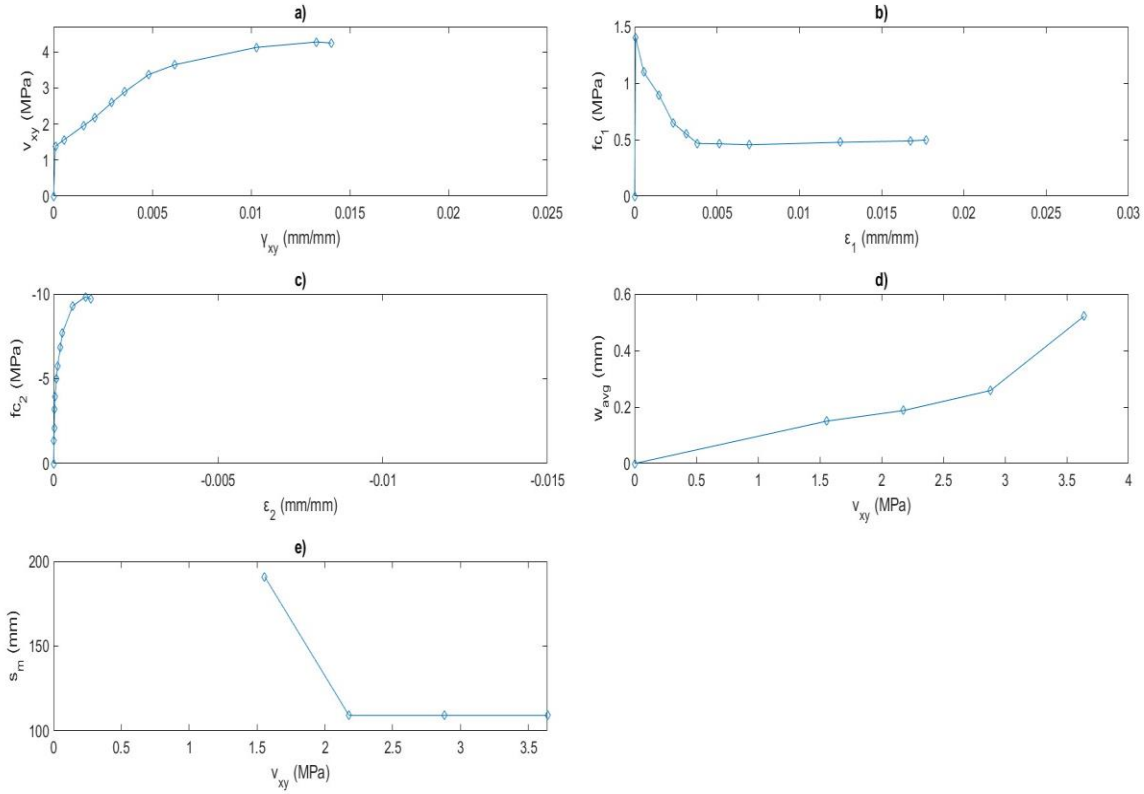

Figure A-2: PFRC-000-029 Results Graphs a) Shear Stress Versus Strain b) Principal Tension c) Principal Compression d) Average Crack Width e) Crack Spacing

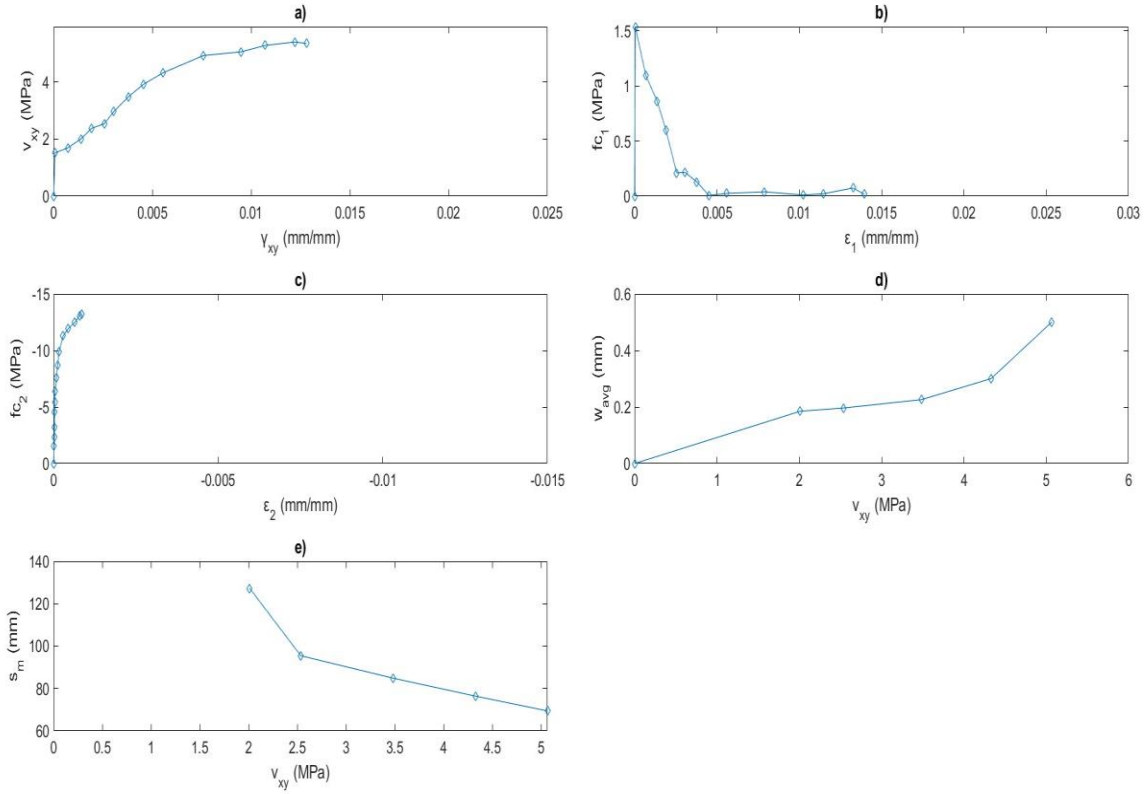

Figure A-3: PFRC-000-058 Results Graphs a) Shear Stress Versus Strain b) Principal Tension c) Principal Compression d) Average Crack Width e) Crack Spacing

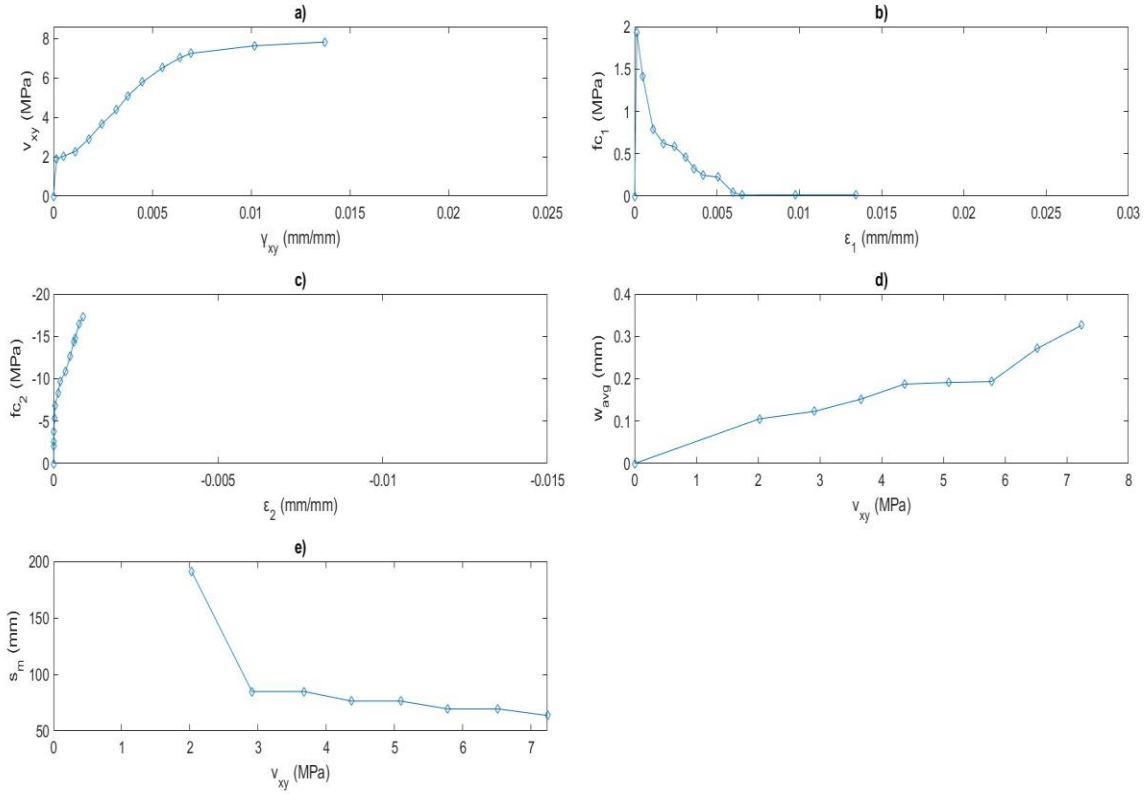

Figure A-4: PFRC-000-114 Results Graphs a) Shear Stress Versus Strain b) Principal Tension c) Principal Compression d) Average Crack Width e) Crack Spacing

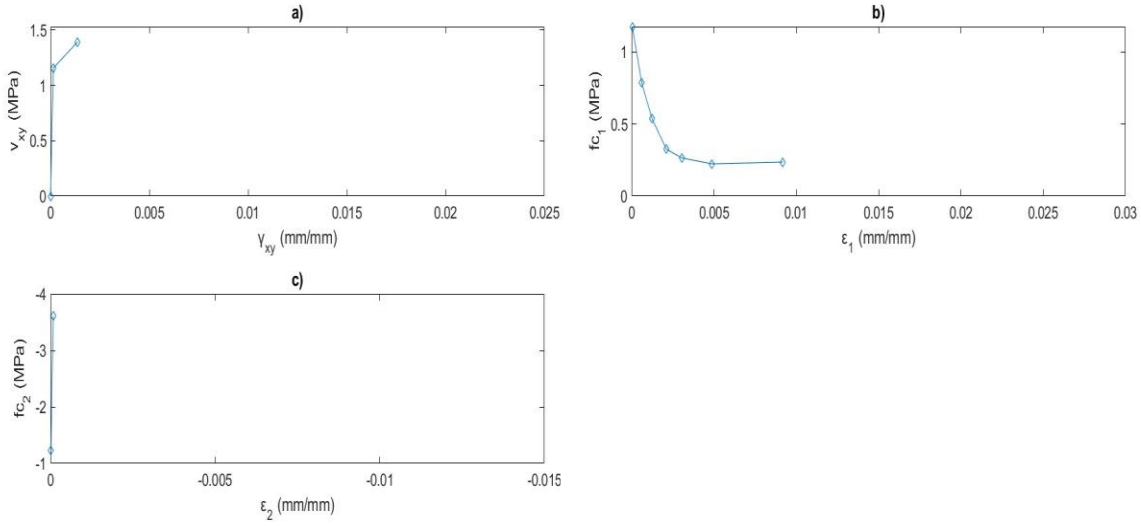

Figure A-5: PFRC-026-000 Results Graphs a) Shear Stress Versus Strain b) Principal Tension c) Principal Compression

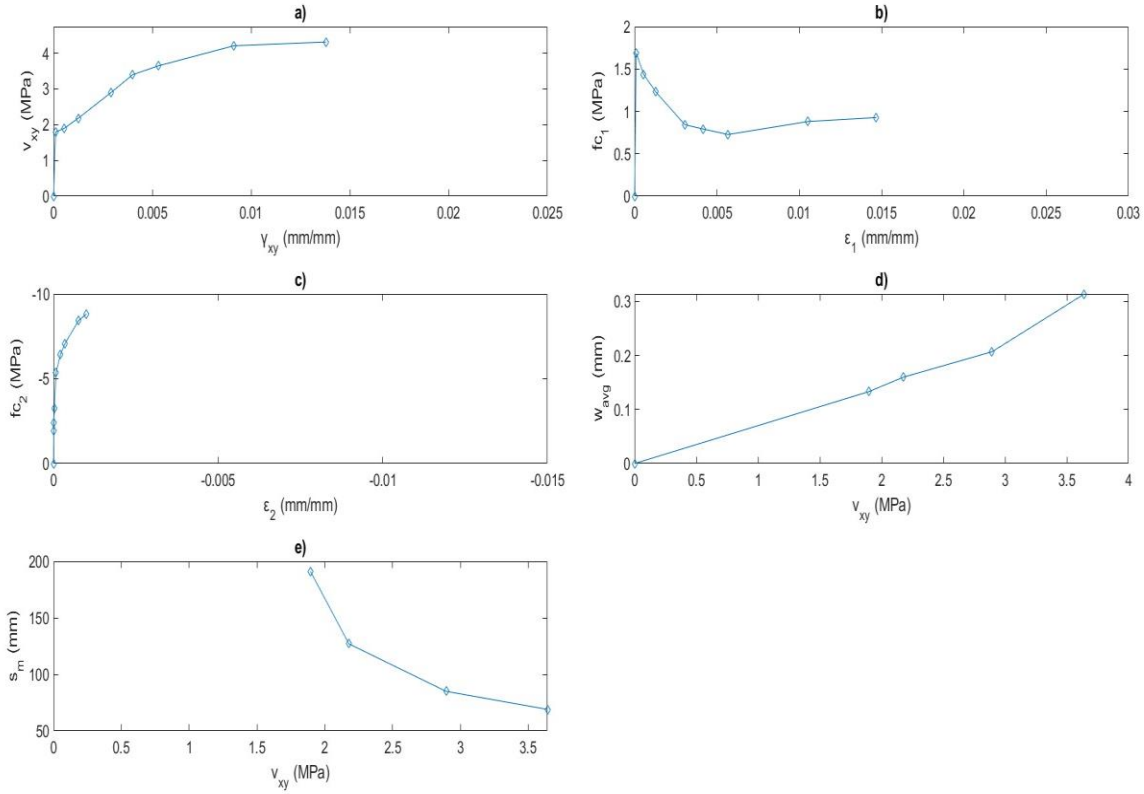

Figure A-6: PFRC-026-029 Results Graphs a) Shear Stress Versus Strain b) Principal Tension c) Principal Compression d) Average Crack Width e) Crack Spacing

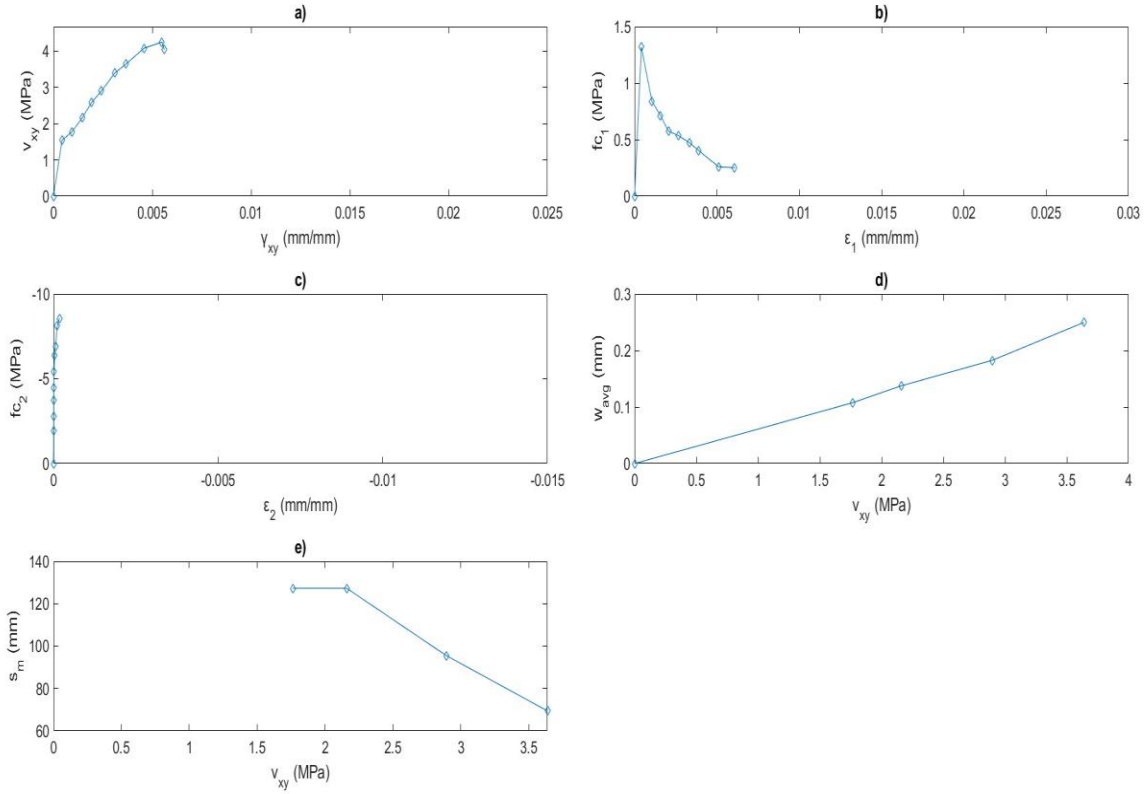

Figure A-7: PFRC-026-058 Results Graphs a) Shear Stress Versus Strain b) Principal Tension c) Principal Compression d) Average Crack Width e) Crack Spacing

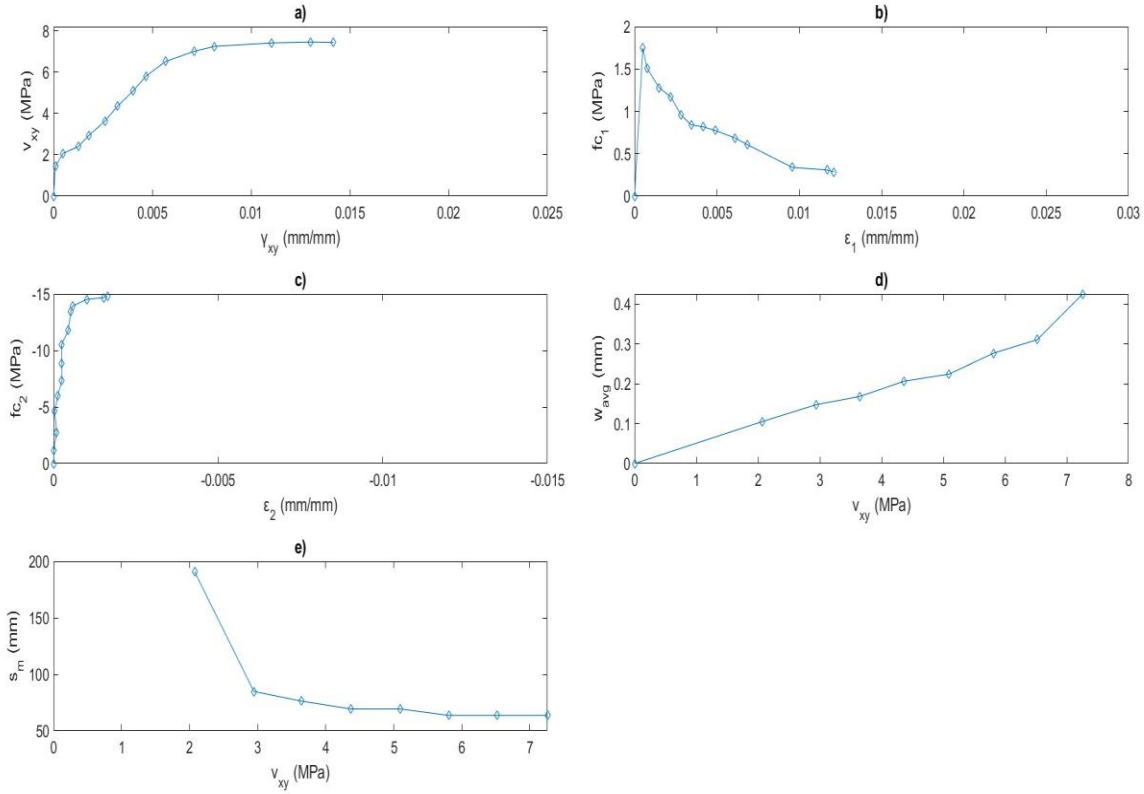

Figure A-8: PFRC-026-114 Results Graphs a) Shear Stress Versus Strain b) Principal Tension c) Principal Compression d) Average Crack Width e) Crack Spacing

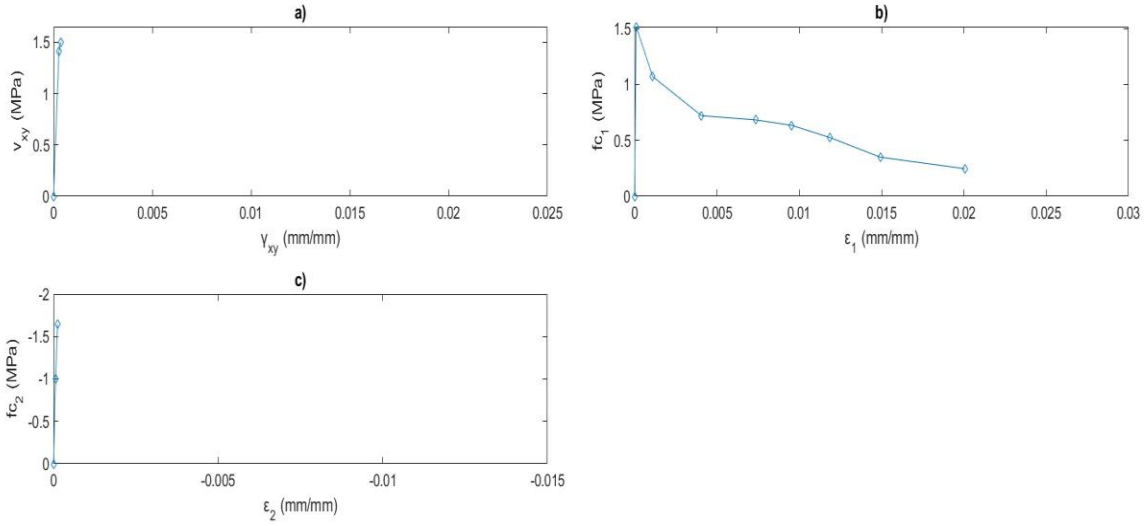

Figure A-9: PFRC-052-000 Results Graphs a) Shear Stress Versus Strain b) Principal Tension c) Principal Compression

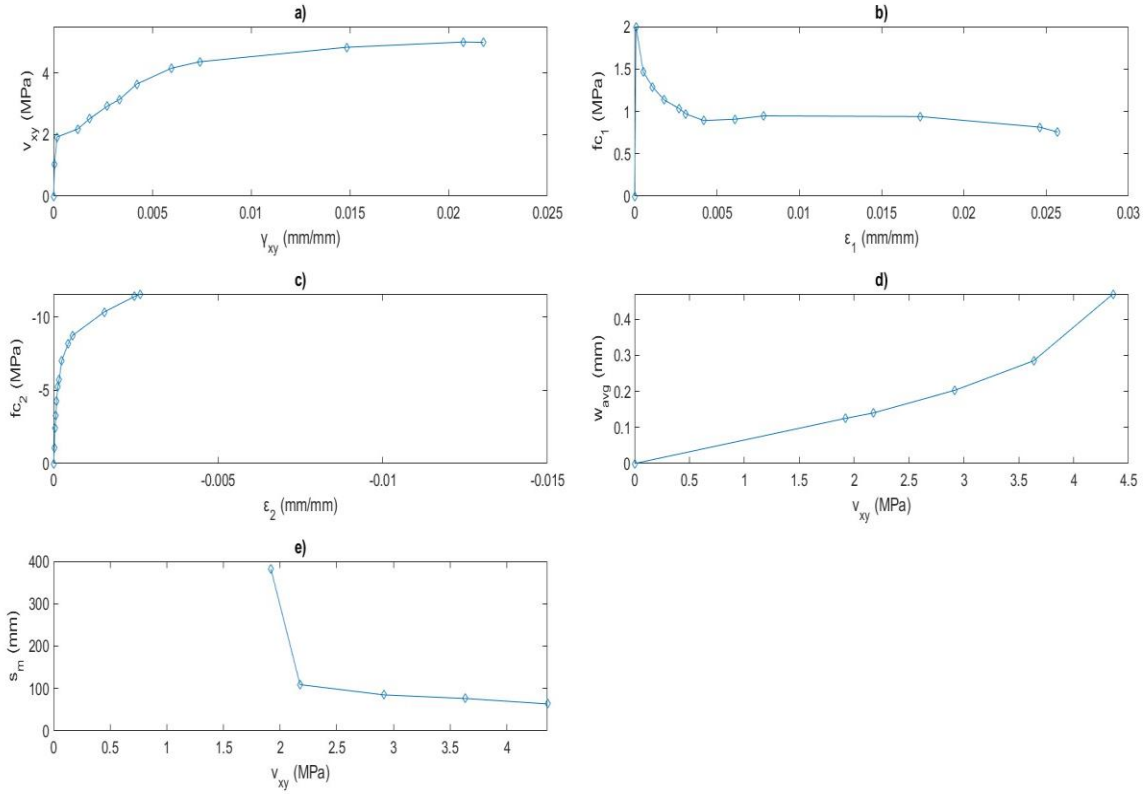

Figure A-10: PFRC-052-029 Results Graphs a) Shear Stress Versus Strain b) Principal Tension c) Principal Compression d) Average Crack Width e) Crack Spacing

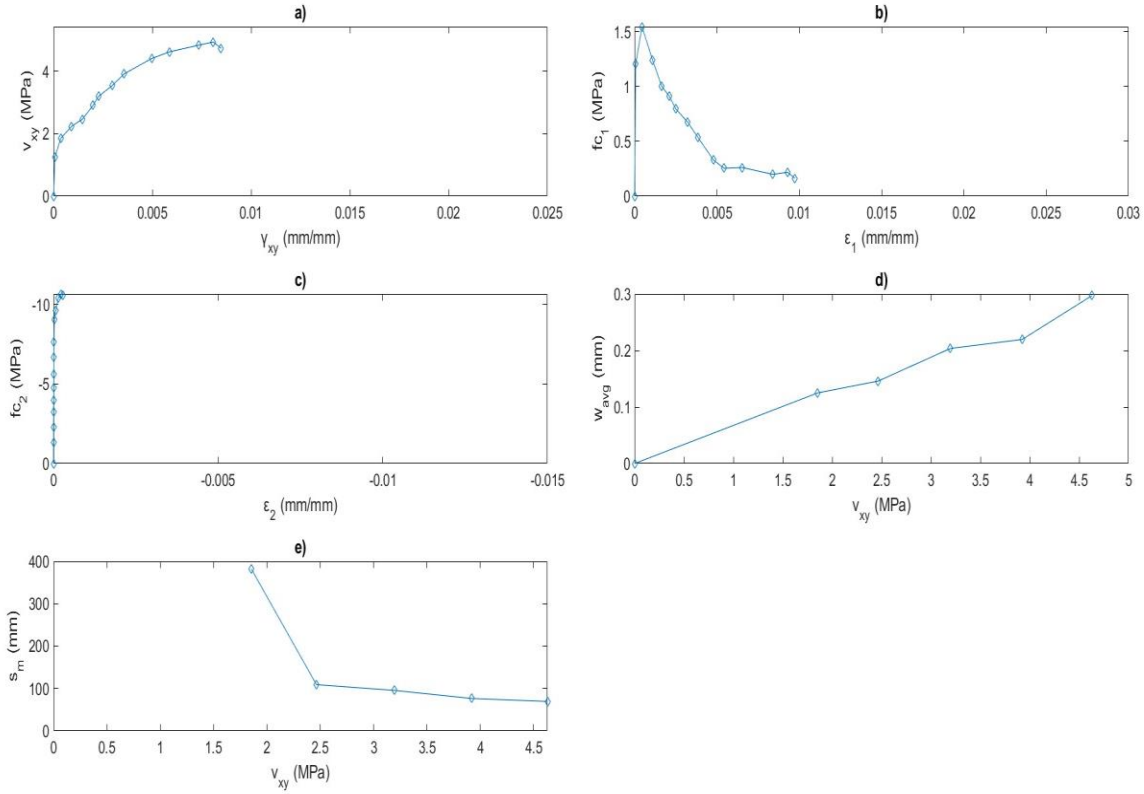

Figure A-11: PFRC-052-058 Results Graphs a) Shear Stress Versus Strain b) Principal Tension c) Principal Compression d) Average Crack Width e) Crack Spacing

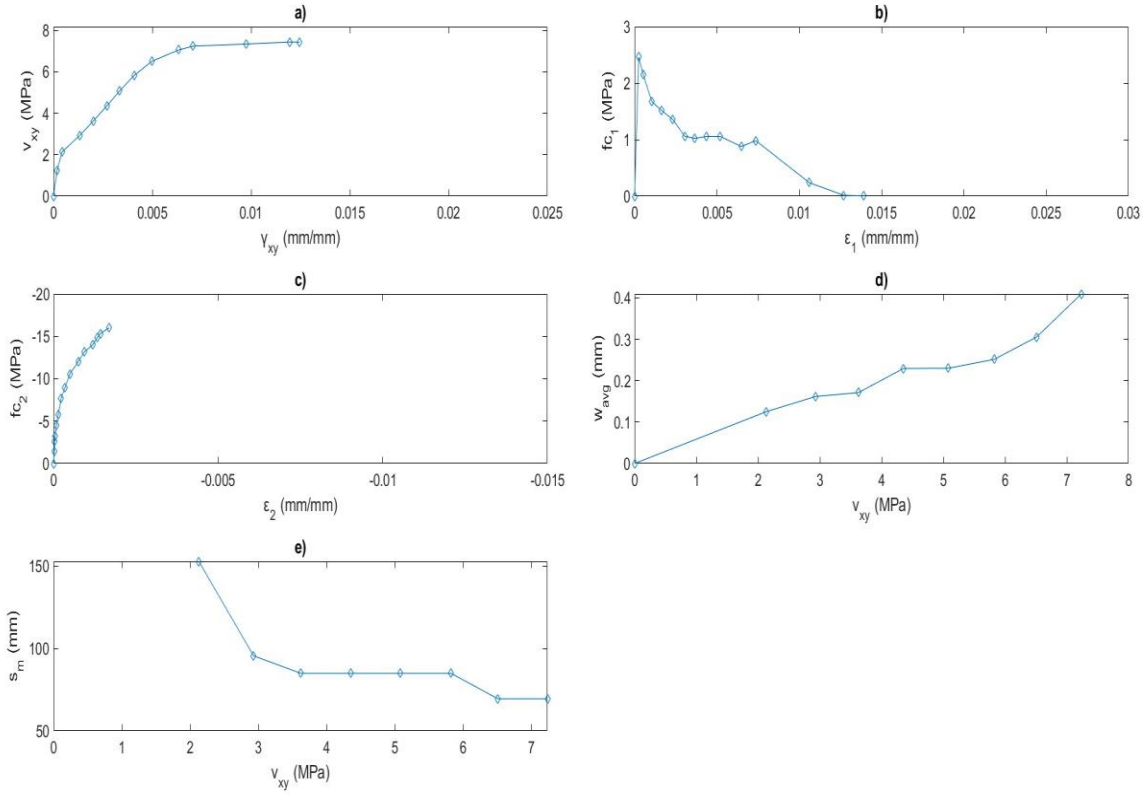

Figure A-12: PFRC-052-114 Results Graphs a) Shear Stress Versus Strain b) Principal Tension c) Principal Compression d) Average Crack Width e) Crack Spacing

A1.1.2 Failure and Heatmaps

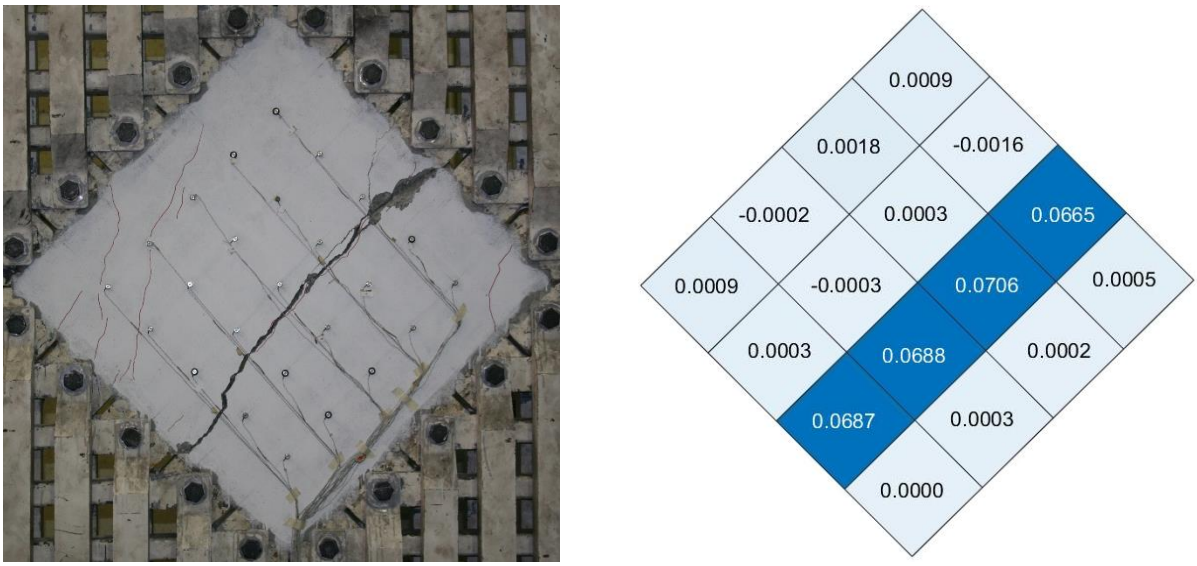

Figure A-13: PFRC-000-000 Failure Picture and Heat Map

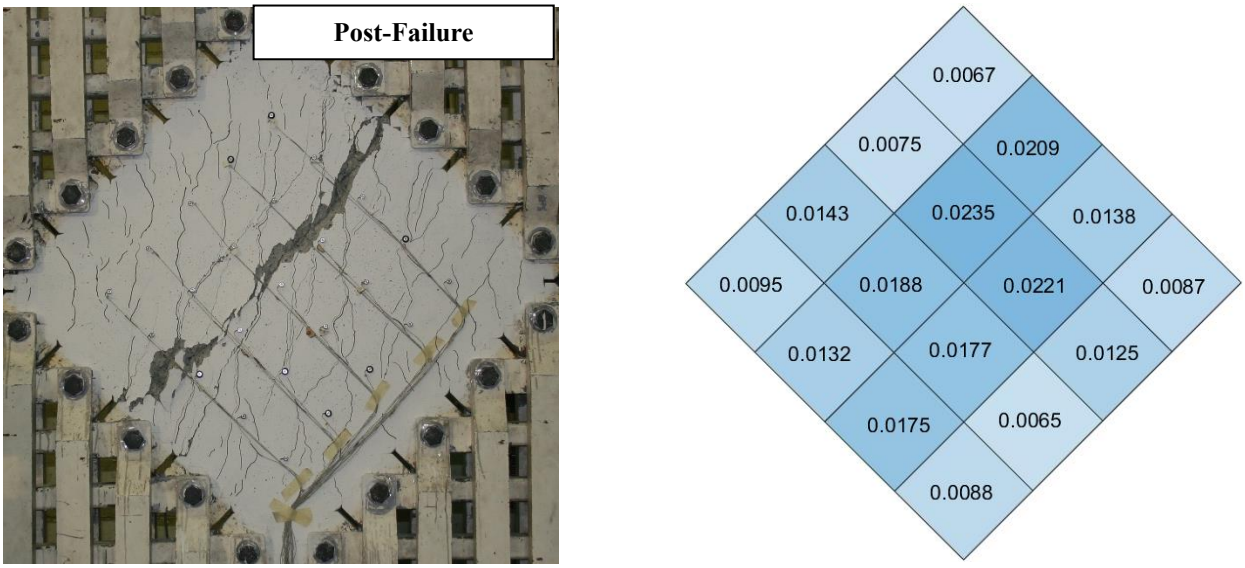

Figure A-14: PFRC-000-029 Failure Picture and Heat Map

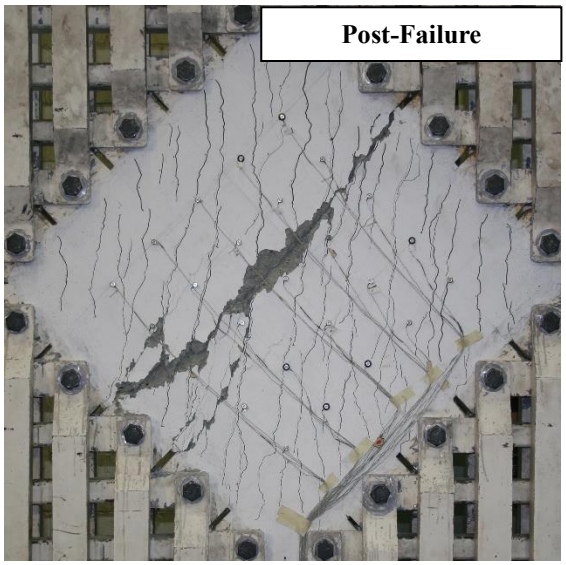

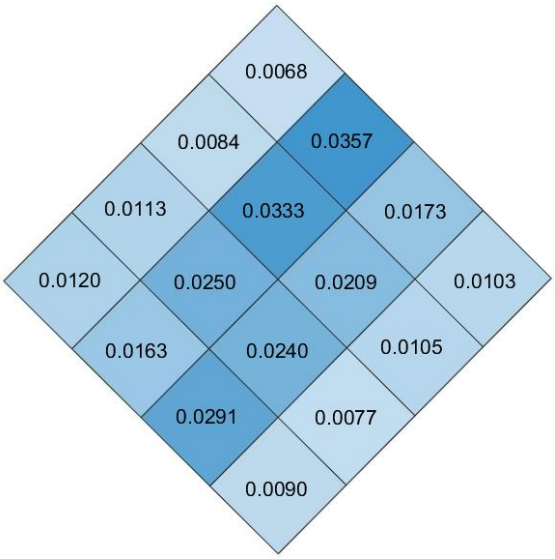

Figure A-15: PFRC-000-058 Failure Picture and Heat Map

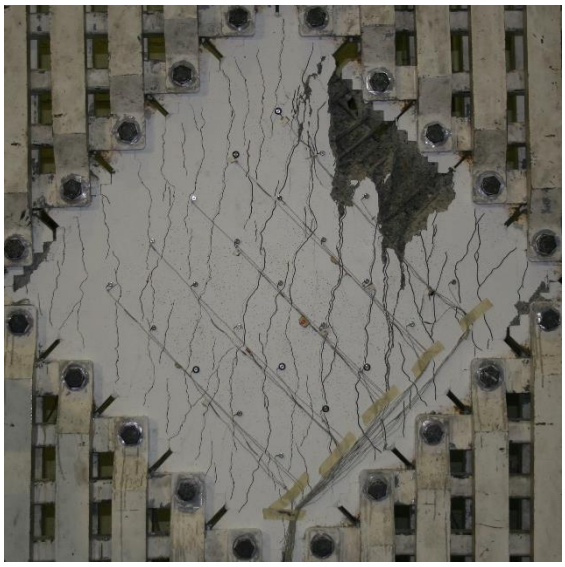

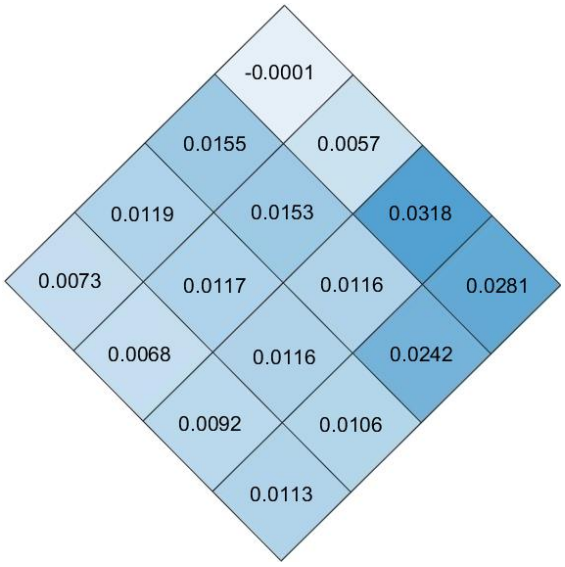

Figure A-15: PFRC-000-114 Failure Picture and Heat Map

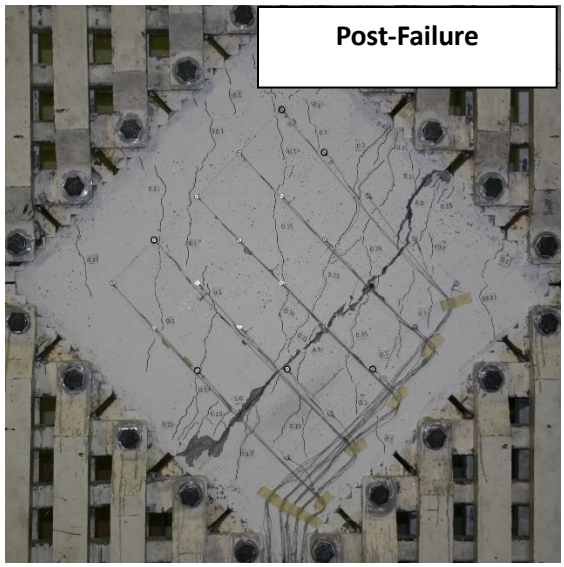

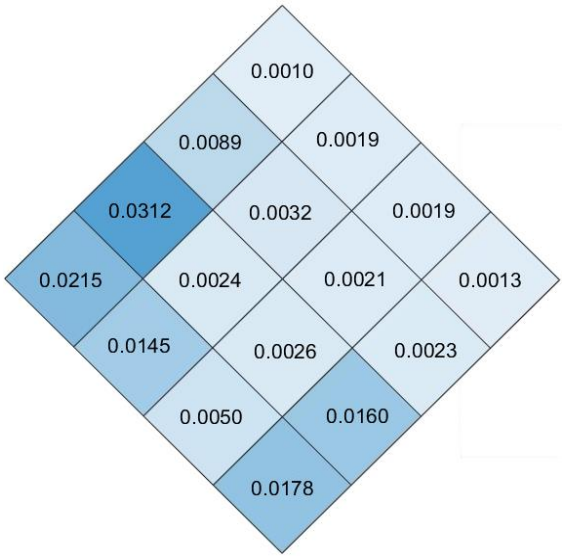

Figure A-16: PFRC-026-000 Failure Picture and Heat Map

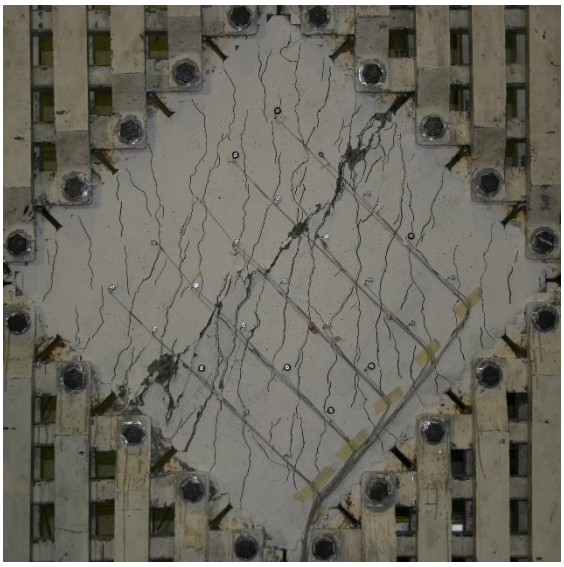

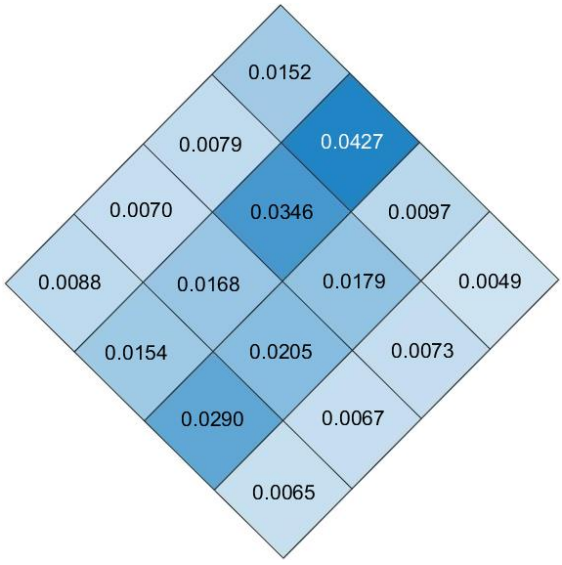

Figure A-17: PFRC-026-029 Failure Picture and Heat Map

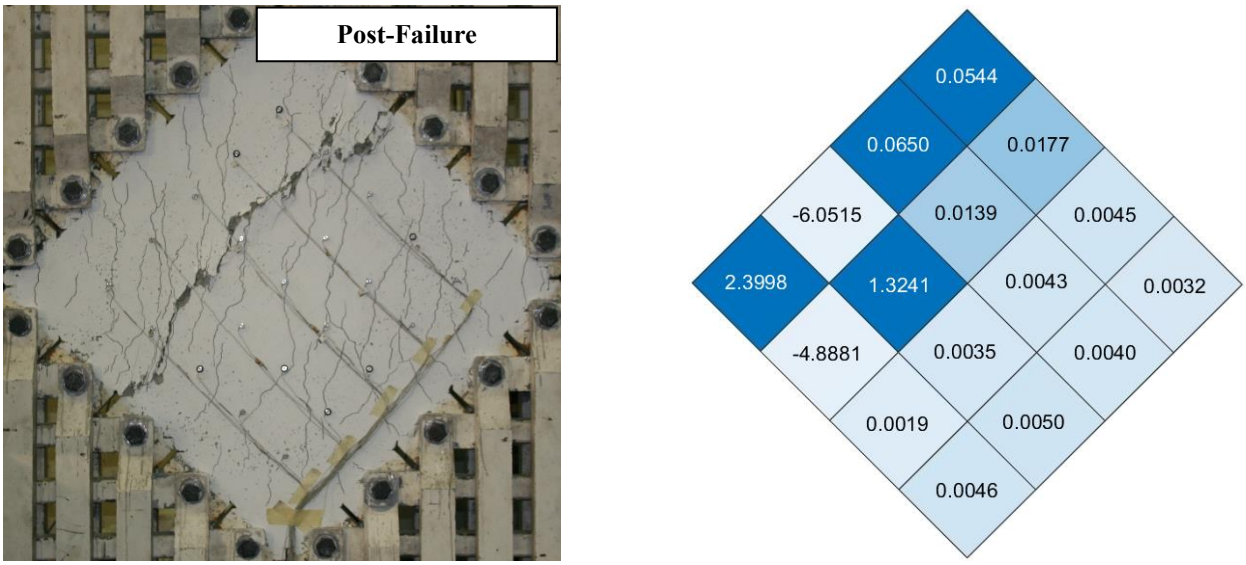

Figure A-18: PFRC-026-058 Failure Picture and Heat Map

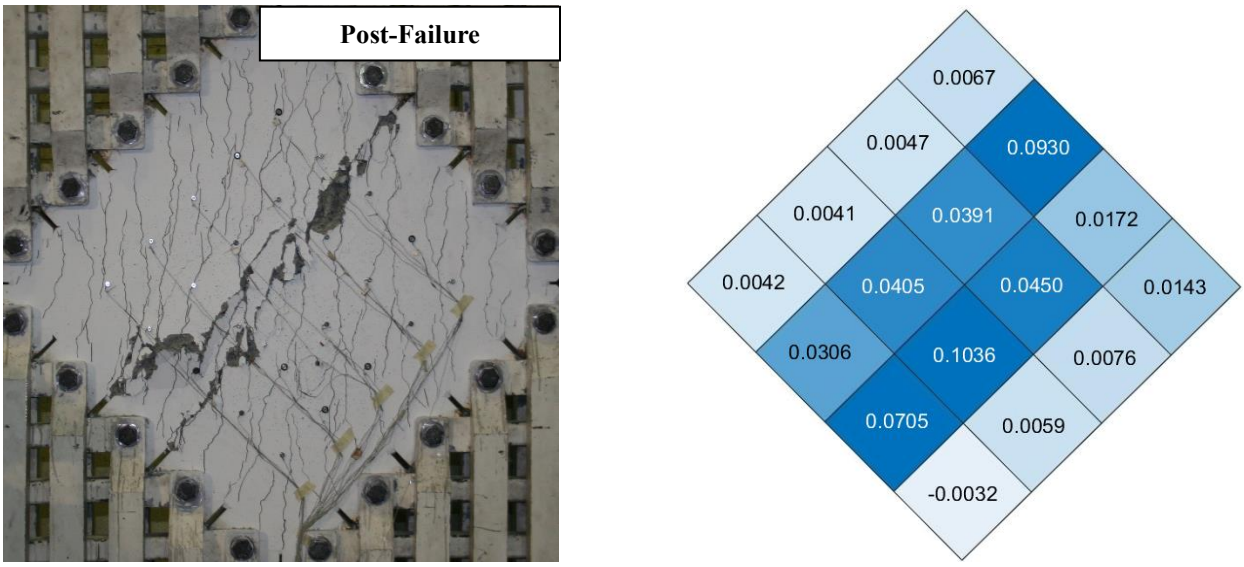

Figure A-19: PFRC-026-114 Failure Picture and Heat Map

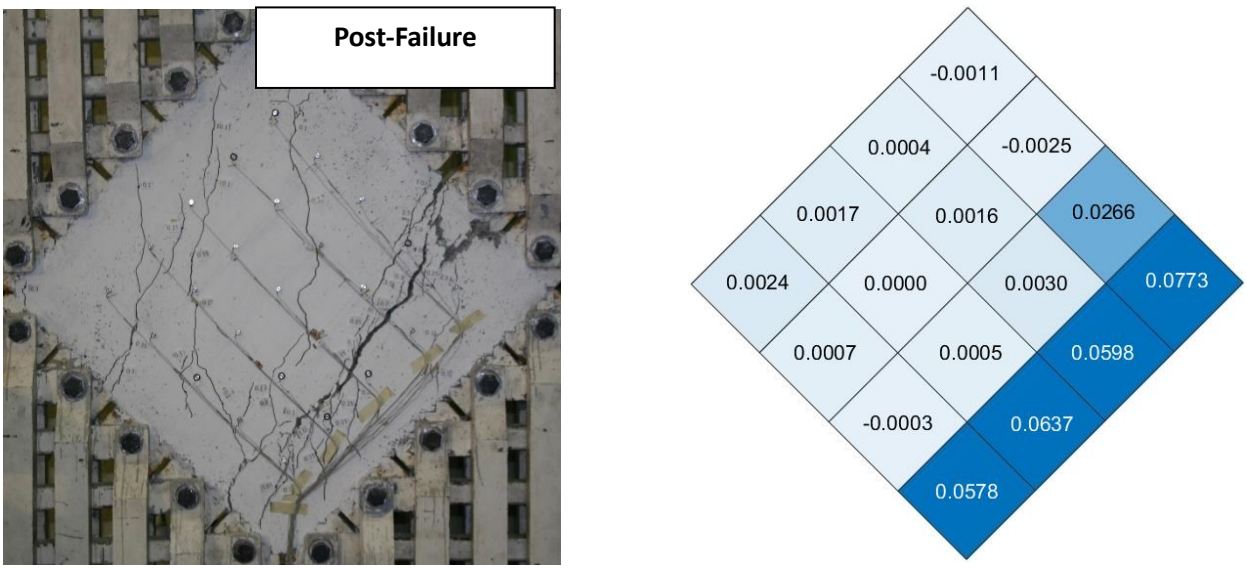

Figure A-20: PFRC-052-000 Failure Picture and Heat Map

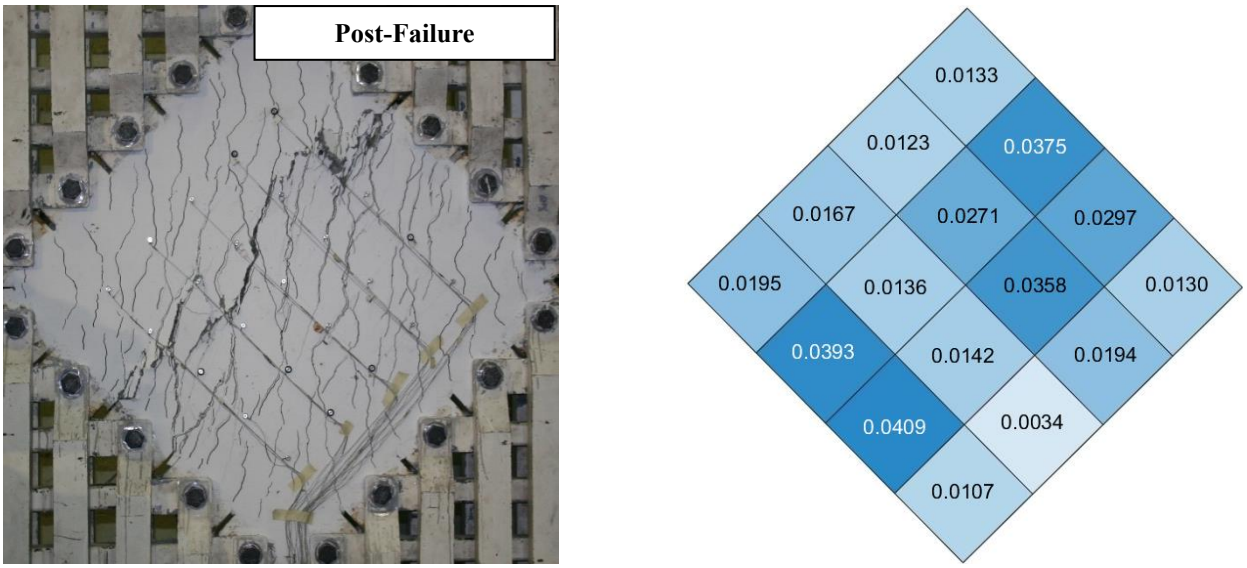

Figure A-21: PFRC-052-029 Failure Picture and Heat Map

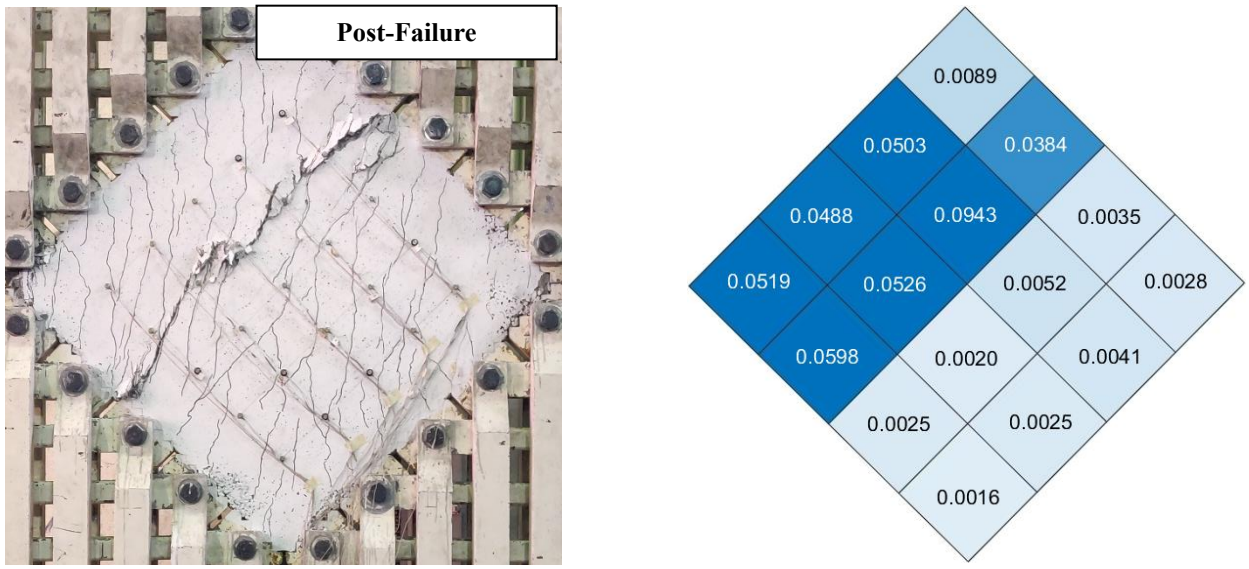

Figure A-22: PFRC-052-058 Failure Picture and Heat Map

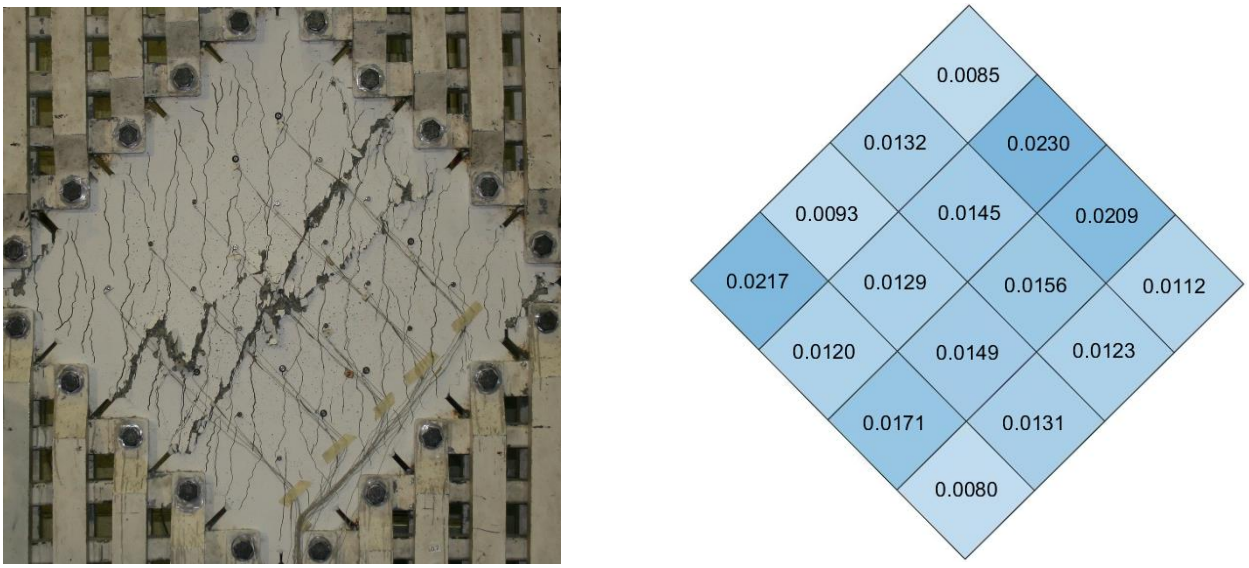

Figure A-23: PFRC-052-114 Failure Picture and Heat Map

A1.1.3 Crack Maps

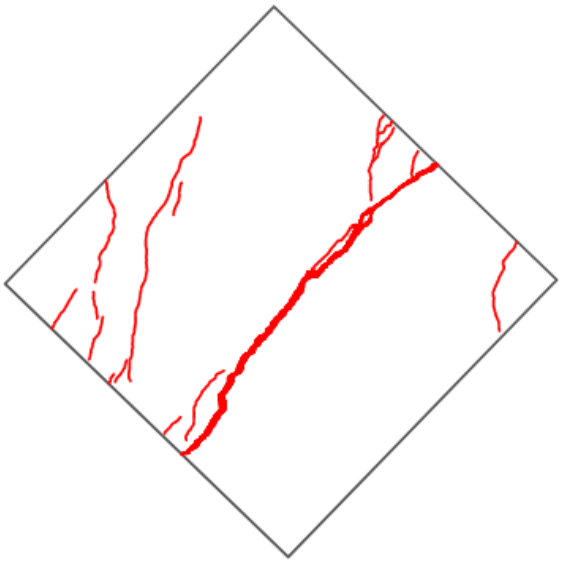

Figure A-24: PFRC-000-000 Crack Map

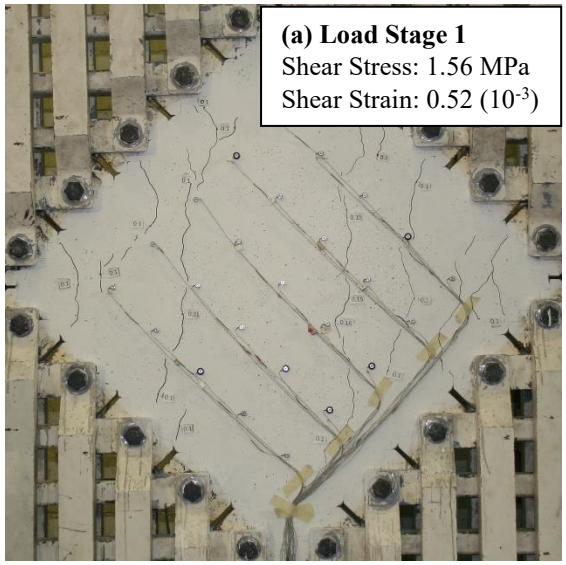

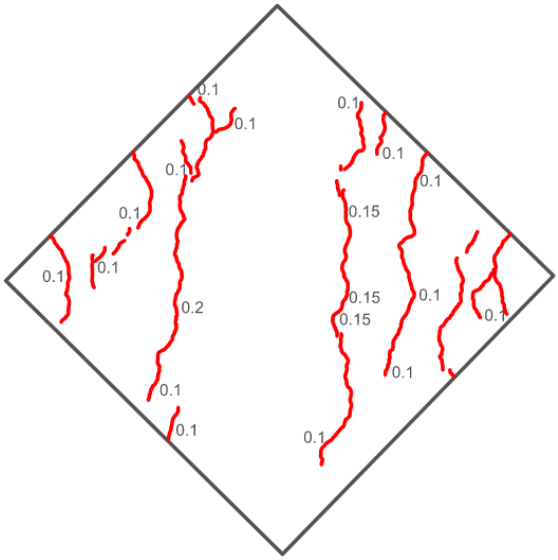

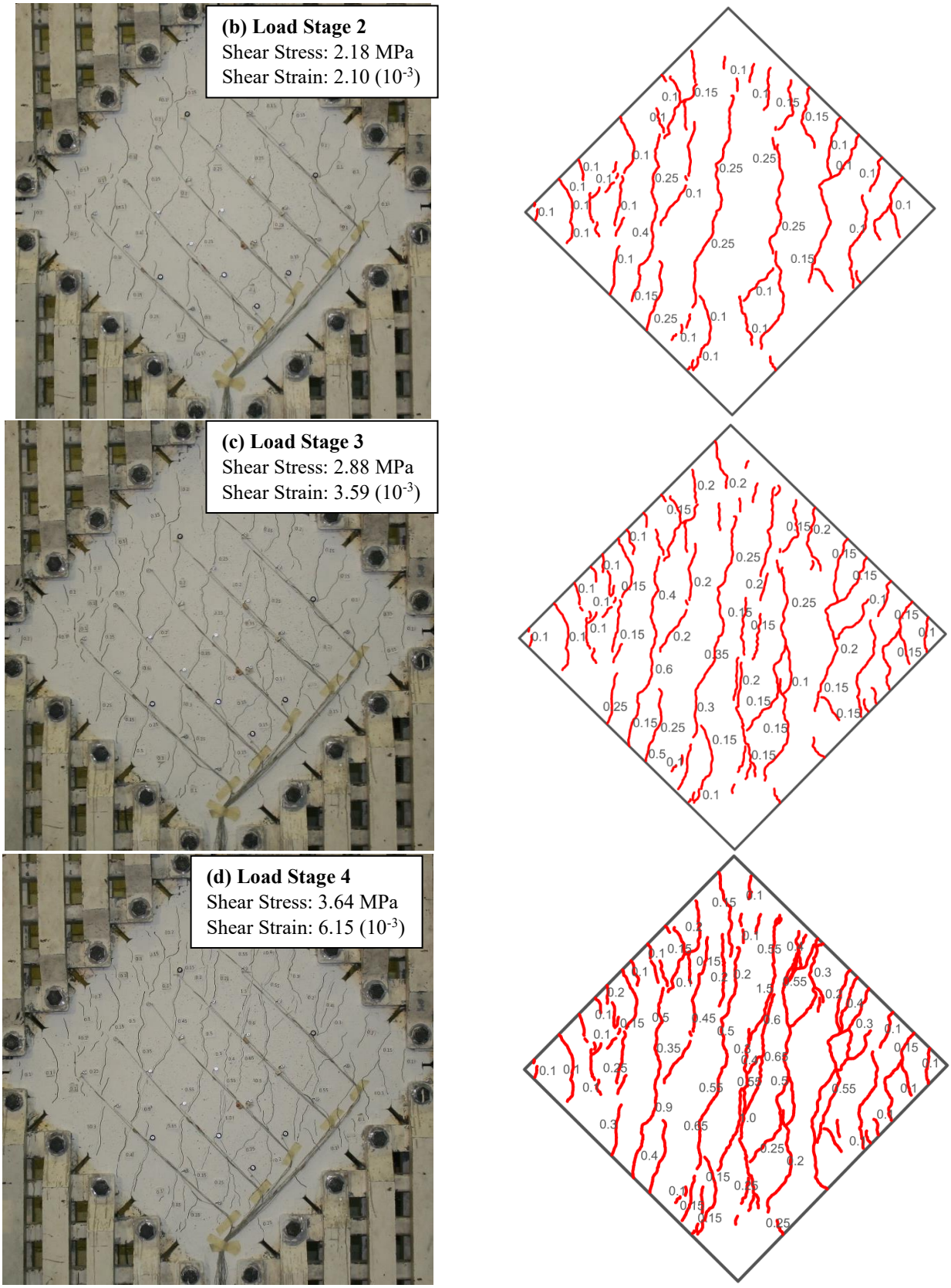

Figure A-25: PFRC-000-029 Photos and Crack Maps at Load Stages

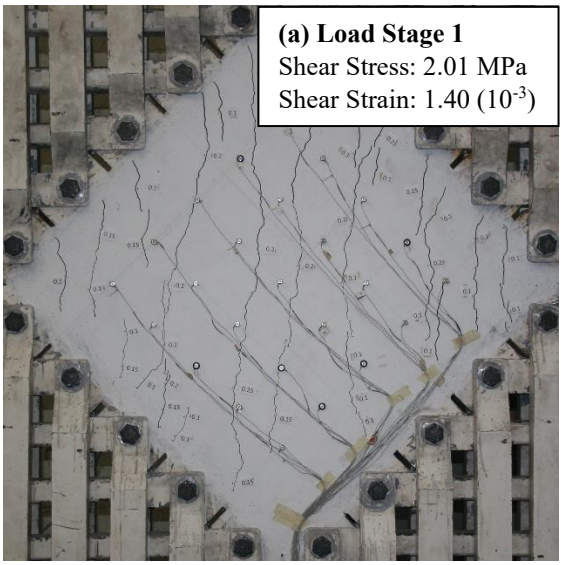

(a) Load Stage 1
Shear Stress: 2.01 MPa
Shear Strain: 1.40 (10^{-3})

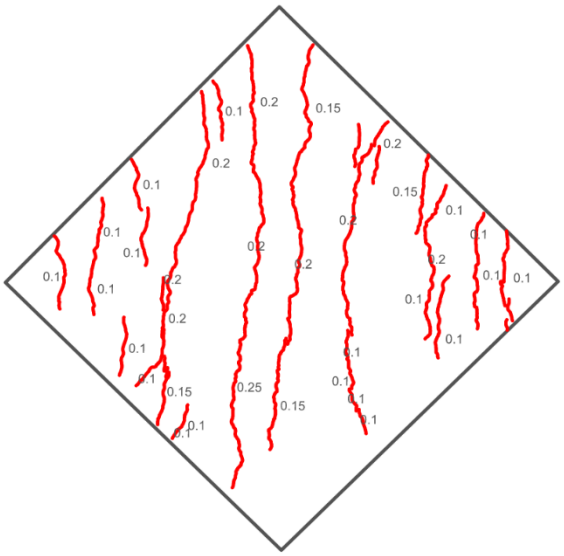

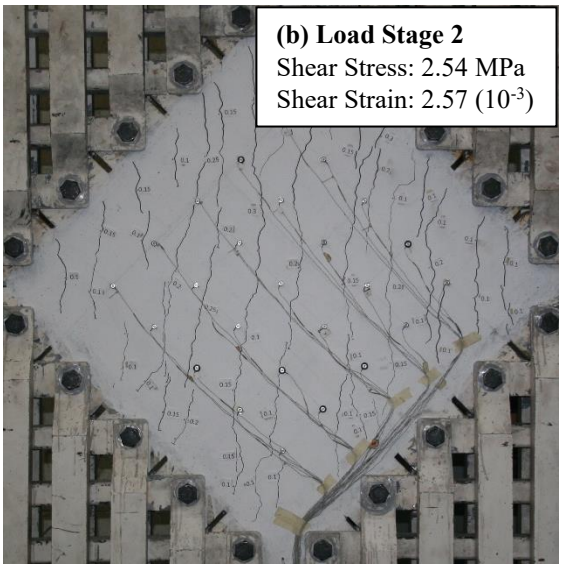

(b) Load Stage 2
Shear Stress: 2.54 MPa
Shear Strain: 2.57 (10^{-3})

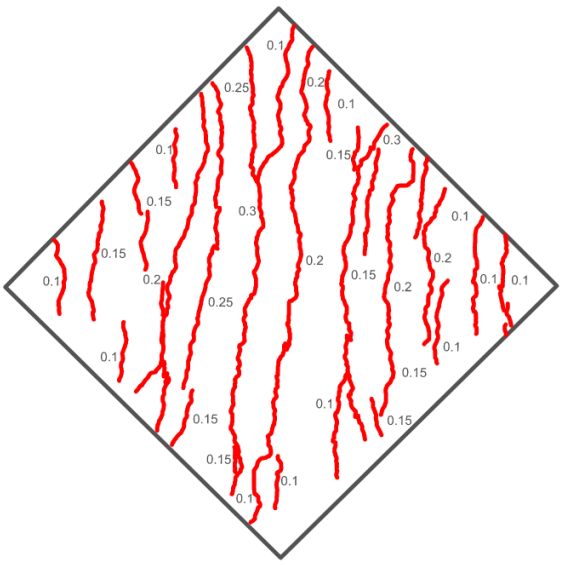

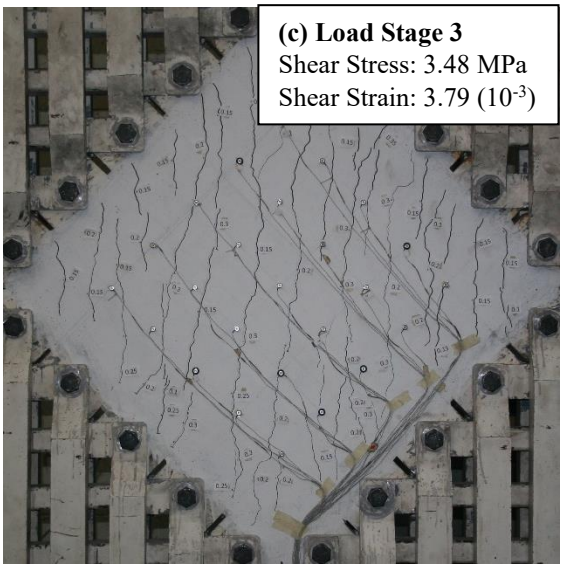

(c) Load Stage 3
Shear Stress: 3.48 MPa
Shear Strain: 3.79 (10^{-3})

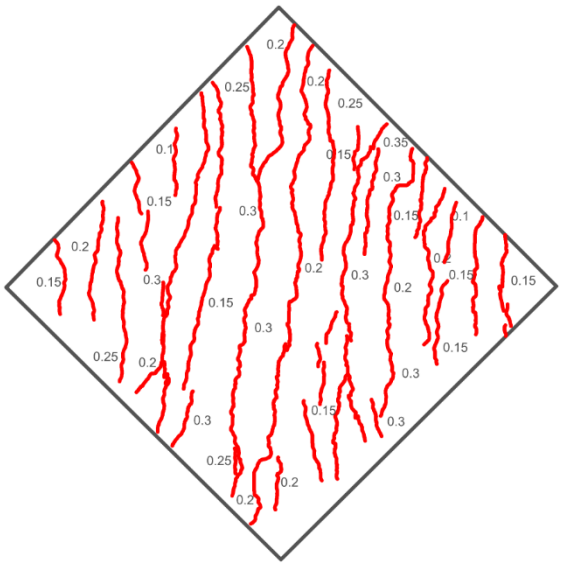

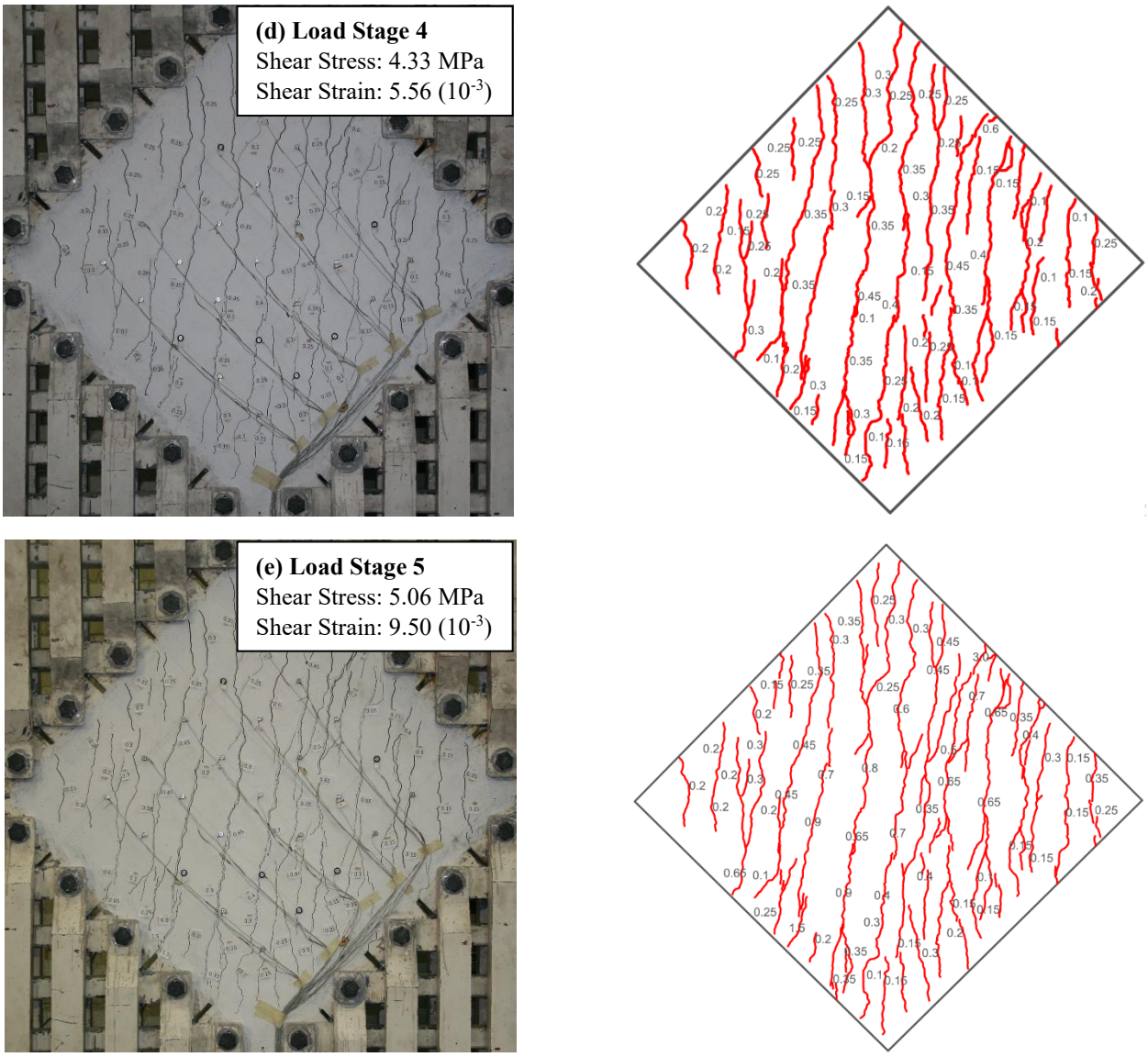

Figure A-26: PFRC-000-058 Photos and Crack Maps at Load Stages

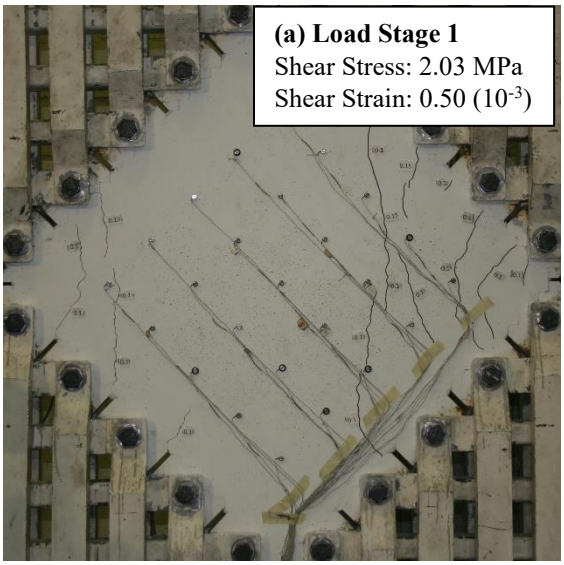

(a) Load Stage 1
Shear Stress: 2.03 MPa
Shear Strain: 0.50 (10^{-3})

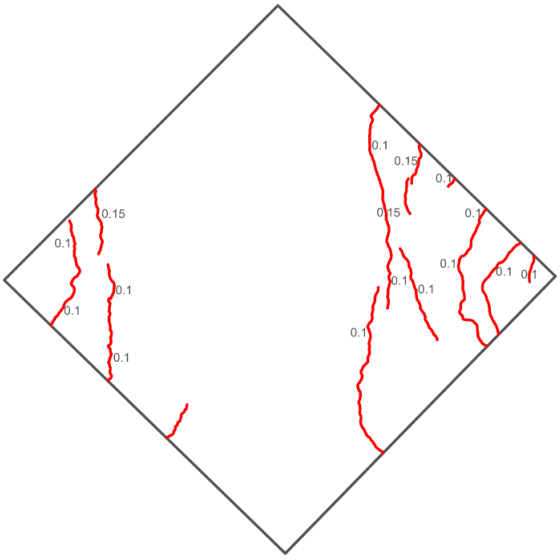

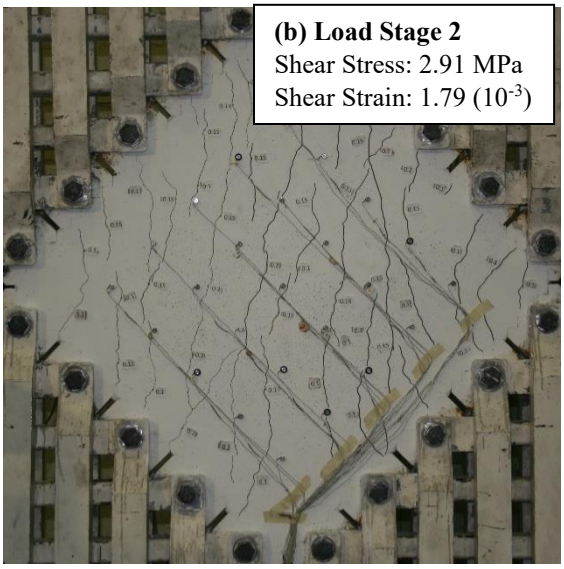

(b) Load Stage 2
Shear Stress: 2.91 MPa
Shear Strain: 1.79 (10^{-3})

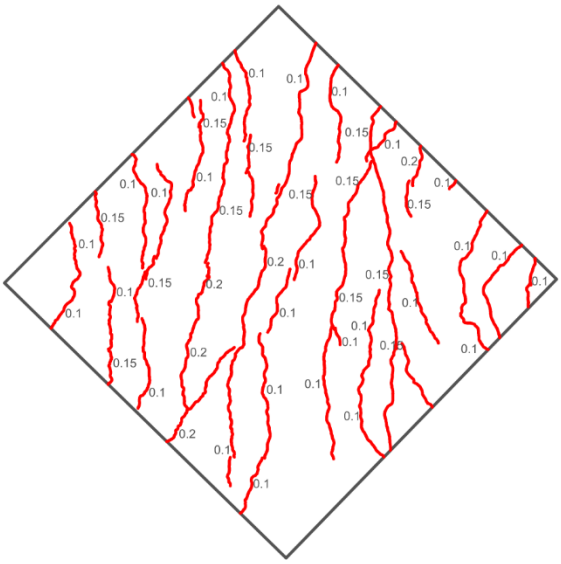

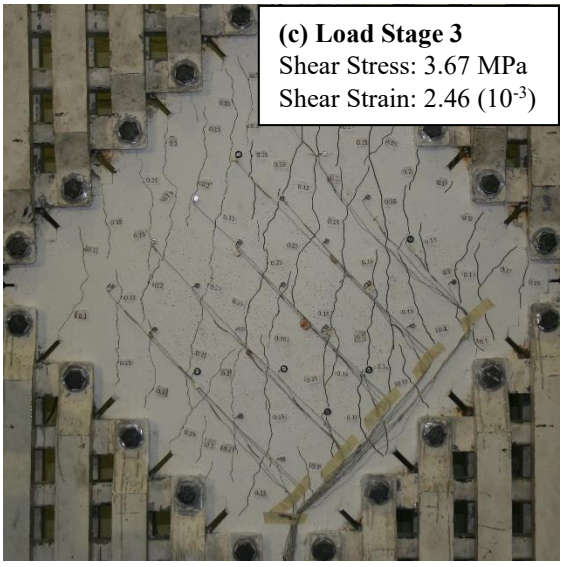

(c) Load Stage 3
Shear Stress: 3.67 MPa
Shear Strain: 2.46 (10^{-3})

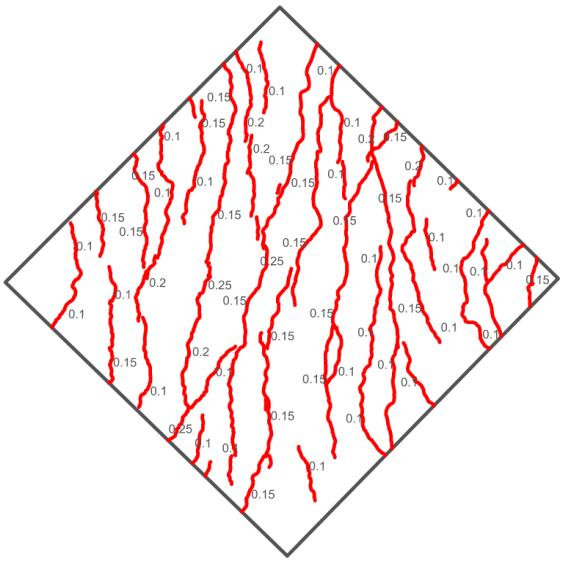

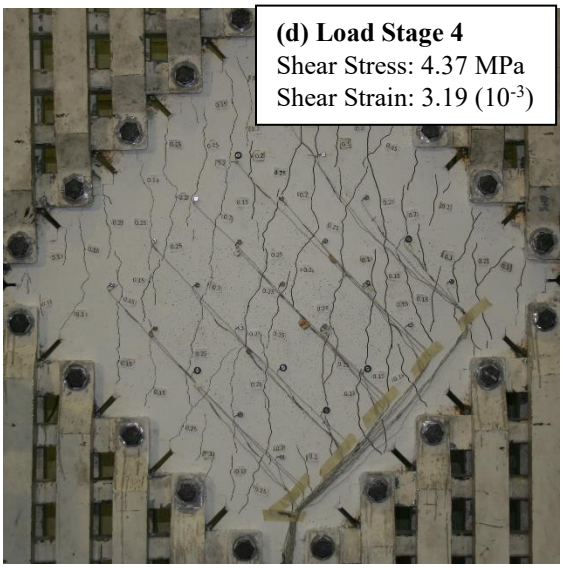

(d) Load Stage 4
Shear Stress: 4.37 MPa
Shear Strain: 3.19 (10^{-3})

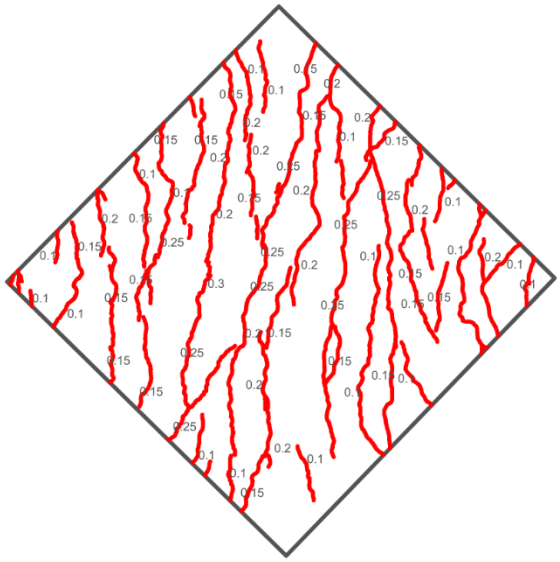

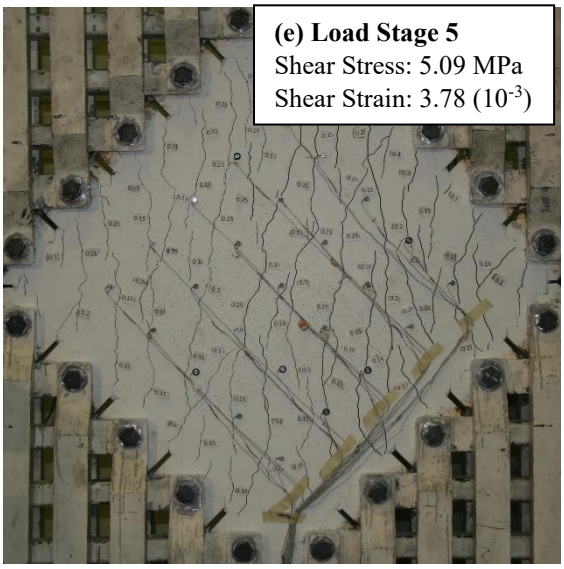

(e) Load Stage 5
Shear Stress: 5.09 MPa
Shear Strain: 3.78 (10^{-3})

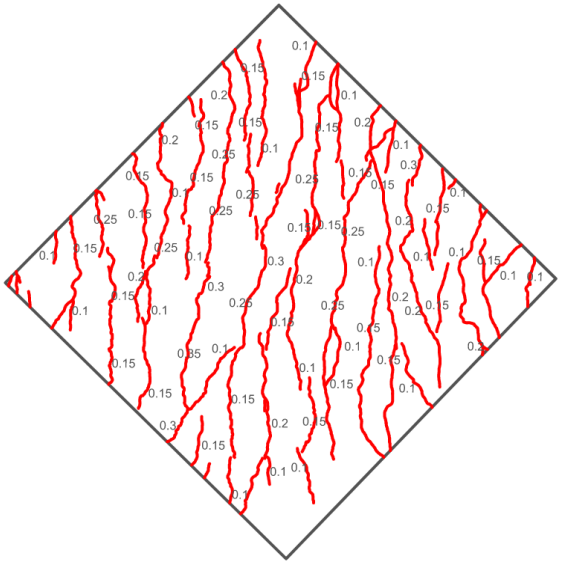

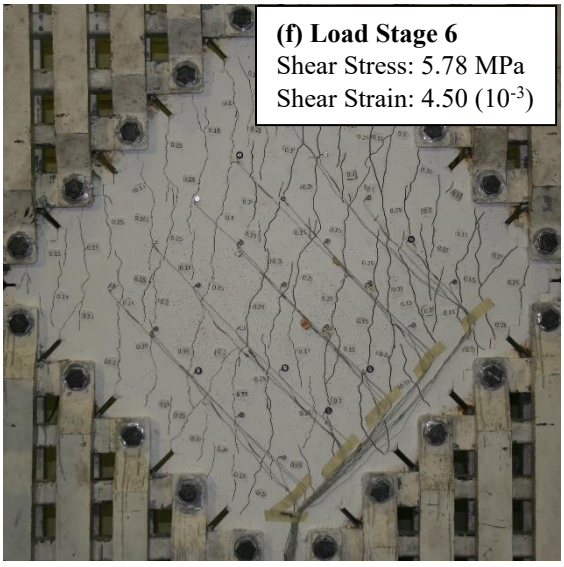

(f) Load Stage 6
Shear Stress: 5.78 MPa
Shear Strain: 4.50 (10^{-3})

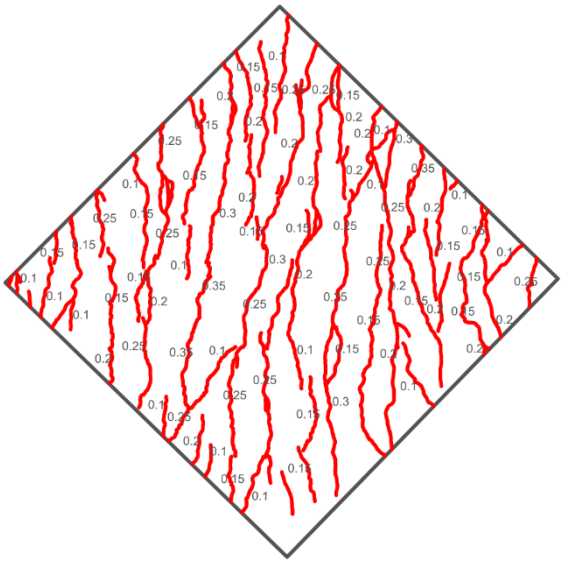

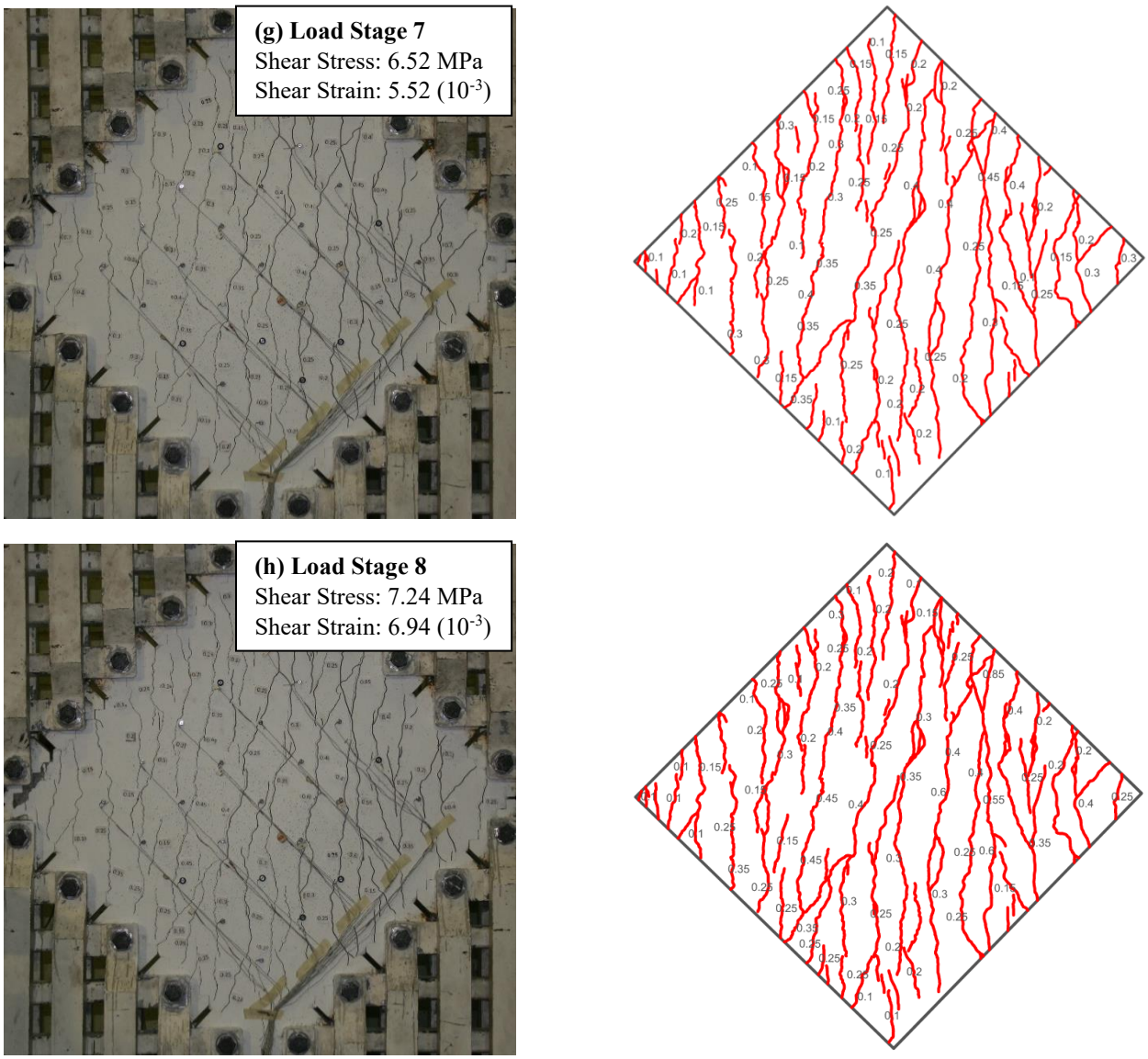

Figure A-27: PFRC-000-114 Photos and Crack Maps at Load Stages

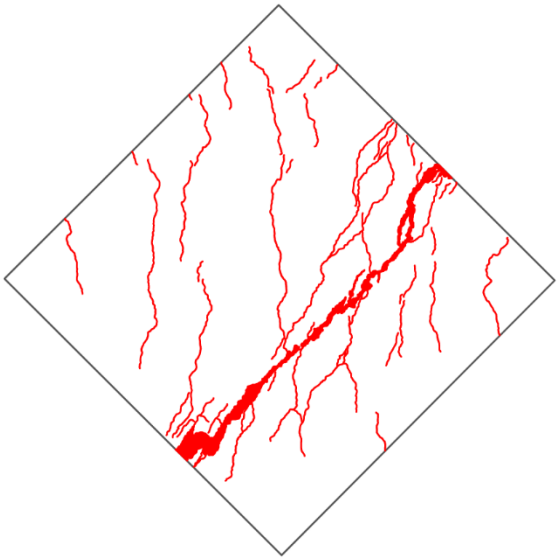

Figure A-28: PFRC-026-000 Crack Map

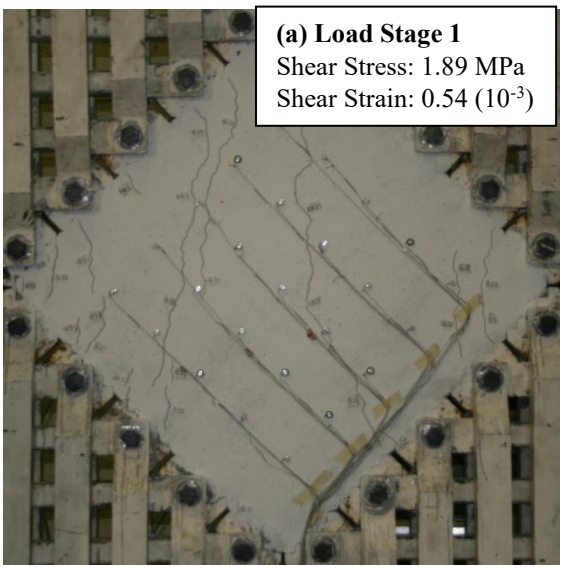

(a) Load Stage 1
Shear Stress: 1.89 MPa
Shear Strain: 0.54 (10^{-3})

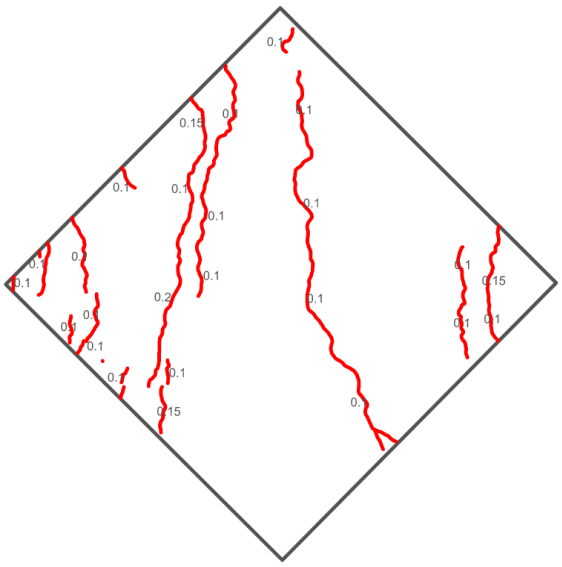

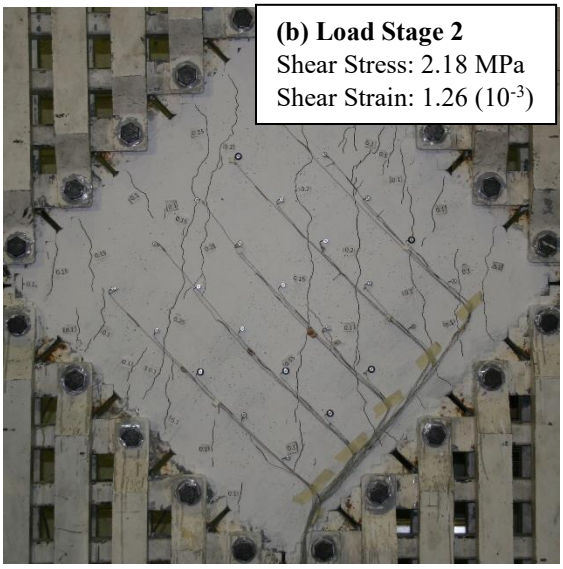

(b) Load Stage 2
Shear Stress: 2.18 MPa
Shear Strain: 1.26 (10^{-3})

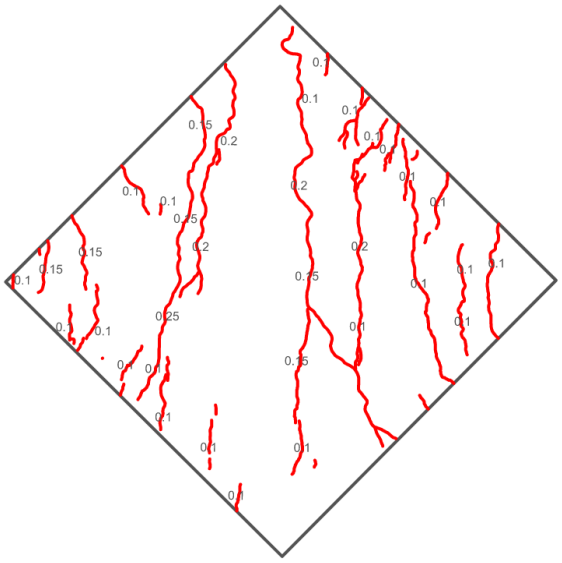

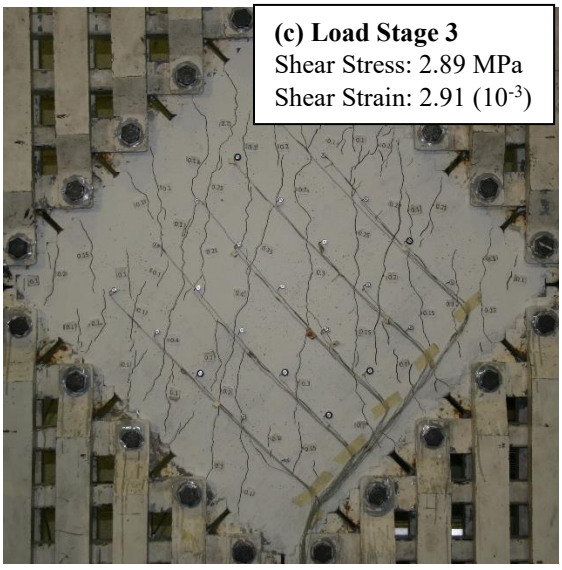

(c) Load Stage 3
Shear Stress: 2.89 MPa
Shear Strain: 2.91 (10^{-3})

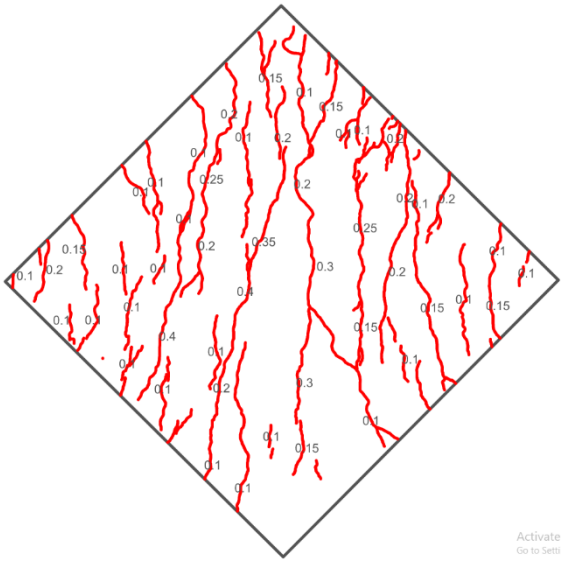

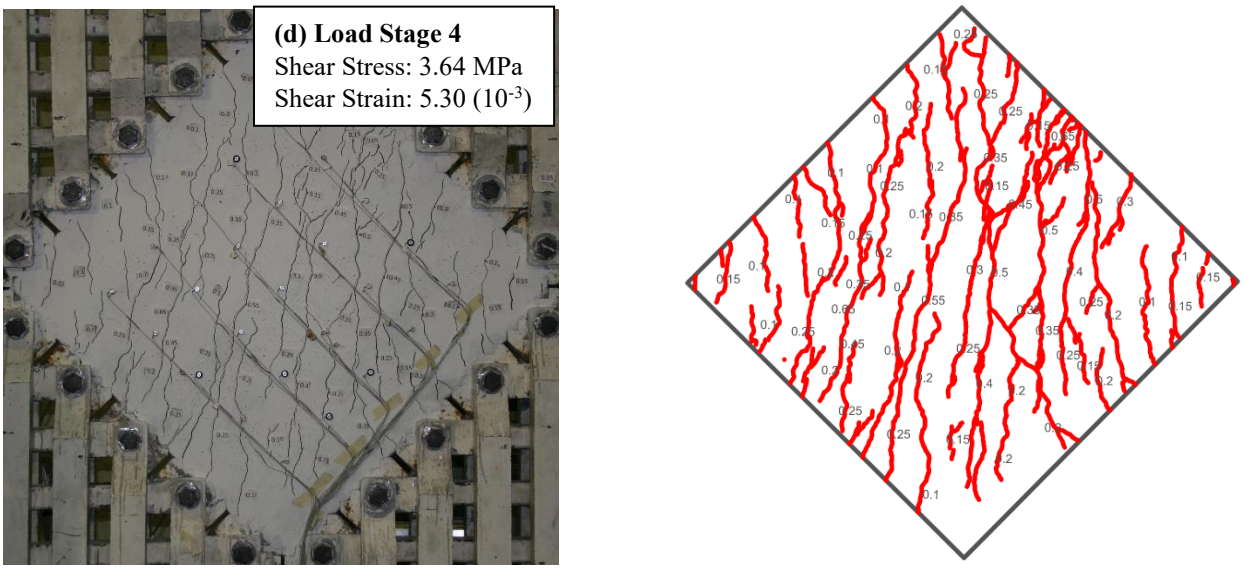

Figure A-29: PFRC-026-029 Photos and Crack Maps at Load Stages

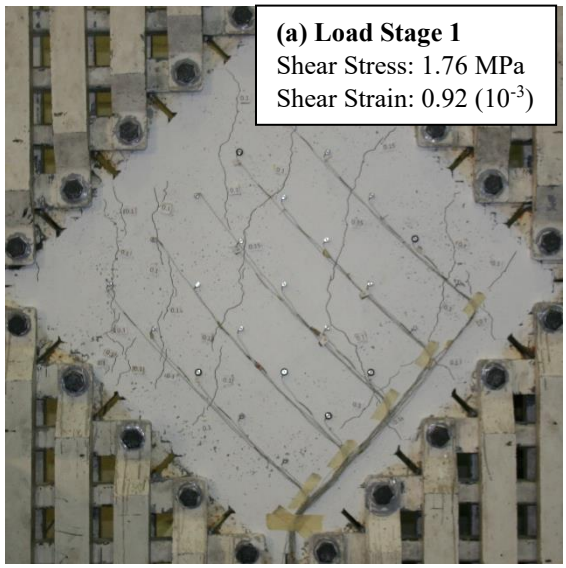
(a) Load Stage 1
Shear Stress: 1.76 MPa
Shear Strain: 0.92 (10^{-3})

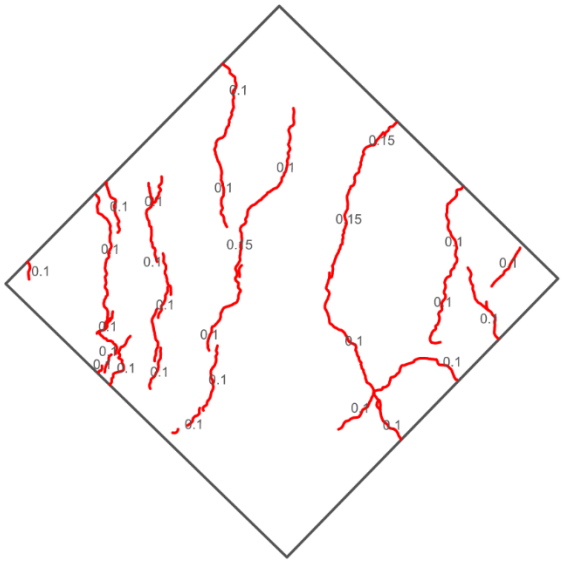

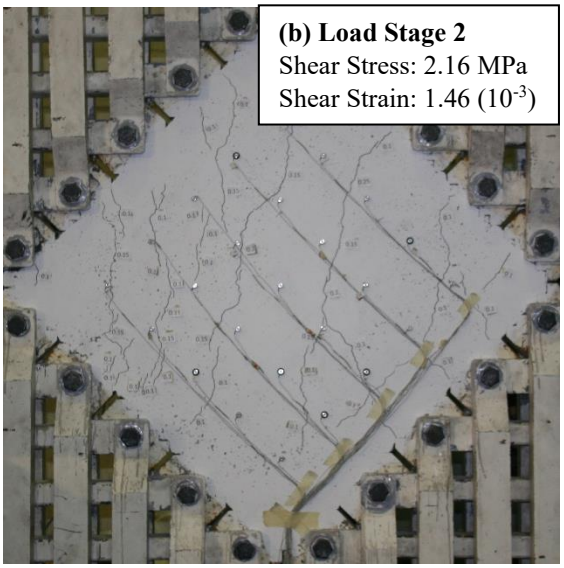
(b) Load Stage 2
Shear Stress: 2.16 MPa
Shear Strain: 1.46 (10^{-3})

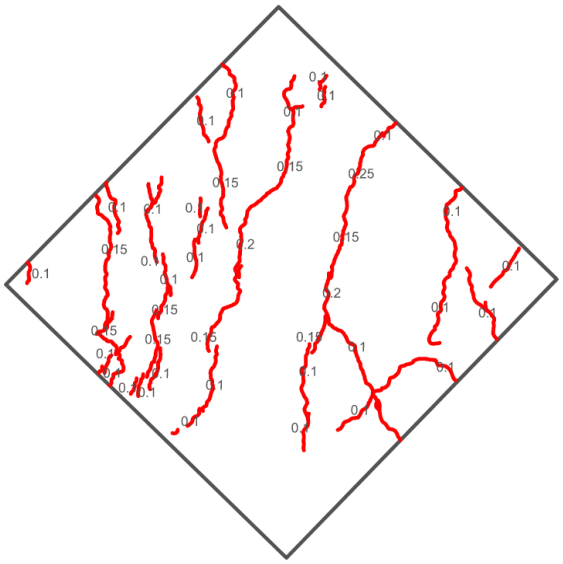

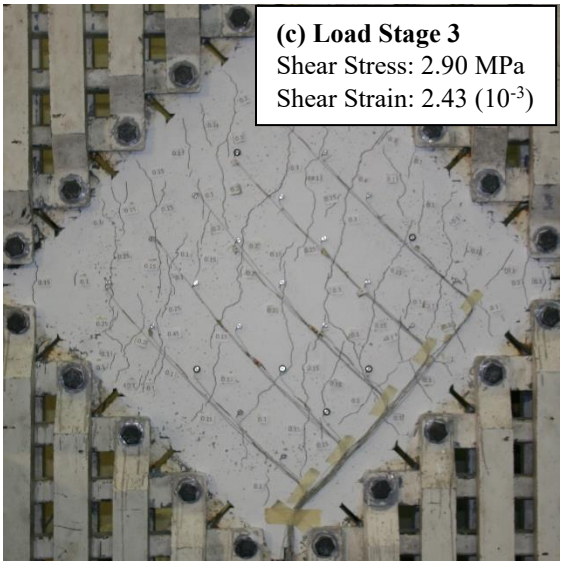
(c) Load Stage 3
Shear Stress: 2.90 MPa
Shear Strain: 2.43 (10^{-3})

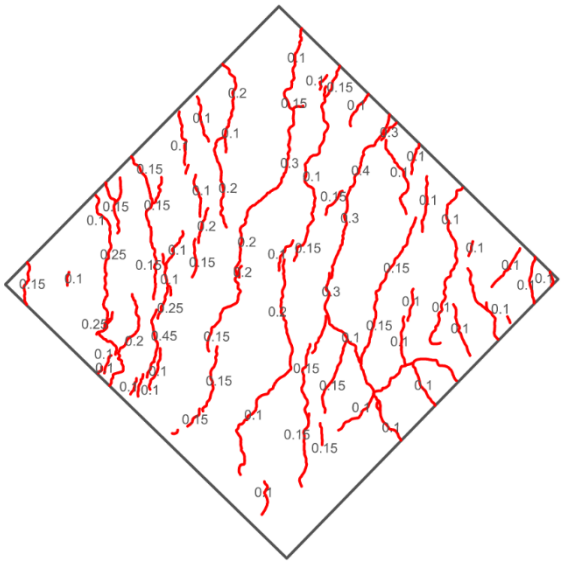

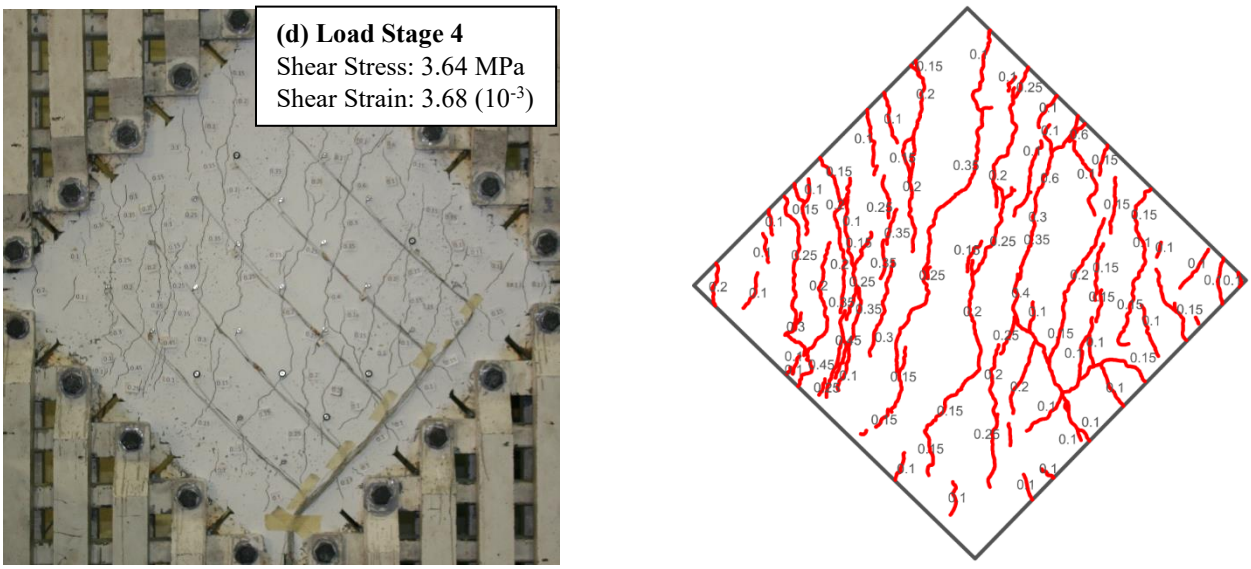

Figure A-30: PFCR-026-058 Photos and Crack Maps at Load Stages

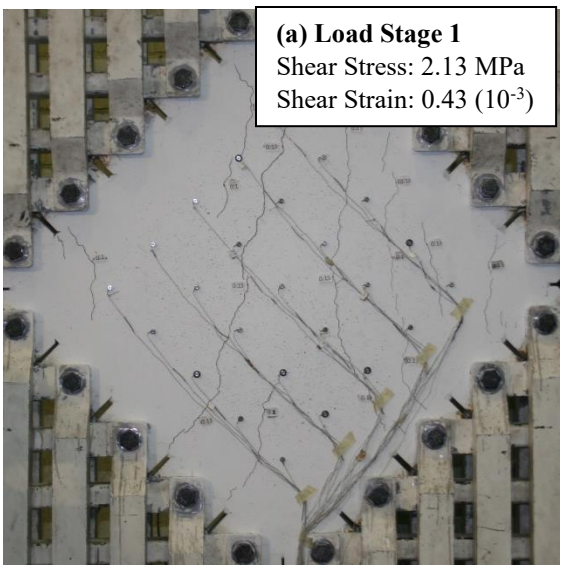

(a) Load Stage 1
Shear Stress: 2.13 MPa
Shear Strain: 0.43 (10^{-3})

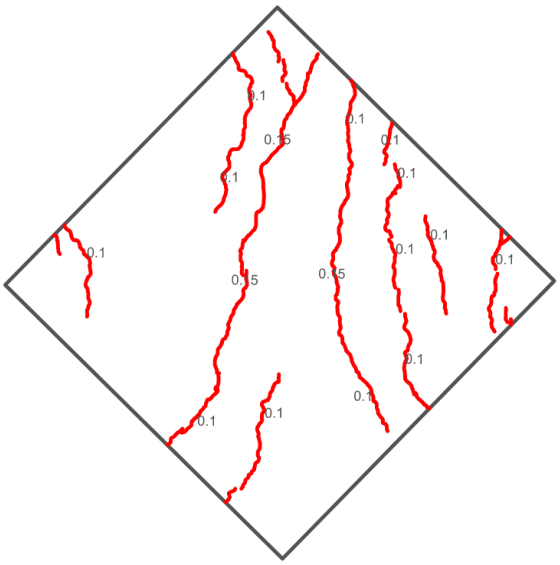

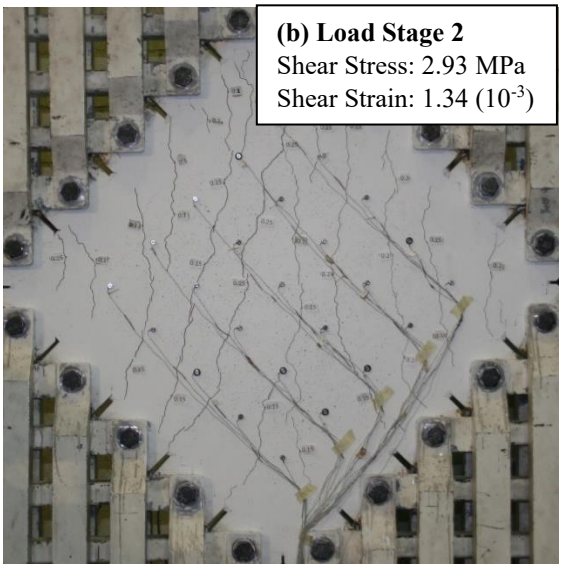

(b) Load Stage 2
Shear Stress: 2.93 MPa
Shear Strain: 1.34 (10^{-3})

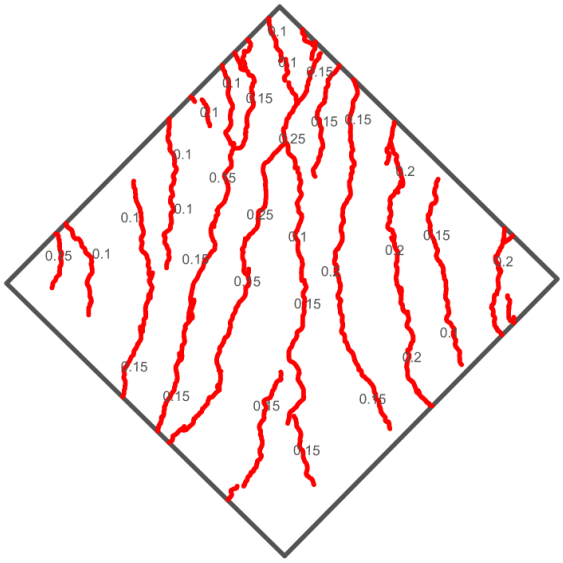

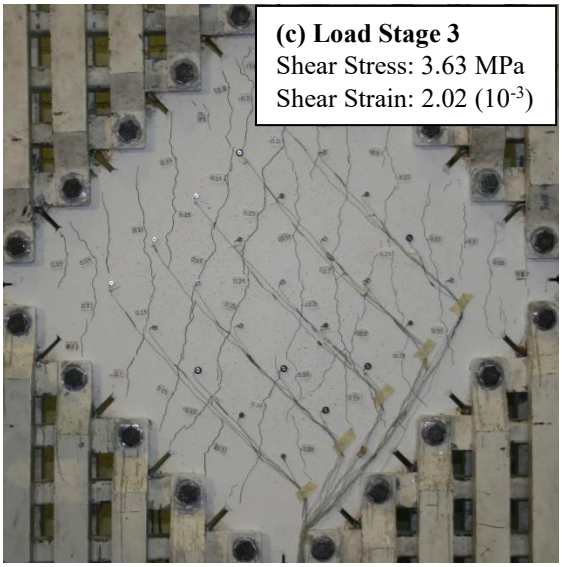

(c) Load Stage 3
Shear Stress: 3.63 MPa
Shear Strain: 2.02 (10^{-3})

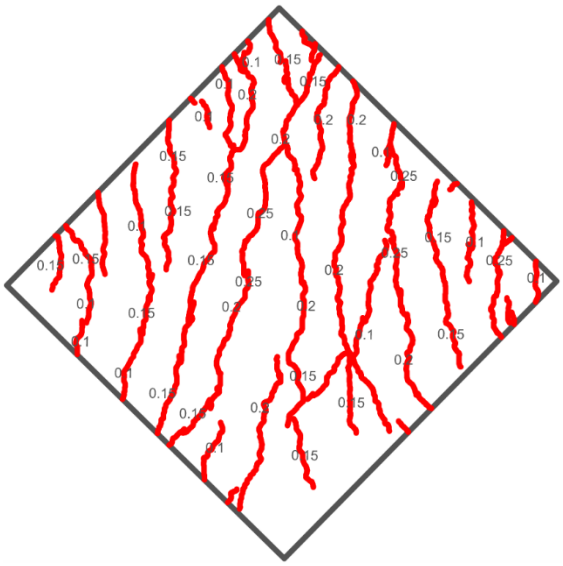

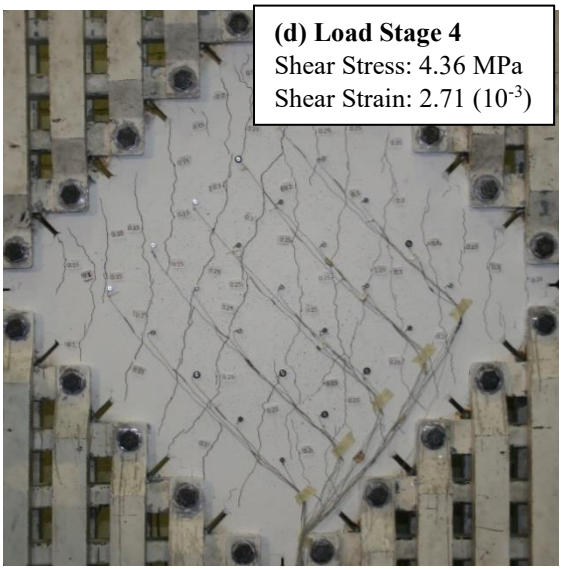

(d) Load Stage 4
Shear Stress: 4.36 MPa
Shear Strain: 2.71 (10^{-3})

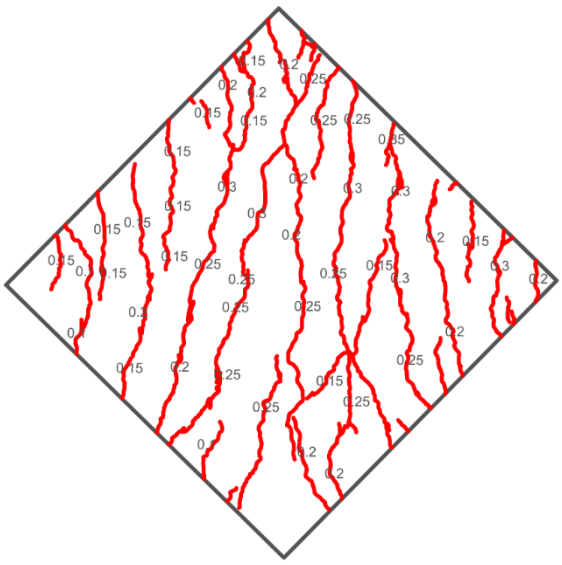

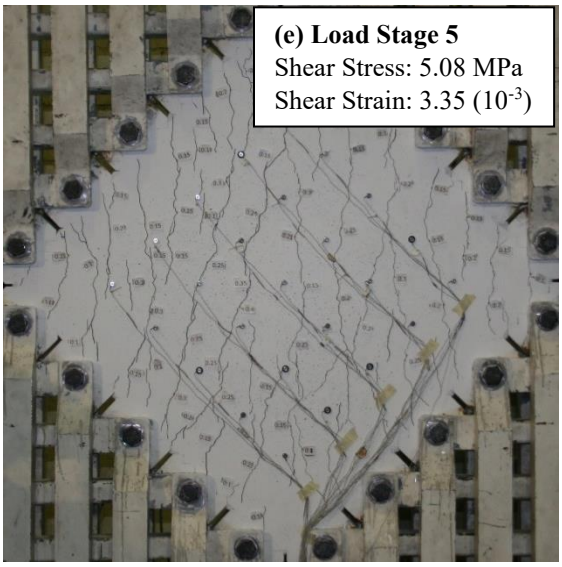

(e) Load Stage 5
Shear Stress: 5.08 MPa
Shear Strain: 3.35 (10^{-3})

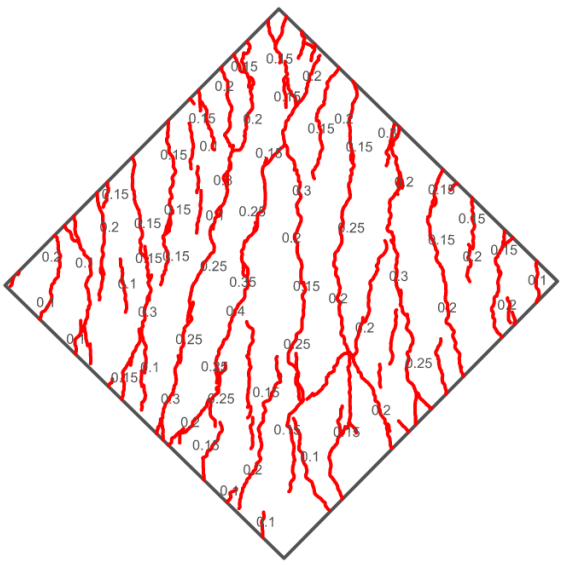

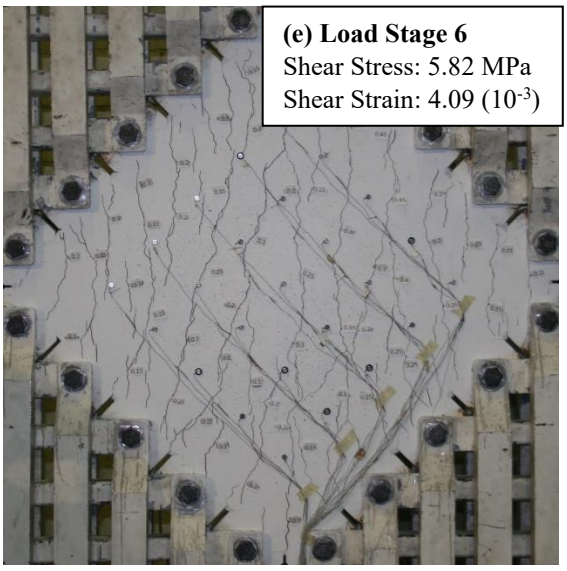

(e) Load Stage 6
Shear Stress: 5.82 MPa
Shear Strain: 4.09 (10^{-3})

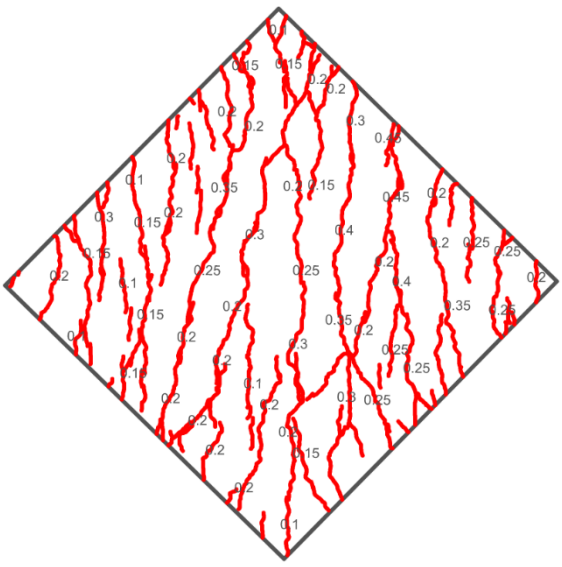

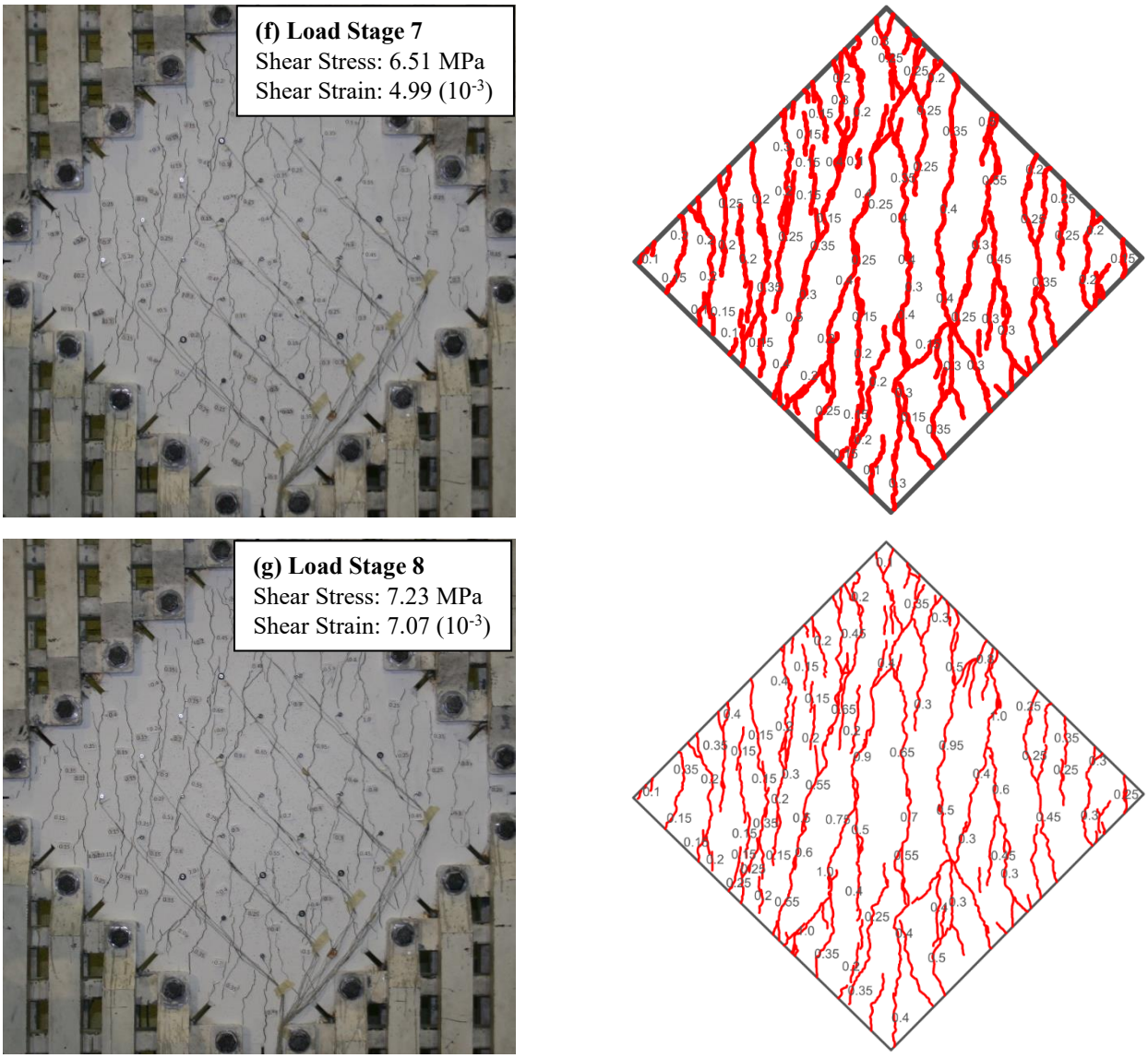

Figure A-31: PFRC-026-114 Photos and Crack Maps at Load Stages

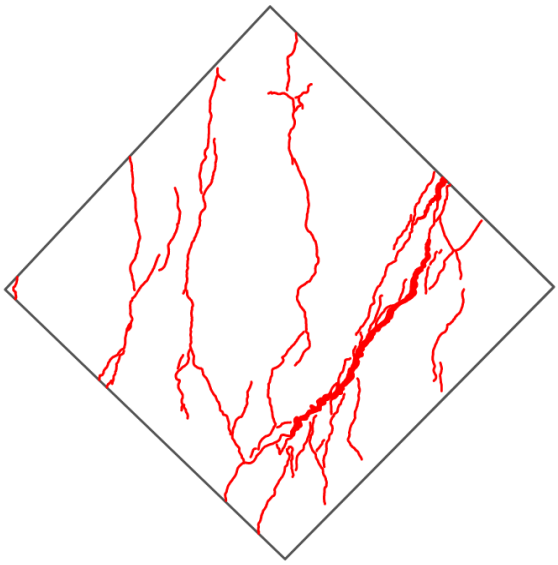

Figure A-32: PFRC-052-000 Crack Map

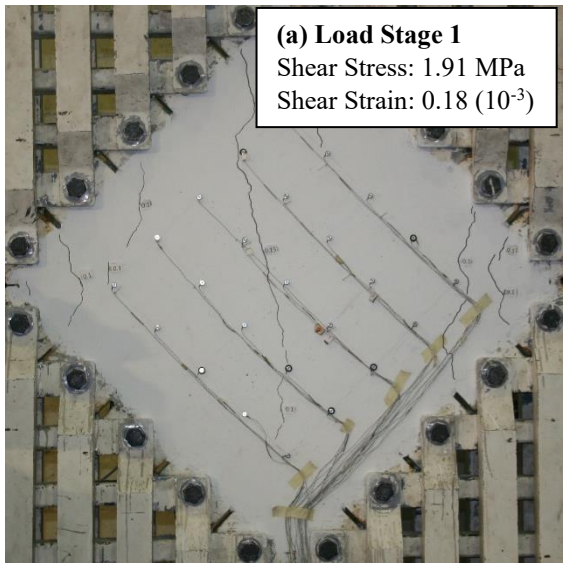

(a) Load Stage 1
Shear Stress: 1.91 MPa
Shear Strain: 0.18 (10^{-3})

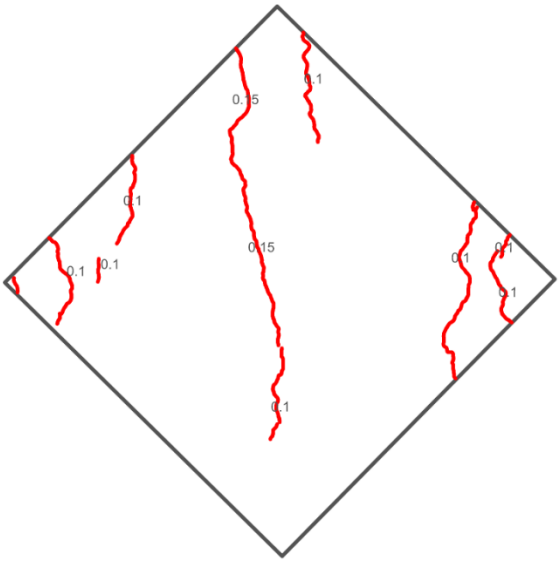

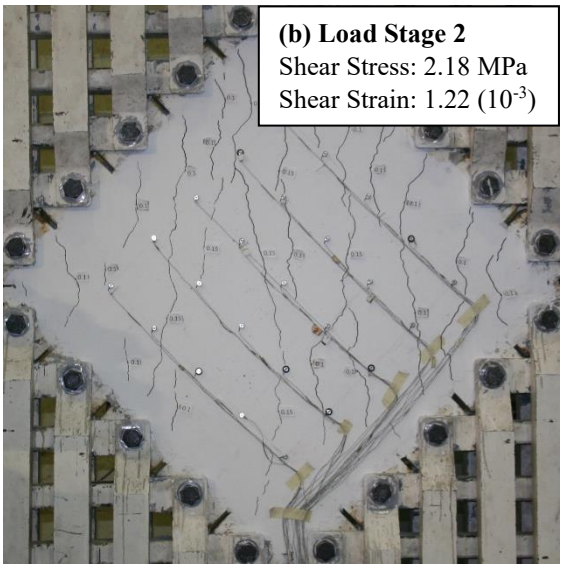

(b) Load Stage 2
Shear Stress: 2.18 MPa
Shear Strain: 1.22 (10^{-3})

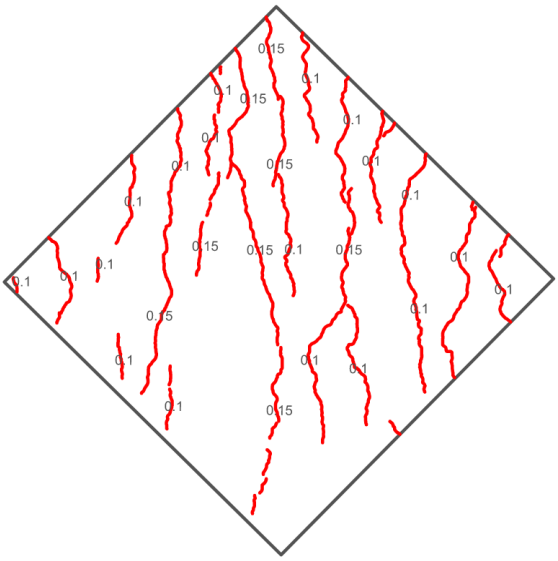

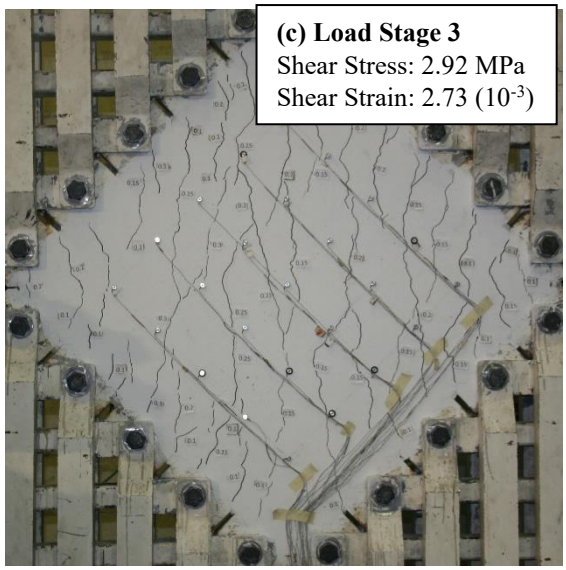

(c) Load Stage 3
Shear Stress: 2.92 MPa
Shear Strain: 2.73 (10^{-3})

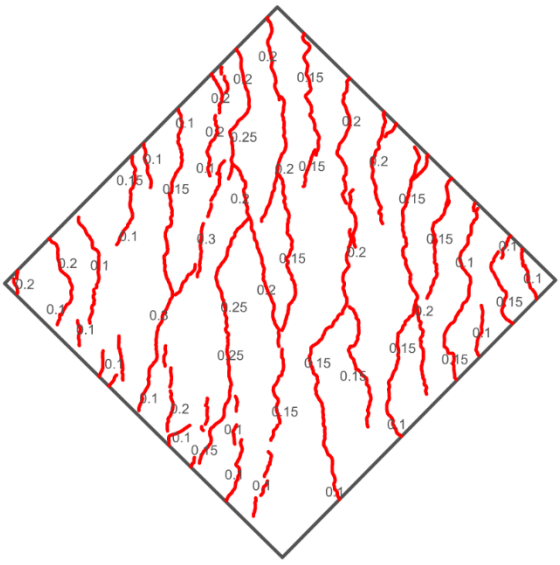

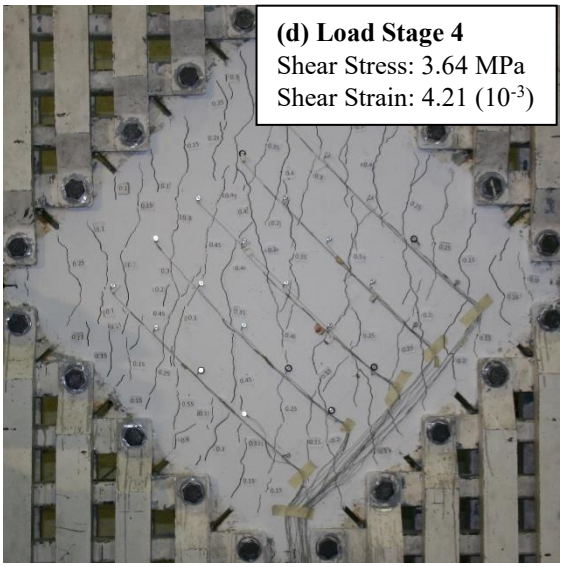

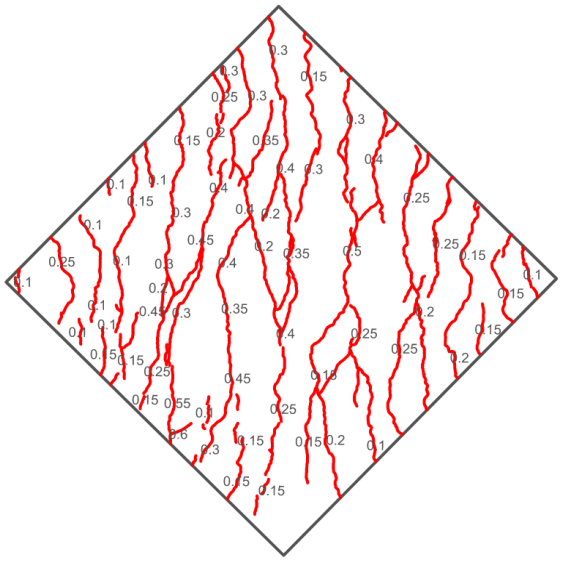

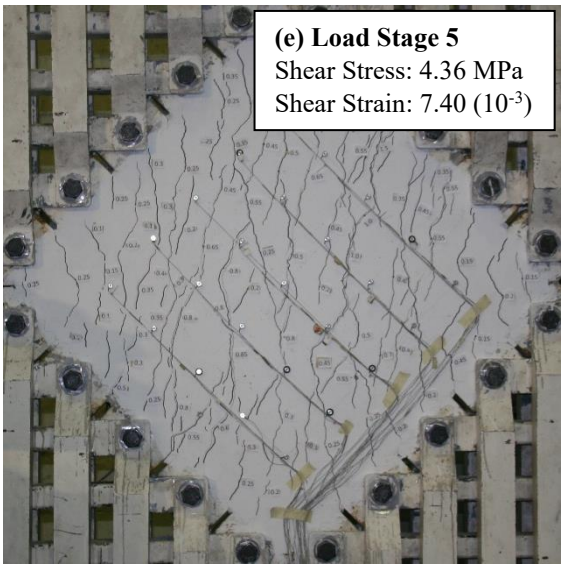

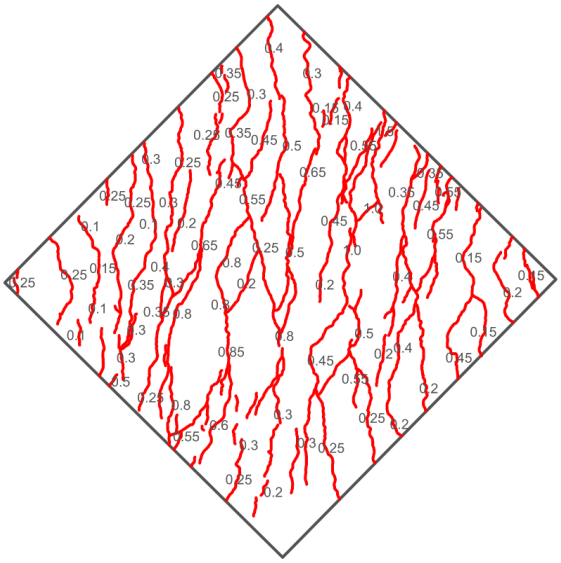

Figure A-33: PFRC-052-029 Photos and Crack Maps at Load Stages

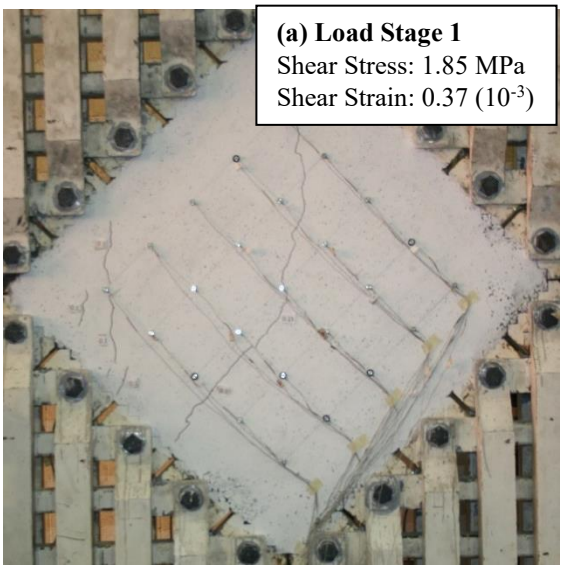

(a) Load Stage 1
Shear Stress: 1.85 MPa
Shear Strain: 0.37 (10^{-3})

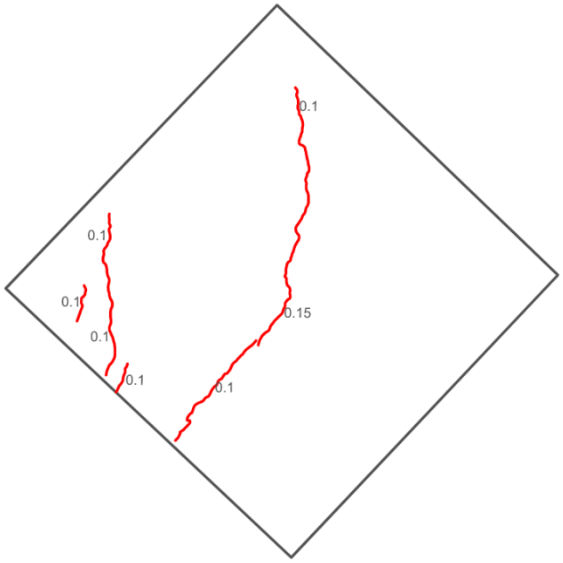

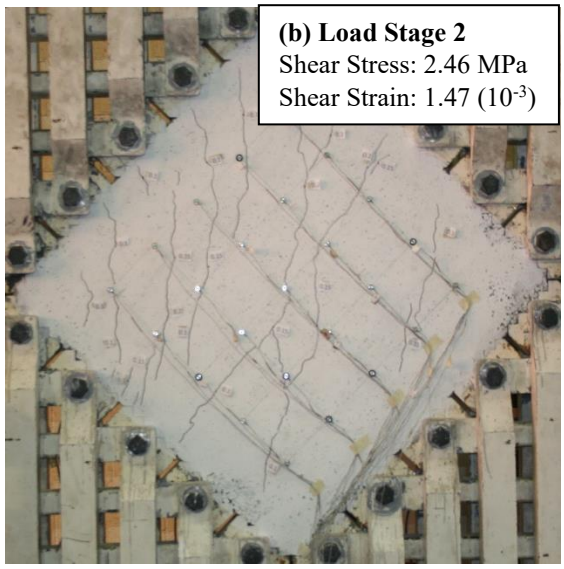

(b) Load Stage 2
Shear Stress: 2.46 MPa
Shear Strain: 1.47 (10^{-3})

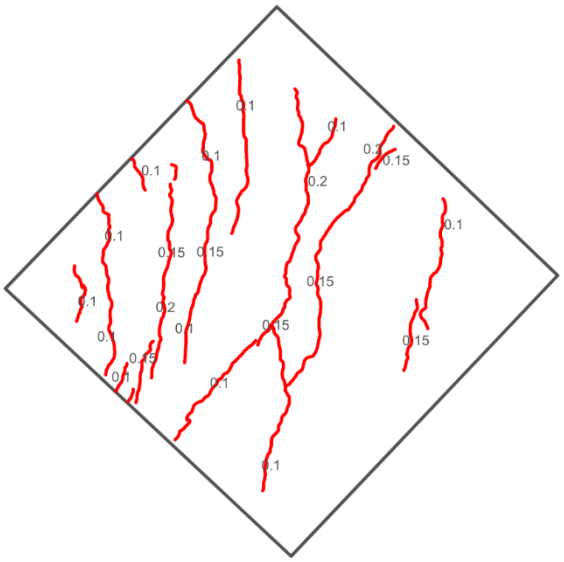

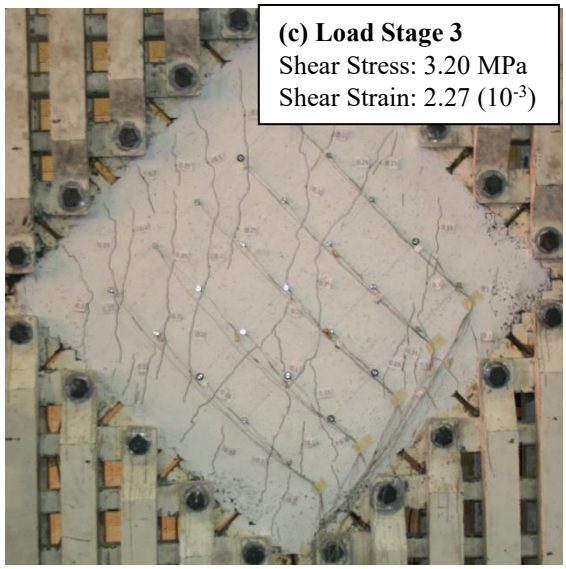

(c) Load Stage 3
Shear Stress: 3.20 MPa
Shear Strain: 2.27 (10^{-3})

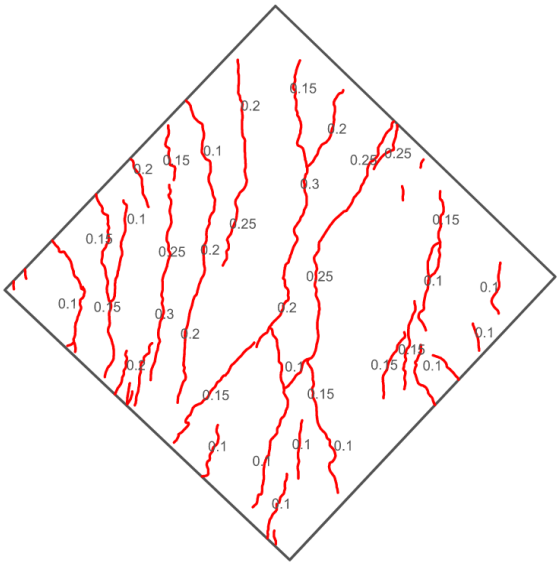

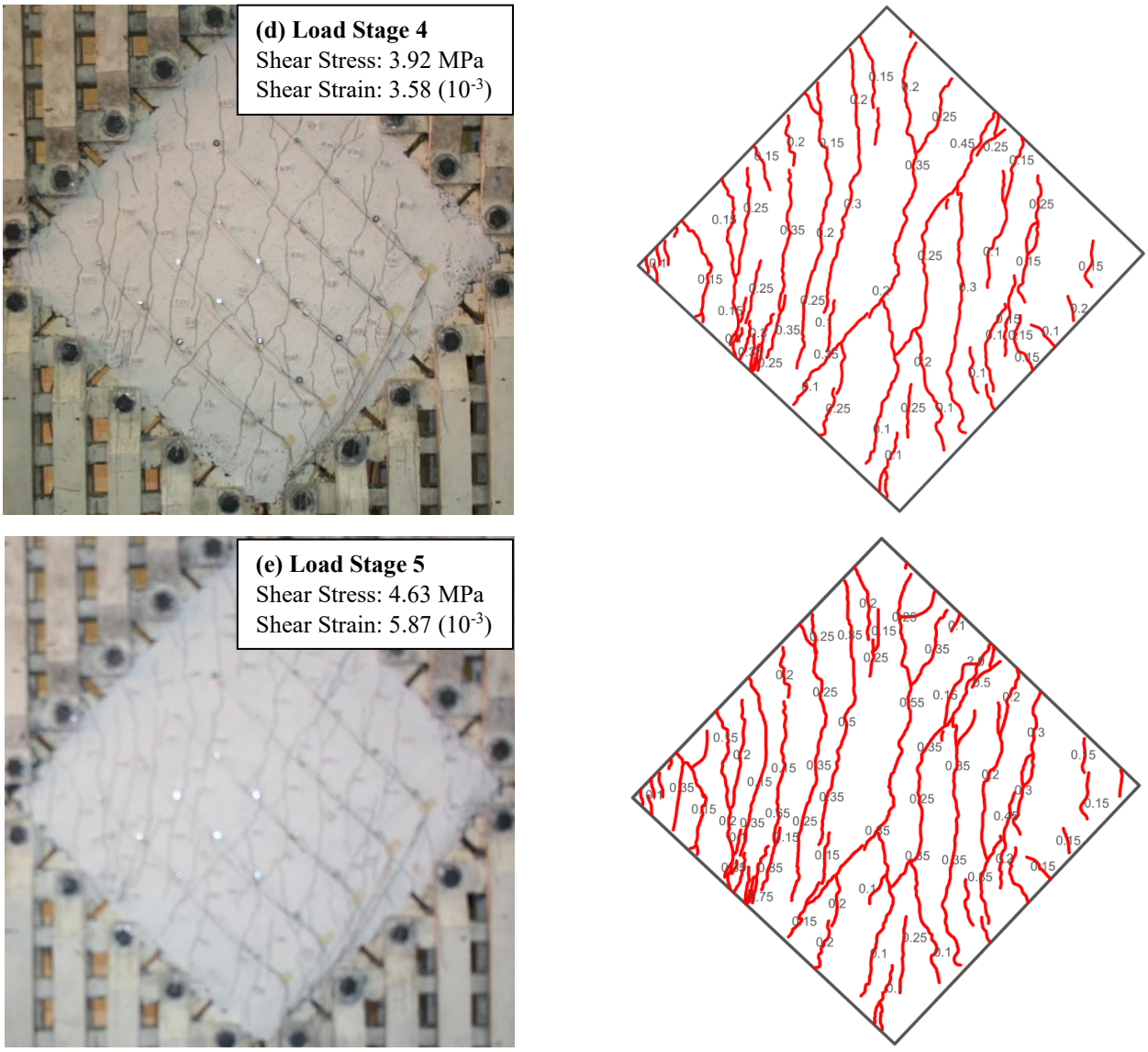

Figure A-34: PFRC-052-058 Photos and Crack Maps at Load Stages

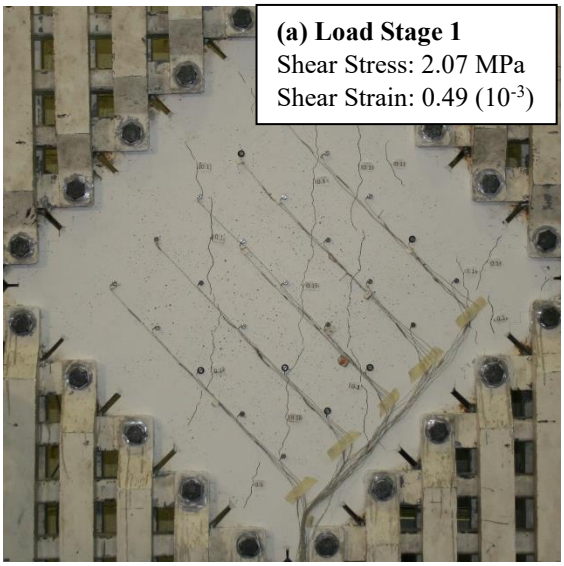

(a) Load Stage 1
Shear Stress: 2.07 MPa
Shear Strain: 0.49 (10^{-3})

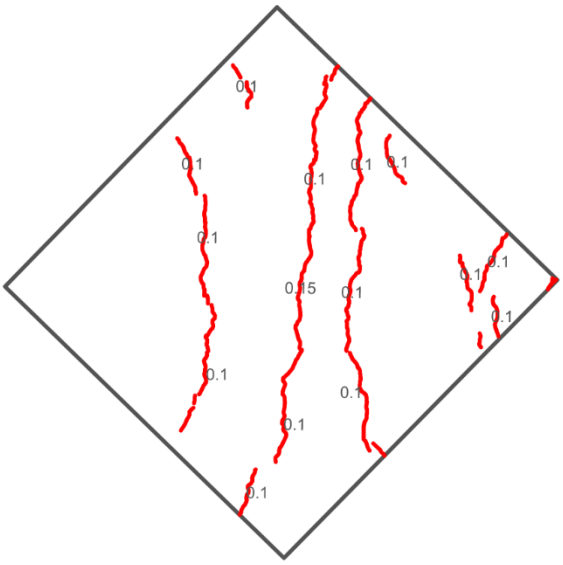

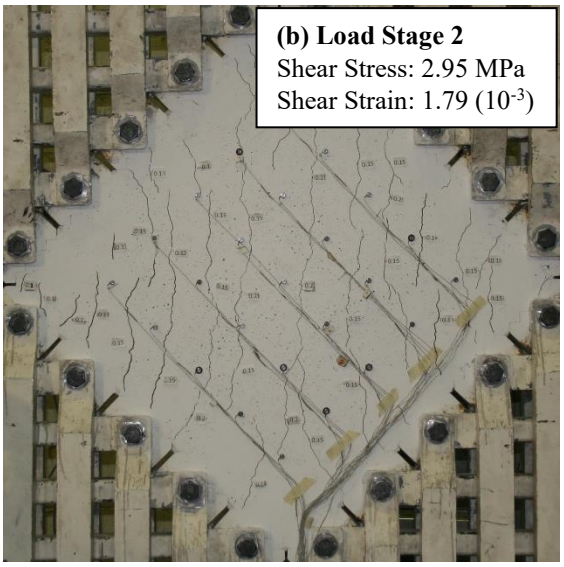

(b) Load Stage 2
Shear Stress: 2.95 MPa
Shear Strain: 1.79 (10^{-3})

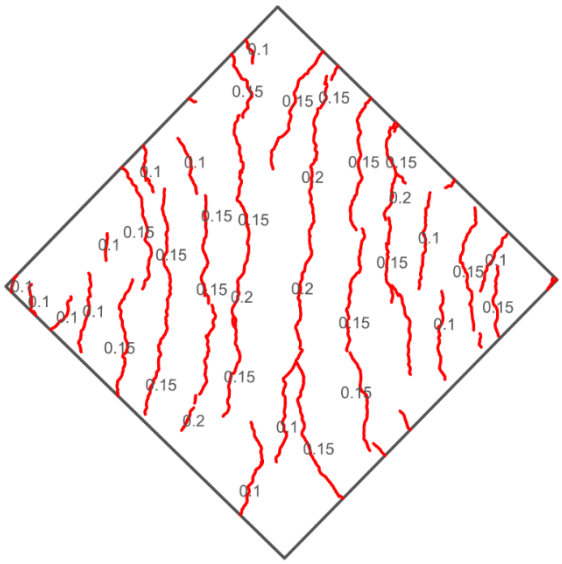

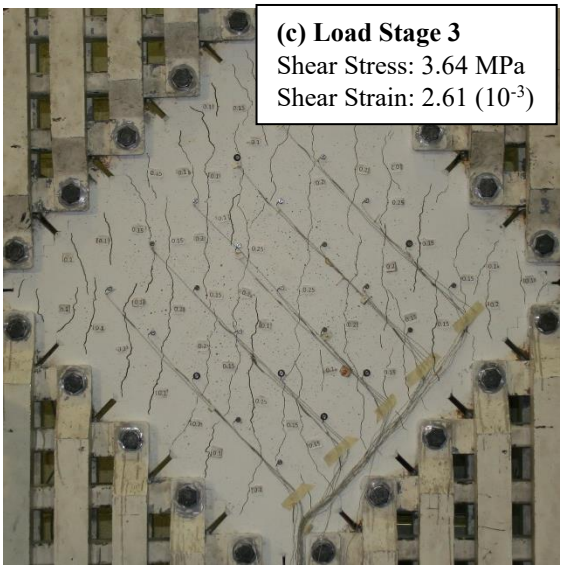

(c) Load Stage 3
Shear Stress: 3.64 MPa
Shear Strain: 2.61 (10^{-3})

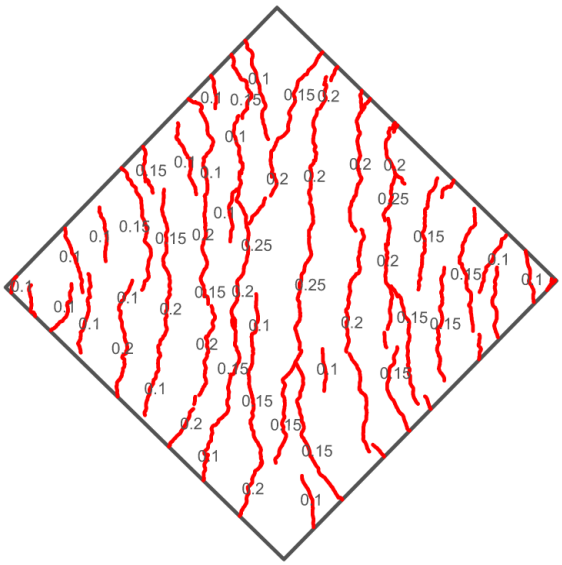

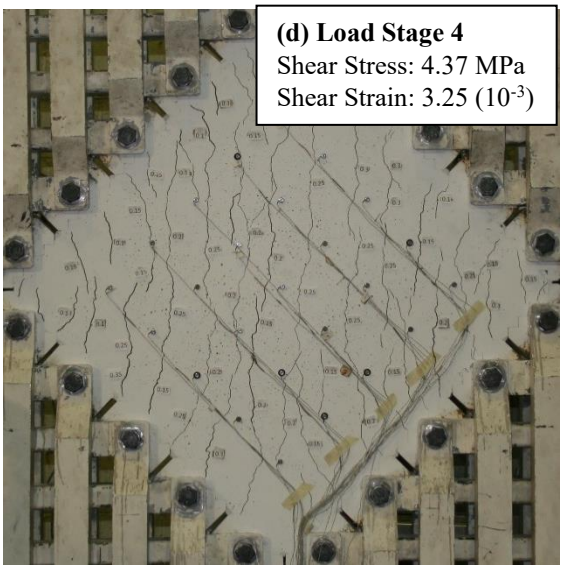

(d) Load Stage 4
Shear Stress: 4.37 MPa
Shear Strain: 3.25 (10^{-3})

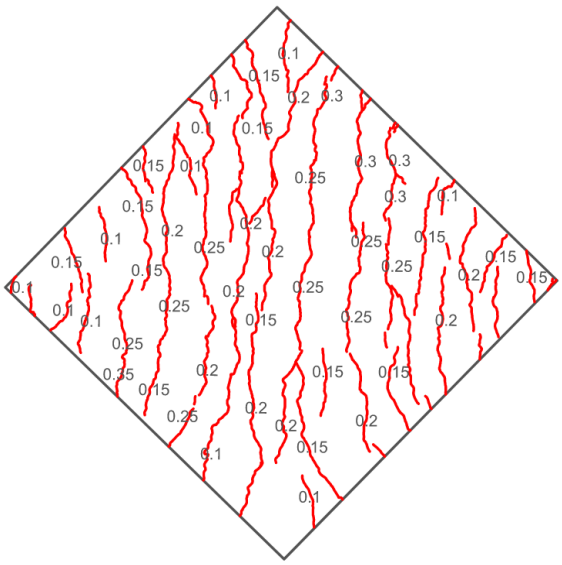

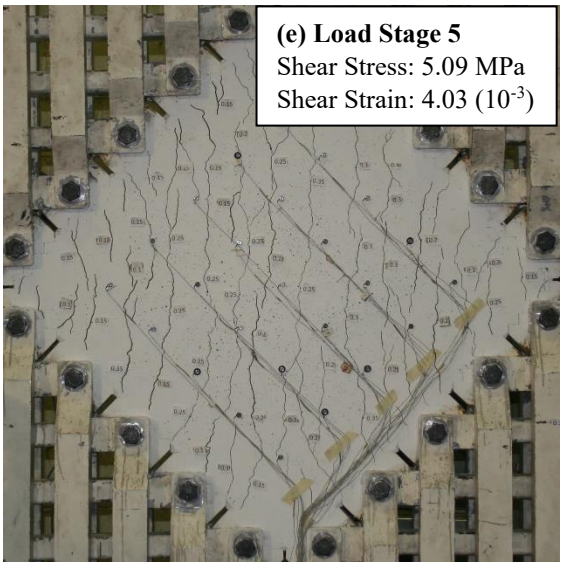

(e) Load Stage 5
Shear Stress: 5.09 MPa
Shear Strain: 4.03 (10^{-3})

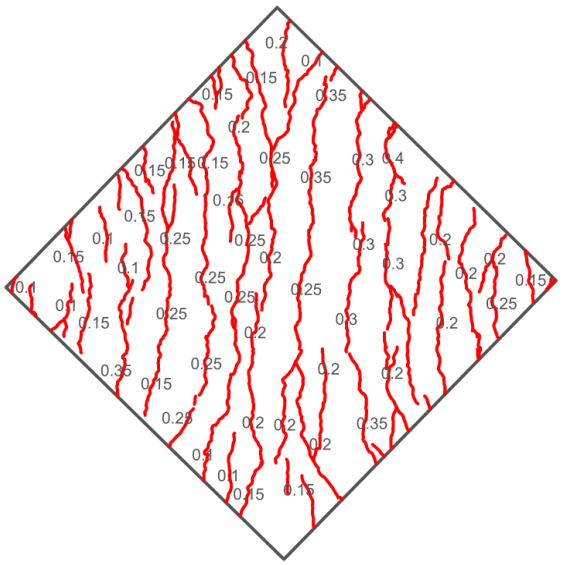

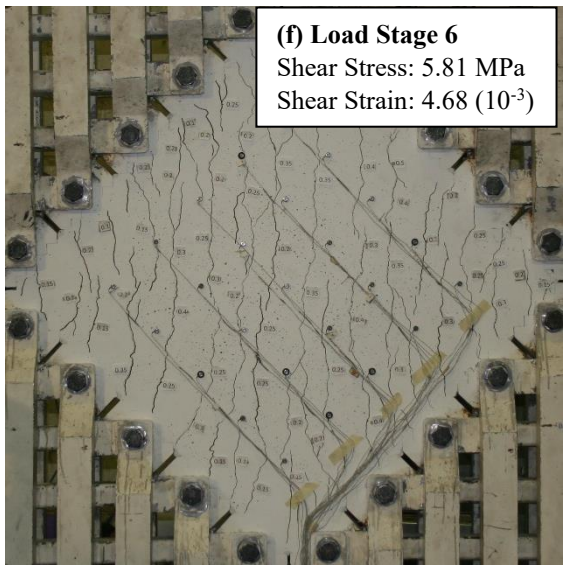

(f) Load Stage 6
Shear Stress: 5.81 MPa
Shear Strain: 4.68 (10^{-3})

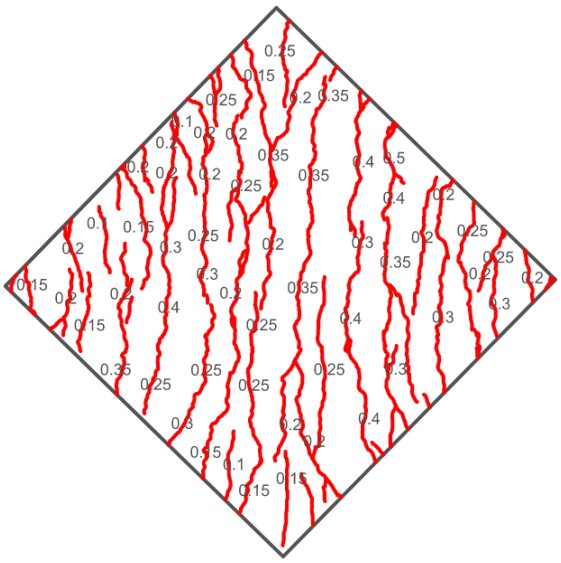

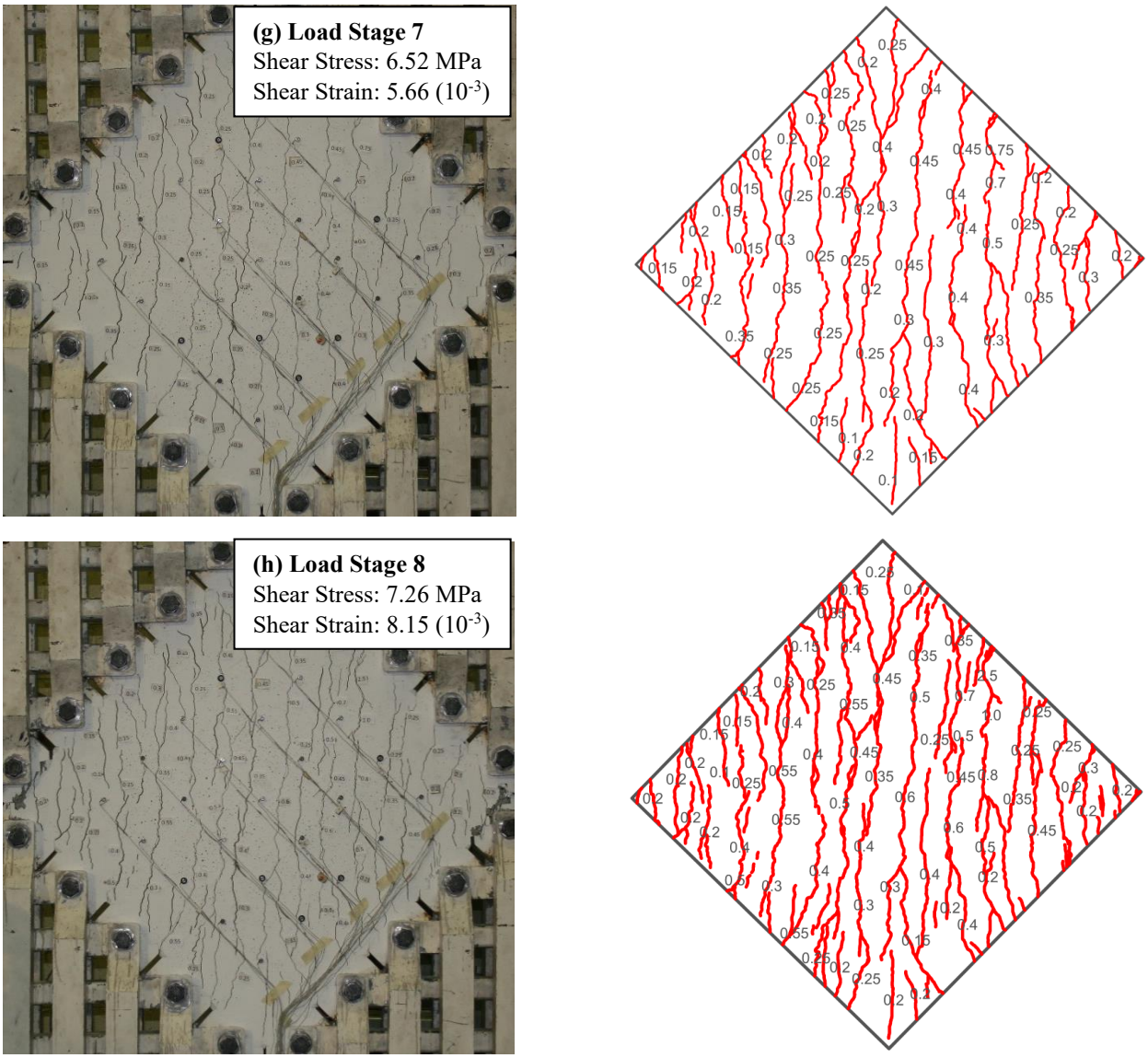

Figure A-35: PFRC-052-114 Photos and Crack Maps at Load Stages